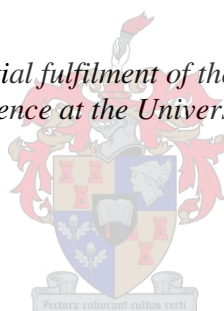


Studying crystallization kinetics using Solution Crystallization Analysis by Laser Light Scattering (Scalls)

by

Divann Robertson

*Thesis presented in partial fulfilment of the requirements for the degree
Master of Science at the University of Stellenbosch*



Supervisor: Prof, Albert J. van Reenen

Faculty of Science
Department of Chemistry and Polymer Science

March 2012

Declaration

By submitting this thesis electronically, I declare that the entirety of the work contained therein is my own, original work, that I am the sole author thereof (save to the extent explicitly otherwise stated), that reproduction and publication thereof by Stellenbosch University will not infringe any third party rights and that I have not previously in its entirety or in part submitted it for obtaining any qualification.

March 2012

ABSTRACT

This study involved the analysis of crystallization kinetics by means of a unique and newly developed Solution crystallization analysis by laser light scattering (Scalls) technique. In the main study we compared two commercial linear low-density polyethylene (LLDPE) polymers (PE-1-octene and PE-1-hexene) and studied the effect of short-chain branching on the solution crystallization of these complex polymer systems. Characterization of the polymers was done by nuclear magnetic resonance spectroscopy (NMR) and high-temperature gel permeation chromatography (HT-GPC).

The second study involved the fractionation of a PE-1-hexene copolymer by temperature rising elution fractionation (Tref) and analyzing the solution crystallization of the different temperature fractions. This resulted in important details on the different molecular regions present in the polymer.

A third additional study was done on the compatibility in polyolefin blends. Two different blends were prepared: isotactic polypropylene (iPP) – low density polyethylene (LDPE) blend and iPP – polypropylene impact copolymer (PPIC) blend. It was found that co-crystallization only occurred for the iPP - PPIC blends. Phase separation occurred for the iPP – LDPE blends, resulting in the formation of two phases for all blend compositions.

Solution crystallization analysis is usually measured by the conventional Crystallization Analysis Fractionation (Crystaf) technique. In this study all crystallization data were compared with Crystaf results and a good correlation was found between the results obtained by Crystaf and Scalls. The major advantages of the Scalls technique are that, results similar to that of Crystaf can be acquired with much shorter analysis times and Scalls also allows for the measurement of solution melting of the crystallized polymer solutions.

OPSOMMING

Hierdie studie het die analise van kristallisasië kinetika behels met behulp van die unieke en nuut ontwikkelde oplossing kristallisasië analise deur laser lig verstrooiing (Scalls) tegniek. In die hoof studie het ons twee kommersiële liniêre lae-digtheid polietileen (LLDPE) polimere (PE-1-okteen en PE-1-hekseen) vergelyk en die effek van kort-ketting vertakking op kristallisasië in oplossing van hierdie komplekse polimeer sisteme bestudeer. Karakterisering van die polimere was gedoen met kern magnetiese resonans spektroskopie (KMR) en hoë-temperatuur gel permeasie kromatografie (HT-GPC).

Die tweede studie het die fraksionering van 'n PE-1-hekseen ko-polieer met behulp van temperatuurstyging eluering fraksionering (Tref) behels asook die analisering van kristallisasië in oplossing van die verskillende temperatuur fraksies. Belangrike informasie oor die verskillende molekuleêre areas teenwoordig in die polimeer was verkry.

'n Derde addisionele studie was gedoen op die versoenbaarheid in poliolefin mengsels. Twee verskillende mengsels was voorberei: isotaktiese polipropileen (iPP) – lae digtheid polietileen (LDPE) mengsel en iPP – polipropileen impak ko-polimeer (PPIC) mengsel. Daar was gevind dat ko-kristallisasië slegs in die iPP – PPIC mengsel plaasgevind het. Fase skeiding het plaasgevind in die iPP – LDPE mengsels wat tot twee fases gelei het vir alle mengsel komposisies.

Kristallisasië in oplossing word gewoonlik gemeet met die konvensionele kristallisasië analise fraksionering (Crystaf) tegniek. In hierdie studie was al die kristallisasië data met Crystaf resultate vergelyk en 'n goeie korrelasie was gevind tussen die resultate van Crystaf en Scalls. Die grootste voordele van die Scalls tegniek is dat resultate soortgelyk aan dië van Crystaf kan verkry word met baie korter analises en Scalls laat ook toe vir die meting van smeltpunt van die ge-kristalliseerde polimeer oplossings.

Dedicated to:

My father, Johan

and

My mother, Sylvia

For their love and support throughout my studies.

Acknowledgements

I would like to thank the following people for their support and contributions during this study:

Prof. A.J. van Reenen – for his support, advice and guidance throughout this study.

Maggie Brand – for assistance with the Scalls setup.

The Olefins research group (Liesl, Madeleine, Maggie and Tiaan)

Sadiq and Dr. Gareth Harding – for the HT-GPC work.

Dr. D.J. Brand and Elsa Malherbe - for the NMR work.

Technical Assistants at Polymer Science

The Laser Research Institute at University of Stellenbosch:

- Prof. E. Rohwer, Dr. P. Neethling, E. Shields, J. Germishuizen, G. Louwrens

NRF – for funding

To all my friends who supported me during this study.

My Mom (Sylvia), Dad (Johan), brother (Heinrich) and the Rinkwest family for their endless support and encouragement.

Contents

List of Contents	I
List of Figures	V
List of Tables	IX
List of Schemes	X
List of Abbreviations	XI

List of contents

Chapter 1: Introduction and Objectives	1
1.1) Introduction.....	2
1.2) Aims and objectives	2
1.3) Structure of this manuscript	2
1.3.1) Chapter 2.....	2
1.3.2) Chapter 3.....	3
1.3.3) Chapter 4.....	3
1.3.4) Chapter 5.....	3
1.4) References	4
Chapter 2: Historical background and Literature review	5
2.1) Polyethylene: An overview	6
2.1.1) Introduction.....	6
2.1.2.) Low-density polyethylene	7
2.1.3) High-density polyethylene.....	7
2.1.4) Linear low-density polyethylene.....	8

2.2) Production of polyethylene.....	9
2.2.1) High pressure processes.....	9
2.2.2) Phillips process	10
2.2.2.1) Cossee mechanism	11
2.2.2.2) Green-Rooney	11
2.2.3) Ziegler process	12
2.2.4) Metallocene processes	14
2.2.4.1) Initiation.....	17
2.2.4.2) Propagation	18
2.2.4.3) Termination.....	19
2.3) Crystallization and crystallinity	20
2.3.1) Crystallization of polyethylene	21
2.4) Fractionation of semi-crystalline polymers	22
2.4.1) Temperature rising elution fractionation (Tref).....	23
2.4.1.1) First step: crystallization.....	23
2.4.1.2) Second step: elution	23
2.4.2) Crystallization analysis fractionation (Crystaf)	25
2.4.2.1) Process.....	26
2.4.3) Turbidity Analysis.....	27
2.4.3.1) Process.....	28
2.5) References	30
Chapter 3: Experimental	35
3.1) Materials	36
3.1.1) Polymers	36

3.1.2)	Solvents	37
3.1.3)	Stabilizers.....	37
3.2)	Preparation of polymer blends	38
3.3)	Differential scanning calorimetry (DSC)	38
3.4)	High temperature gel permeation chromatography (HT-GPC).....	38
3.5)	Nuclear magnetic resonance spectroscopy (NMR)	38
3.6)	Temperature rising elution fractionation (Tref).....	39
3.6.1)	Crystallization step.....	39
3.6.2)	Elution step	39
3.7)	Crystallization analysis fractionation (Crystaf).....	40
3.8)	Solution crystallization analysis by laser light scattering (Scalls)	41
3.9)	Particle size analysis.....	43
3.10)	References	44
 Chapter 4: Results and Discussion		45
4.1)	Introduction.....	46
4.2)	Analysis of LLDPE samples.....	46
4.2.1)	Crystallization analysis.....	46
4.2.1.1)	Particle size analysis.....	55
4.2.2)	Dissolution analysis.....	57
4.3)	Analysis of polymer fractions obtained by Tref.....	61
4.3.1)	Introduction.....	61
4.3.2)	Crystallization analysis.....	62
4.3.3)	Dissolution analysis.....	69
4.4)	Analysis of polymer blends.....	71

4.4.1) Isotactic polypropylene (iPP) – low density polyethylene (LDPE)	71
4.4.1.1) Crystallization analysis.....	71
4.4.1.2) Dissolution analysis.....	74
4.4.2) Isotactic polypropylene (iPP) – polypropylene impact copolymer (PPIC)	76
4.5) References	78
Chapter 5: Conclusions and Recommendations	79
5.1) Conclusions	80
5.1.1) Analysis of LLDPE samples.....	80
5.1.2) Analysis of polymer fractions obtained by Tref	81
5.1.3) Analysis of polymer blends	81
5.2) Recommendations	81
Appendix A: NMR data.....	82
Appendix B: DSC data	85
Appendix C: Crystaf data.....	89

List of Figures

Figure 2.1:	Differences in the microstructure of the three major polyethylenes.....	8
Figure 2.2:	Typical structure of a Ziegler-Natta catalyst.....	13
Figure 2.3:	Structures of some metallocenes.....	15
Figure 2.4:	X-ray diffraction pattern of a highly crystalline poly(ethylene oxide) sample.....	21
Figure 2.5:	Illustration of different layers after Tref crystallization (first step).....	24
Figure 2.6:	Temperature profile of crystallization and elution steps during Tref.....	24
Figure 2.7:	Crystaf profile of a polyolefin blend.....	26
Figure 2.8:	Raw data of a Scalls cooling scan.....	29
Figure 2.9:	First derivative curve of raw data shown in Figure 2.8.....	29
Figure 3.1:	Structure of Irgafos 168.....	37
Figure 3.2:	Structure of Irganox 1010.....	37
Figure 3.3:	Tref column used in this study.....	40
Figure 3.4:	Reactor vessels inside Crystaf oven.....	40
Figure 3.5:	Schematic diagram of Scalls setup (viewed from the top).....	41
Figure 3.6:	Experimental setup of Scalls instrumentation.....	42
Figure 3.7:	Aluminium block mounted on heater stirrer.....	42
Figure 4.1:	Comparison of crystallization data for (A) PE-1-octene and (B) PE-1-hexene at identical conditions (1 °C/min, 2 mg/ml). [Normalized curves].....	47
Figure 4.2:	Comparison of crystallization data for (A) PE-1-octene and (B) PE-1-hexene at identical conditions (0.5 °C/min, 2 mg/ml). [Normalized curves].....	47
Figure 4.3:	Comparison of crystallization data for (A) PE-1-octene and (B) PE-1-hexene at identical conditions (0.2 °C/min, 2 mg/ml). [Normalized curves].....	47
Figure 4.4:	Normalized raw voltage curves for PE-1-octene cooled at 1 °C/min.....	50

Figure 4.5:	Normalized raw voltage curve for PE-1-hexene cooled at 1 °C/min.	51
Figure 4.6:	Crystallization stages for PE-1-octene.....	52
Figure 4.7:	Crystallization stages for PE-1-hexene	52
Figure 4.8:	Raw voltage cooling profiles for Crystaf (0.1 °C/min) and Scalls (0.2 °C/min) for PE-1-hexene. [Normalized curves]	54
Figure 4.9:	First derivative cooling profiles for Crystaf (0.1 °C/min) and Scalls (0.2 °C/min) for PE-1-hexene. [Normalized curves]	55
Figure 4.10:	Intensity distributions of A) PE-1-octene and B) PE-1-hexene.....	56
Figure 4.11:	Volume distributions of A) PE-1-octene and B) PE-1-hexene.....	56
Figure 4.12:	Number distributions of A) PE-1-octene and B) PE-1-hexene.....	56
Figure 4.13:	Heating profiles for PE-1-octene (1 °C/min; 2 mg/ml). [Normalized curves]	57
Figure 4.14:	Heating profiles for PE-1-hexene (1 °C/min, 2 mg/ml). [Normalized curves].....	58
Figure 4.15:	Relative area under melting peaks of different laser signals for PE-1-octene copolymer	59
Figure 4.16:	Relative area under melting peaks of different laser signals for PE-1-hexene copolymer.	59
Figure 4.17:	Normalized cooling profiles for Tref fractions of a PE-1-hexene copolymer analyzed by SCALLS. [blue laser ; 1 °C/min; 2 mg/ml].....	62
Figure 4.18:	Normalized cooling profiles for Tref fractions of a PE-1-hexene copolymer analyzed by SCALLS. [green laser; 1 °C/min; 2 mg/ml].....	62
Figure 4.19:	Normalized cooling profiles for Tref fractions of a PE-1-hexene copolymer analyzed by SCALLS: [red laser; 1 °C/min; 2 mg/ml]	63
Figure 4.20:	Different laser signals of T70 fraction cooling profile. [Normalized; 1 °C/min]	64
Figure 4.21:	Normalized crystaf profiles of PE-1-hexene polymer fractions [0.1°C/min].	65
Figure 4.22:	Normalized cooling profiles for the Tref fractions of a PE-1-hexene copolymer analyzed by Scalls. [blue laser; 0.2 °C/min; 2 mg/ml]	66
Figure 4.23:	Normalized cooling profiles for the Tref fractions of a PE-1-hexene copolymer analyzed by Scalls. [green laser; 0.2 °C/min; 2 mg/ml]	66

Figure 4.24:	Normalized cooling profiles for the Tref fractions of a PE-1-hexene copolymer analyzed by Scalls. [red laser; 0.2°C/min, 2mg/ml].....	66
Figure 4.25:	Crystaf and Scalls crystallization profiles of unfractionated PE-1-hexene polymer.	68
Figure 4.26:	Normalized heating profiles for the Tref fractions of a PE-1-hexene copolymer analyzed by Scalls. [blue laser; 1.5 °C/min; 2 mg/ml].....	69
Figure 4.27:	Normalized heating profiles for the Tref fractions of a PE-1-hexene copolymer analyzed by Scalls. [green laser; 1.5 °C/min; 2 mg/ml].....	69
Figure 4.28:	Normalized heating profiles for the Tref fractions of a PE-1-hexene copolymer analyzed by Scalls: [red laser; 1.5 °C/min; 2 mg/ml].....	70
Figure 4.29:	DSC profiles of 50:50 PP-LDPE blend.....	71
Figure 4.30:	Overlay of Scalls cooling profiles for different lasers. [20:80 wt% PP-LDPE blend; 1 °C/min; 5 mg/ml; normalized peaks].....	72
Figure 4.31:	Overlay of Scalls cooling profiles for different lasers. [10:90 wt% PP-LDPE blend; 1 °C/min; 5 mg/ml; normalized peaks].....	73
Figure 4.32:	Overlay of Scalls cooling profiles for different lasers. [5:95 wt% PP-LDPE blend; 1 °C/min; 5 mg/ml; normalized peaks].....	73
Figure 4.33:	Overlay of Scalls heating profiles for different lasers. [20:80 wt% PP-LDPE blend, 1 °C/min; 5 mg/ml normalized peaks].....	74
Figure 4.34:	Overlay of Scalls heating profiles for different lasers. [10:90 wt% PP-LDPE blend, 1 °C/min; 5 mg/ml normalized peaks].....	75
Figure 4.35:	Overlay of Scalls heating profiles for different lasers. [5:95 wt% PP-LDPE blend, 1 °C/min; 5 mg/ml normalized peaks].....	75
Figure 4.36:	DSC profiles of 50:50 wt% PP-PPIC blend.	76
Figure 4.37:	Overlay of Scalls cooling profiles for different lasers. [50:50 wt% PP-EPR blend; 1°C/min; 2 mg/ml; normalized peaks].....	77
Figure 4.38:	Overlay of Scalls heating profiles for different lasers. [50:50 PP-EPR blend; 1.5°C/min; 2mg/ml; normalized peaks]	77

Figure A-1:	^{13}C NMR spectrum of PE-1-octene.....	82
Figure A-2:	^1H NMR spectrum of PE-1-octene.....	82
Figure A-3:	^{13}C NMR spectrum of PE-1-hexene used in first study	83
Figure A-4:	^1H NMR spectrum of PE-1-hexene used in first study.	83
Figure A-5:	^{13}C NMR spectrum of PE-1-hexene used in fractionation study.....	84
Figure A-6:	^1H NMR spectrum of PE-1-hexene used in fractionation study.....	84
Figure B-1:	DSC results for PE-1-octene.....	85
Figure B-2:	DSC results for PEH1.....	85
Figure B-3:	DSC results for PEH2.....	86
Figure B-4:	DSC endotherms for Tref fractions of PEH2.....	86
Figure B-5:	DSC exotherms for Tref fractions of PEH2.	87
Figure B-6:	DSC results for iPP.	87
Figure B-7:	DSC results for LDPE.	88
Figure B-8:	DSC results for PPIC.....	88
Figure C-1:	Crystaf profile of PE-1-octene.....	89
Figure C-2:	Crystaf profile of PEH1.....	89
Figure C-3:	Crystaf profile of iPP.....	90
Figure C-4:	Crystaf profile of PEH2.....	90
Figure C-5:	Crystaf profile of PEH2 T60 fraction.....	91
Figure C-6:	Crystaf profile of PEH2 T70 fraction.....	91
Figure C-7:	Crystaf profile of PEH2 T80 fraction.....	92
Figure C-8:	Crystaf profile of PEH2 T90 fraction.	92

List of Tables

Table 2.1:	Contrasting features between Metallocene and Ziegler-Natta catalysts.	15
Table 2.2:	Zirconocene/aluminoxane efficiency.	16
Table 2.3:	Ethylene polymerization with different metallocene-aluminoxane systems. (330ml toluene, 8 bar pressure, 5×10^{-3} mol (Al-O) units).....	17
Table 2.4:	Comparison between preparative Tref and analytical Tref.	25
Table 3.1:	Molecular weight data of polymers used during this study.....	36
Table 4.1:	Characterization data of LLDPE samples used	46
Table 4.2:	Data of crystallization peak temperatures	49
Table 4.3:	Duration of crystallization at different cooling rates for Stage 1.....	53
Table 4.4:	Duration of crystallization at different cooling rates for Stage 2.....	53
Table 4.5:	Relative areas under melting peaks.....	58
Table 4.6:	Tref fractions of PE-1-hexene copolymer collected for study.....	61
Table 4.7:	Molecular weight data for fractions and bulk sample.....	61
Table 4.8:	Crystallization peak temperatures for the different Tref fractions at cooling rate of $1^{\circ}\text{C}/\text{min}$	63
Table 4.9:	Peak temperatures for the T70 fraction cooled at $1^{\circ}\text{C}/\text{min}$	64
Table 4.10:	Comparison of Crystaf and Scalls results done at similar conditions.....	67
Table 4.11:	Duration of crystallization for Tref fractions analyzed by Scalls at different cooling rates.....	68
Table 4.12:	Comparison of Tref elution temperatures and Scalls solution melting temperatures.....	70

List of Schemes

Scheme 2.1: Polyethylene polymerization	6
Scheme 2.2: Chemical reaction according to Bamberger and Tschiner	6
Scheme 2.3: Disproportionation and recombination of polyethylene chains.....	10
Scheme 2.4: Reaction of chromium compound with dehydrated silica to form the Phillips-type catalyst.....	11
Scheme 2.5: Ethylene polymerization mechanism with Phillips-type catalyst.....	12
Scheme 2.6: A mechanism for Ziegler-Natta catalysis of ethylene.....	14
Scheme 2.7: Initiation step of ethylene polymerization with metallocene catalyst.....	18
Scheme 2.8: Propagation step of ethylene polymerization with metallocene catalyst.....	18
Scheme 2.9: Chain transfer through β -elimination with hydride transfer to monomer.....	19
Scheme 2.10: Chain transfer through β -elimination with hydride transfer to metal.....	19
Scheme 2.11: Hydrogenolysis	20
Scheme 2.12: Illustration of Tref elution (second step).....	24

List of Abbreviations

AIBN	Azobis - isobutyronitrile
Crystaf	Crystallization Analysis Fractionation
DLS	Dynamic Light Scattering
DSC	Differential Scanning Calorimetry
HDPE	High – density polyethylene
HT – GPC	High Temperature Gel Permeation Chromatography
iPP	Isotactic polypropylene
LDPE	Low – density polyethylene
LLDPE	Linear low – density polyethylene
MAO	Methylaluminoxane
MFI	Melt flow index
M_n	Number average molecular weight
M_w	Weighted average molecular weight
NMR	Nuclear Magnetic Resonance
p - Tref	preparative temperature rising elution fractionation
PDI	Polydispersity index
PE	Polyethylene
PPIC	Polypropylene impact copolymer
Scalls	Solution Crystallization Analysis by Laser Light Scattering
SCB	Short chain branching
TCB	1,2,4 - Trichlorobenzene
TCE	1,1,2,2 - Tetrachloroethane
TEAL	Triethylaluminum

TFA	Turbidity Fractionation Analyzer
Tref	Temperature Rising Elution Fractionation

Chapter 1

Introduction and Objectives

This chapter provides a brief overview on the techniques used for analyzing solution crystallization events in polymers as well as an outline for the rest of the chapters in this thesis.

1.1) Introduction

The crystallization events in polymers are important processes that determine the physical and mechanical properties of polymer systems. These events are usually studied by solution crystallization techniques. Solution crystallization analysis of polymers has ordinarily been studied by a “delayed” technique like Crystallization analysis fractionation (Crystaf). This means that the information obtained is not immediate. Due to this, many smaller and significant events that occur during crystallization could be missed completely, ignored or misinterpreted.

Although Crystaf requires shorter analysis times than temperature rising elution fractionation (Tref), both of these techniques are time consuming. The chemical composition distribution of polyolefins, especially LLDPE, has extensively been studied using these two techniques^{1,2,3}. In this study we analyze the solution crystallization of mainly LLDPE with an instrument built in-house for our research group⁴ and initially developed by Shan et al.⁵ Results were then compared to those obtained by Tref and Crystaf.

1.2) Aims and objectives

The main objective of this study was to evaluate the use of Solution Crystallization Analysis by Laser Light Scattering (Scalls) in the study of the crystallization of polymer systems, mainly LLDPE. Under this objective, the aims are:

- The use of Scalls to differentiate between chemically similar but morphologically different polymers.
- To look at responses of different lasers (blue – 405 nm, green – 532 nm, red – 635 nm) and see what information regarding crystallization and melting events can be obtained.
- Fractionation of a polyolefin by Tref and analysis of the fractions by Scalls.
- Analysis of polyolefin blends.

1.3) Structure of this manuscript

1.3.1) Chapter 2

This chapter shares some background information and previous work done on the polymerization and crystallization of polyethylene as well as the fractionation of semi-crystalline polymers.

1.3.2) Chapter 3

An overview of the materials analyzed and experimental techniques used during this study is given in this chapter.

1.3.3) Chapter 4

This chapter focuses on the results obtained by Scalls and the comparison with Crystaf and Tref data.

1.3.4) Chapter 5

A summary of the conclusion for the study is given in this chapter.

1.4) References

- 1) Britto L.J.D., Soares J.B.P., Penlidis A., Monrabal B., *Polyolefin analysis by single-step crystallization fractionation*. Journal of Polymer Science Part B: Polymer Physics, 1999, vol 37, no. 6, pp. 539-552.
- 2) Gabriel C., Lilge D., *Comparison of different methods for the investigation of the short-chain branching distribution of LLDPE*, Polymer, 2001, vol 42, no. 1, pp. 297-303.
- 3) Müller A.J., Arnal M.L., Spinelli A.L., Cañizales E., Puig C.C., Wang H., Han C.C., *Morphology and crystallization kinetics of melt miscible polyolefin blends*, Macromolecular Chemistry and Physics, 2003, vol 204, no. 12, pp. 1497-1513.
- 4) Van Reenen A.J., Rohwer E.G., Walters P., Lutz M., Brand M., *Development and use of a turbidity analyzer for studying the solution crystallization of polyolefins*, Journal of Applied Polymer Science, 2008, vol. 109, no. 5, pp. 3238-3243.
- 5) Shan C.L.P., Degroot W.A., Hazlitt L.G., Gillespie D., *A new turbidimetric approach to measuring polyethylene short chain branching distributions*, Polymer, 2005, vol. 46, no. 25, pp. 11755-11767.

Chapter 2

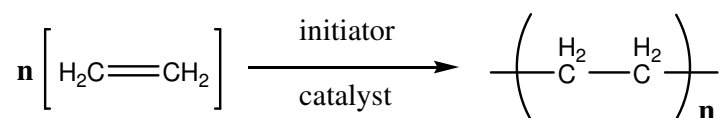
Historical background and Literature review

In this chapter some background information and previous work done on the polymerization and crystallization of polyethylene as well as the fractionation of semi-crystalline polymers is discussed.

2.1) Polyethylene: An overview

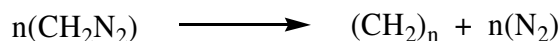
2.1.1) Introduction

Polyethylene is part of a group of polymers known as polyolefins. This group of polymers only consists of carbon and hydrogen atoms and polyethylene has the simplest formula of all polyolefins, namely $-(CH_2)_n$. A typical polymerization reaction is shown in Scheme 2.1:



Scheme 2.1: Polyethylene polymerization

The first synthesis of polyethylene was reported as long ago as 1898 when von Pechmann observed that on standing, a white substance formed after the dissolution of diazomethane in ether. He called the composition “polymethylene”. Bamberger and Tschirner later stated that this substance had a melting point of 128 °C and after analysis concluded that the chemical structure was $(CH_2)_n$ ¹. The chemical reaction leading to the formation of this substance was reported to be (Scheme 2.2):



Scheme 2.2: Chemical reaction according to Bamberger and Tschirner

The development of the industrially practical synthesis of polyethylene can be traced back to the 1930's. In 1933 a small amount of polyethylene was produced at the Alkali Division of Imperial Chemical Industries Limited but development only proceeded after eight grams were made in December 1935 and the substance went under the generic name of polyethylene². The history can be divided into several phases:

- 1935-1939: Development of manufacturing processes and suitable uses for the material.
- 1939-1945: Attention was focused on the production of polyethylene in the United Kingdom and United States of America for wartime uses.

1945- present: Development of polyethylene as a plastic material. In this period it has found a wide range of applications including packaging materials, domestic articles and films.

In the era after 1945, the evolution of industrial polyethylene includes some important milestones. Hogan and Banks produced linear polyethylene by transition metal catalysts in 1950. This work was done independently to Ziegler who applied a different method. Through the 1960's and 1970's, supported catalyst systems and gas-phase processes emerged. During this time, linear low-density polyethylene (LLDPE) materialized as well. The commercialization of metallocene single-site catalysts occurred during the 1990's³. The types of polyethylene are summarized in the next few sections.

Depending on the process conditions, a wide variety of polyethylene can be synthesized. Certain factors that influence these variations in microstructure, composition, molecular weight, density etc. includes the specific polymerization conditions, catalyst type and cocatalyst type. By far the most common and major polyethylenes are low-density polyethylene (LDPE), high-density polyethylene (HDPE) and linear low-density polyethylene (LLDPE). Figure 2.1 shows the differences in molecular structure of the three polymers.

2.1.2.) Low-density polyethylene

Low-density polyethylene is produced by free radical polymerization of the ethylene monomer. The polymerization is a high pressure process and range from 180 to 350MPa. The temperature during polymerization is in the ranges of 180 to 350°C. The typical density values for this polymer range between 0.915 g/cm³ and 0.930 g/cm³.

2.1.3) High-density polyethylene

Unlike LDPE, high-density polyethylene cannot be made via a free radical polymerization mechanism. High-density polyethylene is produced by polymerization of ethylene monomer with the use of a Ziegler-Natta catalyst or a Phillips catalyst. Typical density values for this polymer are

0.940 g/cm³ – 0.970 g/cm³. The higher density is due to the linearity of the polymer chains and increased crystallinity compared to LDPE and LLDPE. Thus HDPE cannot match up in terms of clarity and is used for pipes and bottles etc.

2.1.4) Linear low-density polyethylene

Similar to HDPE, linear low-density polyethylene cannot be polymerized through a free radical mechanism. LLDPE is produced by copolymerization of ethylene monomer with α -olefins. This is done using a Phillips catalyst, Ziegler-Natta catalyst or single site catalyst. Copolymerization results in a polymer structure with short chain branching. The branching distributions are dependent on the comonomer used as well as the comonomer content. The inclusion of the comonomer results in branched structures with ethyl branches if 1-butene is used; butyl branches if 1-hexene is used, and so on. Comonomer reactivities are very important in the production of LLDPE⁴. Various α -olefins have been studied to analyze their use and effects as comonomers to form LLDPE's^{5,6}.

Single site catalysts based on metallocene/methylaluminoxane (MAO) systems are extremely useful for these copolymerizations. These types of catalysts lead to polymer structures that are more homogeneous and uniform in both comonomer distribution and molecular weight distribution.

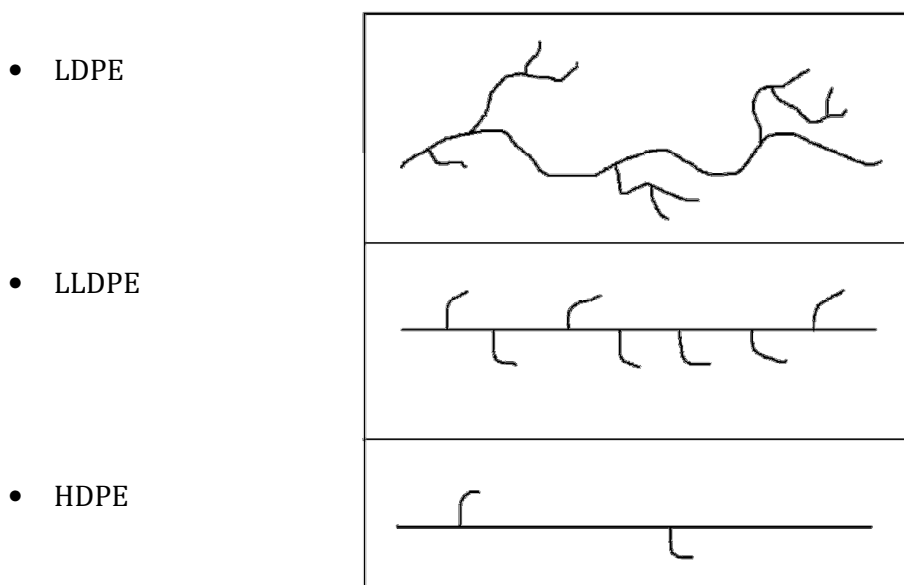


Figure 2.1: Differences in the microstructure of the three major polyethylenes.

2.2) Production of polyethylene

There are a number of different methods for the preparation of ethylene polymers. Some of these methods are listed below.

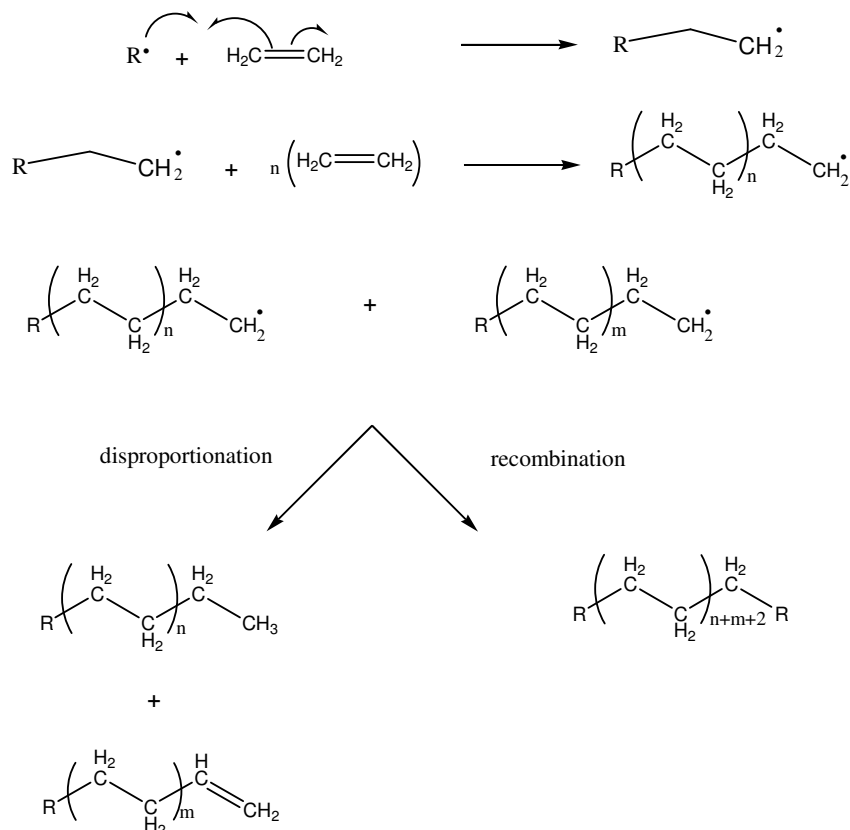
- 1) High pressure processes
- 2) Phillips process
- 3) Ziegler process
- 4) Metallocene process

2.2.1) High pressure processes

This process involves a free-radical polymerization mechanism and usually free-radical initiators such as azobis-isobutyronitrile (AIBN) or benzoyl peroxide are used. This is a continuous process. During the continuous operation, the reactants are passed through stirred reactors (also known as autoclaves). Tubular reactors are also used for the manufacturing polyethylene. The free-radical-type mechanism has two major characteristics namely the critical dependence on the monomer concentration as well as a high exothermic reaction⁷.

Characteristics such as molecular weight, molecular weight distribution and branching are easily influenced with a variation in reaction conditions. Factors that can be altered in order to vary these characteristics are; temperature, pressure, type of initiator and the incorporation of chain-transfer agents. The propagation of polymer chains is controlled by disproportionation or recombination of these chains (illustrated in Scheme 2.3).

Polyethylene produced via the high-pressure free-radical process usually has lower densities in the range of (0.915-0.940 g/cm³) as well as a lower molecular weight range, in comparison to those prepared by other processes.



Scheme 2.3: Disproportionation and recombination of polyethylene chains.

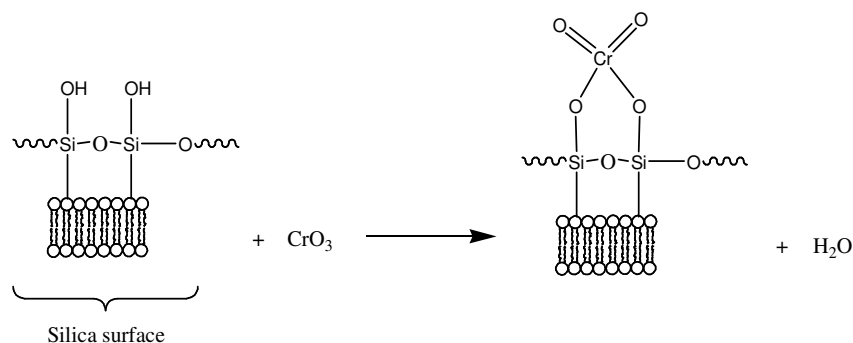
2.2.2) Phillips process

The discovery of transition metal catalysts, supported on metal oxides for the polymerization of ethylene, was made just after World War II when ways to convert olefins to gasoline-type fuels were explored⁸. The Phillips catalyst is a chromium-based catalyst supported on silica (e.g. Cr/SiO₂) and was discovered by Hogan and Banks⁹. The formation of the catalyst is shown in Scheme 2.4. Since the discovery of the Phillips-type catalysts, the same questions are still asked today¹⁰:

- Oxidation state of active site?
- Molecular structure of catalyst?
- The exact polymerization mechanism?

No unified picture has yet been achieved regarding previously mentioned questions¹¹. Polymerization can be broken into three steps namely initiation, chain propagation and chain

termination. During the initiation step the monomer attaches to the active catalytic site. Subsequent monomer units attach during the propagation step and result in a growing polymer chain. These units form alkyl chains that are fixed to the catalyst's chromium center¹². Separation of the polymer chain from the catalyst happens during termination.



Scheme 2.4: Reaction of chromium compound with dehydrated silica to form the Phillips-type catalyst.

The propagation and termination steps for ethylene polymerization are well understood but this is not the case for initiation with the Phillips catalyst. Several groups have suggested mechanisms for the initiation step⁽¹³⁻¹⁵⁾. The propagation can proceed through a Cossee¹⁶ or Green-Rooney¹⁷ mechanism depending on the method of monomer initiation.

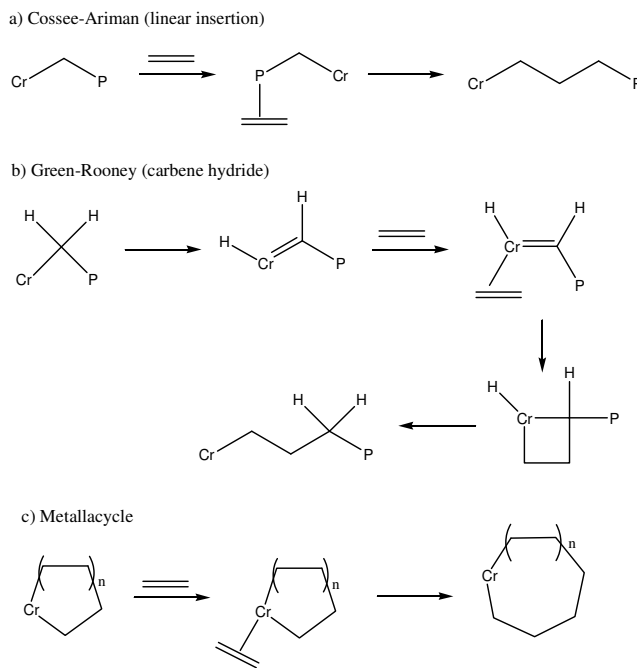
2.2.2.1) Cossee mechanism

A vacant site is required at the metal center in a position adjacent to the growing alkyl chain. This vacant site is needed for coordination of the monomer unit. Coordination occurs through π -bonding between the monomer and metal.

2.2.2.2) Green-Rooney

Two vacant sites are required at the metal center. The propagating chain first eliminates a α -hydrogen to form a metal-carbene specie before the monomer coordinates to the metal via the remaining vacant site.

Some mechanistic schemes for ethylene polymerization are given below in Scheme 2.5¹⁵, where P represents the polymer chain:



Scheme 2.5: Ethylene polymerization mechanism with Phillips-type catalyst.

2.2.3) Ziegler process

The start of Ziegler catalysis for polymerization as well as the use of Ziegler-Natta catalysts can be traced way back to the 1950's when Karl Ziegler was the first to discover that zirconium and titanium salts, when combined with an aluminum co-catalyst, are able to produce polyethylene of high molecular weights¹⁸. Soon after Ziegler's discovery, Giulio Natta found that isotactic polypropylene can be polymerized with certain preparations and conditioning of the catalyst¹⁹. The combination of these discoveries led to the extensive commercialization of some major thermoplastics that include LLDPE, HDPE and polypropylene¹⁸.

This process is commonly referred to as coordination polymerization due to the formation of a monomer-catalyst complex during the approach of the monomer unit towards the growing polymer chain. The catalysts involved are heterogeneous systems and the formation of these catalysts takes

place through the interaction of alkyls of groups' I-III metals with halides or other derivatives of the transition metals in groups' IV-VIII of the periodic table⁷. The structure of a typical Ziegler-Natta catalyst is shown in Figure 2.2, where R is an alkyl group from an alkyl metal, M is a transition metal and \square is the vacant orbital through which the monomer coordinates to the metal.

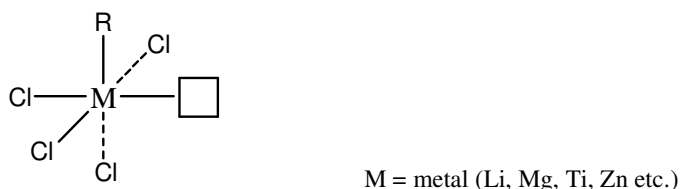
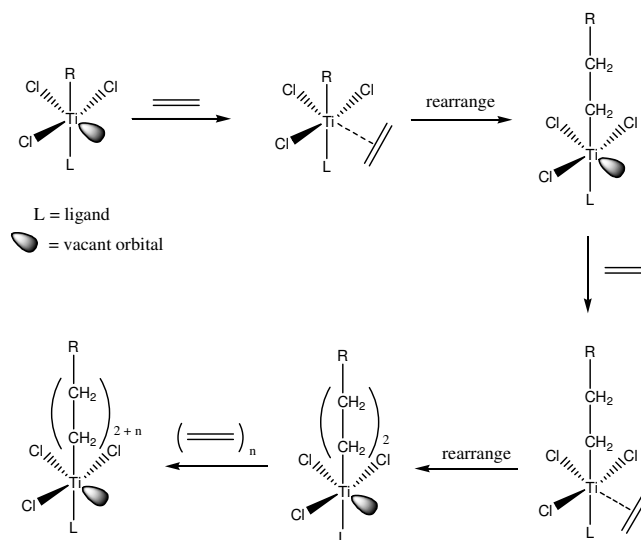


Figure 2.2: Typical structure of a Ziegler-Natta catalyst.

Monomer is introduced into a reactor at very mild conditions relative to the free-radical polymerization process. Introduction of the catalyst to the monomer kicks off the polymerization event. Oxygen and water need to be absent from the system for effective operation of the catalyst. Polymers produced by this process usually have density values between those produced by high-pressure processes and the Phillips process. Molecular weights can be varied by altering a number of factors in the system namely:

- Ratios in catalyst system
- Variation of reaction temperature
- Use of hydrogen as chain-transfer agent
- Monomer concentration

Supported catalysts have higher activity than non-supported catalysts due to the fact that the active centers are much more dispersed and highly accessible for monomer coordination. In the case of olefin polymerization, MgCl_2 supported Ziegler-Natta catalysts have become the most important catalysts²⁰. In both catalyst systems the active site become wrapped due to the growing polymer chain but in unsupported catalysts, a vast majority of potential active sites are buried inside the TiCl_3 crystallite and lowers the activity of the catalyst. Monomer addition becomes extremely difficult at this stage. The mechanism of Ziegler-Natta polymerization can be seen in Scheme 2.6. All Ziegler-Natta type polymerizations take place at a metal-carbon bond and the stereoregulation that prevails at this bond depends mainly on two things: i) whether the center is part of a crystalline catalyst particle or ii) whether the center is part of a soluble complex (bimetallic or trimetallic)²¹.



Scheme 2.6: A mechanism for Ziegler-Natta catalysis of ethylene.

Polymer chain length depends on the competition between propagation and chain termination reactions. Chain propagation occurs much easier than termination, thus in most industrial polymerization processes molecular hydrogen is injected into the reactor to regulate chain growth in both Ziegler-Natta and metallocene catalysis²².

2.2.4) Metallocene processes

Metallocenes have been known since 1951 with ferrocene being the first to be discovered²³. In 1957, Breslow and Newburg first reported the use of metallocene catalysts for the production of polyethylene²⁴. These catalysts were based on bis(cyclopentadienyl)-titanium dichloride-alkylaluminum complexes. Since then, a number of significant developments have been reported regarding metallocene catalysis⁽²⁵⁻²⁹⁾. One of the key discoveries at this time was the increase in catalyst activity with the incorporation of methylaluminoxanes as cocatalysts.

Metallocene catalysts are organometallic compounds. The transition metal centers are sandwiched between aromatic ligands. The ligands are mainly dicyclopentadienyl or indenyl groups and has a dramatic influence on polymer molar mass, polymerization activity, microstructure as well as comonomer insertion³⁰. Examples of some metallocenes are illustrated in Figure 2.3.

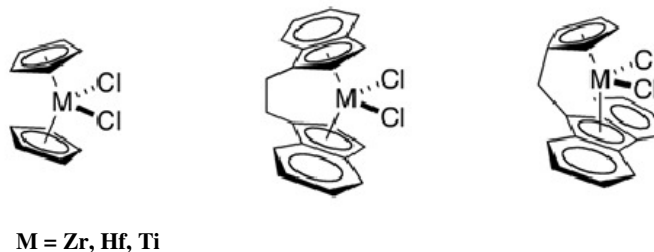


Figure 2.3: Structures of some metallocenes.

Several contrasting features exist between single-site and Ziegler-Natta catalysts. Some of these characteristics are listed in Table 2.1. Most metallocene single-site catalysts are homogeneous species and the active sites are cationic, where in the case of Ziegler-Natta catalysts the species are heterogeneous in nature and the active sites are neutral octahedral complexes with open coordination sites³¹. Polymerization with Ziegler-Natta catalysts results in polymers with very broad polydispersities. This is mainly due to the presence of multiple active sites that polymerize in somewhat different ways. Narrow polydispersities are obtained when single-site catalysts are used because as the name suggests there is only a “single site” or one type of active site through which polymerization proceeds.

Table 2.1: Contrasting features between Metallocene and Ziegler-Natta catalysts.

	Ziegler-Natta	Metallocene
Typical catalyst:	amorphous solid containing Ti	metallocenes of Zr and Ti
Cocatalyst:	TEAL ^a	MAO ^b
Active centers:	multiple active sites	single active site
Polymer polydispersities:	Broad ($4 \leq$)	Narrow (2-3)

^a triethylaluminum; ^b methylaluminoxanes

Zirconocene/aluminoxane catalyst systems have been found to have high efficiency in the polymerization of olefins. The efficiency can be seen in Table 2.2, where some of the different polymer systems, obtained by these specific catalyst-cocatalyst combinations, are listed. An overview on different metallocene-aluminoxane combinations for the polymerization of ethylene can be found in Table 2.3.

Table 2.2: Zirconocene/aluminoxane efficiency.

Ethylene polymerization	<ul style="list-style-type: none"> • Very high activity ($\approx 40 \times 10^6$ g PE/g Zr-h)
Ethylene copolymerization	<ul style="list-style-type: none"> • LLDPE • Comonomers: propene, butene, hexene, diolefins, cycloalkenes
EPDM elastomers	<ul style="list-style-type: none"> • Narrow MWD • Low concentration of transition metal in polymer
Propene polymerization	<ul style="list-style-type: none"> • Highly isotactic PP • Atactic PP • Syndiotactic PP • Isoblock PP • Stereoblock PP
Cyclopentene polymerization	<ul style="list-style-type: none"> • Polymerization to isotactic polymers • High melting points
Oligomerization to optically active hydrocarbons	
Polymerization in presence of filling materials	

Table 2.3: Ethylene polymerization with different metallocene-aluminoxane systems³². (330ml toluene, 8 bar pressure, 5 x 10⁻³ mol (Al-O) units)

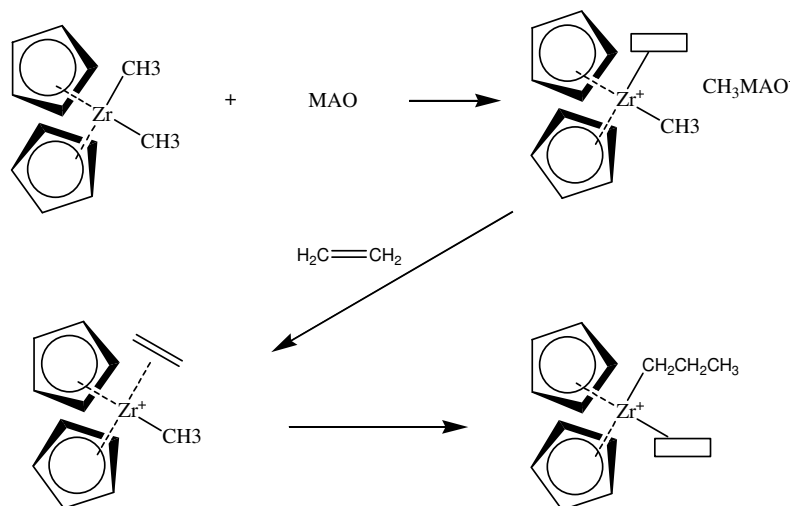
Metalocene	Cocatalyst	Temperature (°C)	Activity (g PE/g Zr.h.bar)	M _n (g/mol)
Cp ₂ Ti(CH ₃) ₂	MAO	20	5000	520 000
Cp ₂ Ti(CH ₃)Cl	MAO	20	50 000	490 000
Cp ₂ TiCl ₂	MAO	20	90 000	430 000
Cp ₂ Zr(CH ₃) ₂	MAO	20	9 000	730 000
Cp ₂ Zr(CH ₃) ₂	MAO	70	70 000	190 000
Cp ₂ Zr(CH ₃) ₂	MAO	90	3 100 000	106 000
Cp ₂ Zr(CH ₃) ₂	PAO	70	175 000	500 000
Cp ₂ ZrCl ₂	MAO	90	5 000 000	122 000
Cp ₂ ZrCl ₂	EAO	60	23 000	500 000
Cp ₂ Hf(CH ₃) ₂	MAO	70	60 000	441 000
Cp ₂ HfCl ₂	MAO	70	69 000	490 000

^amethylaluminoxane, ^bisopropylaluminoxane, ^cethylaluminoxane

The mechanism of polymerization with metallocene single-site catalysts is illustrated in Scheme 2.7 – 2.11 with dimethylzirconocene as catalyst and methylaluminoxane as cocatalyst. The steps are discussed in the following sections.

2.2.4.1) Initiation

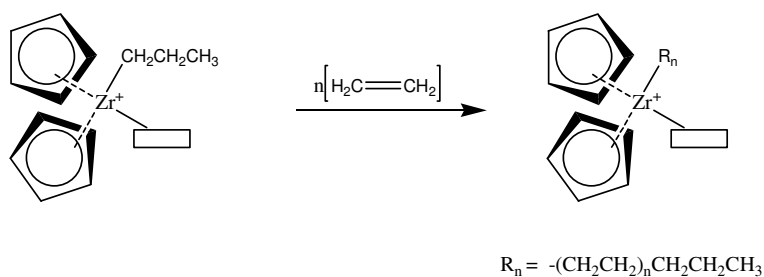
The first step is the generation of a cationic specie which acts as the active site for monomer coordination. This happens through complexation of the catalyst and cocatalyst. Generation of the active site is due to ligand abstraction by the MAO. A vacant site is produced but the anionic counter ion, formed by ligand abstraction, is still weakly coordinated to the metal center. The next step is the coordination of the monomer unit to the metal center. Once the monomer is inserted, rearrangement of the vacant orbital takes place. Growth of the polymer chain takes place through subsequent addition of monomer units.



Scheme 2.7: Initiation step of ethylene polymerization with metallocene catalyst.

2.2.4.2) Propagation

After the initiation step, the propagation process takes over. Subsequent monomer units coordinate to the metal center and inserts into the polymer chain. As more monomer units coordinate, the polymer chain starts growing longer and longer. After the insertion of each monomer unit rearrangement of the vacant site follows.

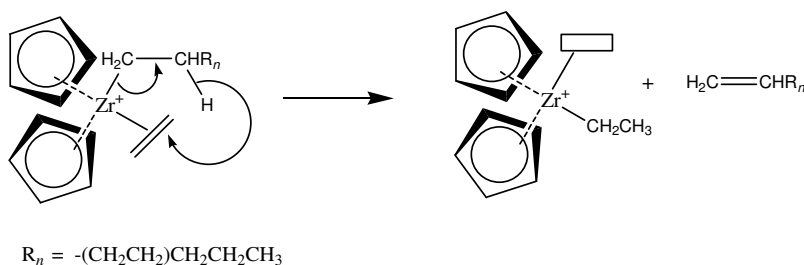


Scheme 2.8: Propagation step of ethylene polymerization with metallocene catalyst.

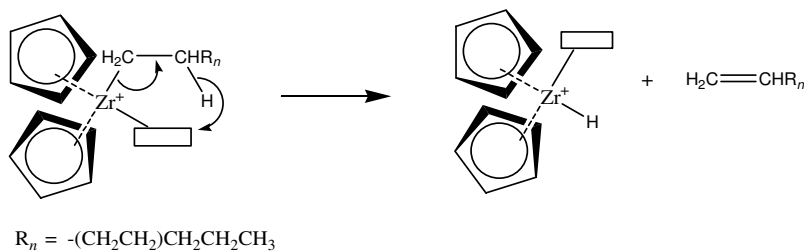
2.2.4.3) Termination

This is when polymer chain-growth stops. Several termination reactions can occur and some are illustrated in Scheme 2.9 - 2.11. Termination during metallocene catalysis is similar to the termination steps in Ziegler-Natta catalysis. This may occur in several modes:

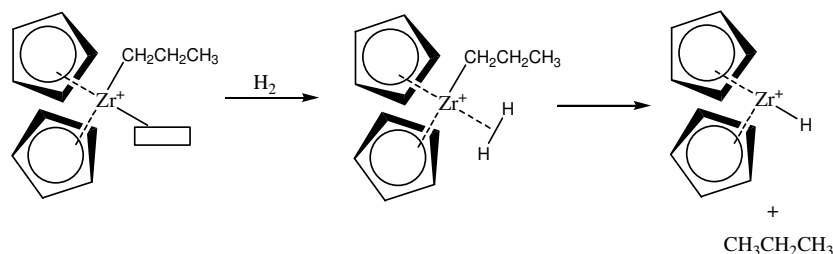
- chain transfer through β -elimination with hydride transfer to monomer
- chain transfer through β -elimination with hydride transfer to metal
- hydrogenolysis: chain transfer to hydrogen



Scheme 2.9: Chain transfer through β -elimination with hydride transfer to monomer.



Scheme 2.10: Chain transfer through β -elimination with hydride transfer to metal.



Scheme 2.11: Hydrogenolysis

2.3) Crystallization and crystallinity

Crystallinity is a very important structural feature in determining polymer properties. There are some requirements for crystallization in polymers, one of which is geometrical regularity of the polymer chains¹. This means that crystallization is influenced by the size and shape of substituent groups on a polymer backbone. A second factor affecting the crystallizability of polymers is considered to be the packing efficiency of the polymer chains³³.

A polymer can be classified as being amorphous or semi-crystalline, depending on the polymeric regions present. Amorphous polymers do not have any crystalline regions. Semi-crystalline polymers contain crystalline regions that will conform in a specific order under certain conditions. The formation and presence of crystals in polymer systems, as stated earlier, largely influences the physical properties of a polymer. During crystallization, polymer chains pack close together to form an ordered structure. These chains form lamellae, which in turn are organized into spherulites. Spherulites are very dominant features of bulk crystallization³⁴.

Although semi-crystalline polymers contain crystalline regions, amorphous areas are also present. The amorphous regions do not partake in polymer crystallization and only consist of random coiled chains. An easy way to observe the presence of these different regions is by looking at the X-ray diffraction patterns of the polymer. This method is based on the fact that crystalline regions will give sharp diffraction maxima³⁵. The reason why crystallinity can be measured is due to the exact spacing between crystalline structures which reflects light in a unique way. Crystalline regions show discrete Bragg reflections which is visible in the form of concentric circles whereas non-

crystalline polymers results in a diffused halo³⁴. An example of the X-ray pattern for a crystalline polymer can be seen in Figure 2.4.

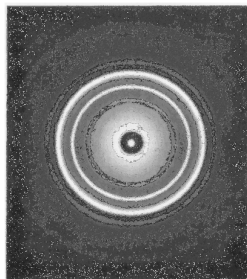


Figure 2.4: X-ray diffraction pattern of a highly crystalline poly(ethylene oxide) sample³⁴.

2.3.1) Crystallization of polyethylene

During crystallization spherulitic growth starts at central nucleation points and spread outwards from away from these points. Spherulitic growth continues until adjacent spherulites meet³⁶. Although the completely formed spherulites have cluster-like appearances, it does not originate in that form. Each spherulite is formed by a single-crystal nucleus, which then grows into a rod-like structure. As crystal growth proceeds from the nucleation point the spherulites start taking on a radial structure. Crystallization usually initiates in the areas where the polymer chains roughly lie parallel one another. This implies that growth can take place longitudinally along the polymer chain direction or laterally over sections of adjacent molecules. The crystallization process occurs with some difficulties, no matter in what direction it proceeds. The main reason for this is the entanglement of polymer chains in all directions. Longitudinal growth requires the close packing of polymer. Thus, in low-density polyethylene the branching distribution has a huge influence in the growth of crystals along the chain axis. Lateral growth only requires re-organization of neighboring chains. The opaque nature of thick polyethylene samples is not due to individual crystalline regions but well due to larger structural units.

2.4) Fractionation of semi-crystalline polymers

In the past various classical analytical methods have been used to investigate polymer crystallization but not enough information could be given on the heterogeneity of the polymer samples being analyzed. Due to this lack of information obtained by the classical techniques, more sophisticated techniques were developed during recent years. The aim of this development was to study chemical heterogeneity. Temperature rising elution fraction (Tref) and crystallization analysis fractionation (Crystaf) are two well-known recently developed analytical techniques for determining the chain crystallization distribution of semi-crystalline polymers. Both techniques are based on polymer crystallization from dilute solution and rely heavily on intermolecular differences in crystallizability of polymer chains. It is accepted that under these conditions, polymer chains with a fixed level of short chain branching are able to crystallize at a given temperature³⁷. When looking from a thermodynamic point of view, the thermodynamic equilibrium of concentrated polymer solutions is described by the Flory-Huggins equation³⁸. The equation is also known as the Flory-Huggins equation for free energy of mixing and is shown in **Equation 2.1**.

Equation 2.1: Flory-Huggins equation for free energy of mixing.

$$\frac{1}{T_m} - \frac{1}{T_m^0} = \left(\frac{R}{\Delta H_u} \right) \left(\frac{V_u}{V_1} \right) \left[-\frac{\ln(v_2)}{x} + \left(1 - \frac{1}{x} \right) v_1 - \chi_1 v_1^2 \right]$$

Where:

- T_m = equilibrium melting temperature of polymer in solution
- T_m^0 = melting temperature of pure polymer
- ΔH_u = heat of fusion per repeating unit
- V_1 = molar volume of diluent
- V_u = molar volume of polymer repeating unit
- v_1 = volume fraction of diluent
- v_2 = volume fraction of polymer
- x = number of segments
- χ_1 = Flory-Huggins thermodynamic interaction parameter

2.4.1) Temperature rising elution fractionation (Tref)

Wild and Ryle³⁹ first proposed the acronym Tref. Temperature rising elution fractionation was first used for LDPE and LLDPE⁴⁰. The study with Tref has moved on to polypropylene (PP) and also olefin alloys. It was found that determination for example, of molecular weight averages of polymers with techniques like osmometry or light scattering did not deliver results that could uniquely define a polymer sample. After the development of Tref, it became the main technique for the analysis of composition distribution of polymers with high crystallizability⁴¹. The mechanism is based on fractionation according to the molecular structure which influences the crystallinity. Tref can only be used to fractionate semi-crystalline polymers. Important detailed information on molecular structures can be obtained and this data can then be correlated to properties on a macroscopic level which can then again be correlated to the final applications of different semi-crystalline polymers. Major drawbacks of this technique are the operational complexity and long analysis times.

The Tref process consists of two sequential steps:

2.4.1.1) First step: crystallization

The polymer is dissolved in a good solvent and put into contact with an inert support. Support that can be used in Tref includes glass beads, chromosorb P, stainless steel shots/balls and silica gel⁴¹. Through controlled cooling, the polymer starts to crystallize out of solution. It is important to control the cooling in order to obtain reproducible results. Polymer segments with higher crystallizability will crystallize first. Thus the most branched polymer will crystallize out last. This results in the formation of different layers around the support which starts with highly crystalline polymer at the inside and less crystalline polymer when moving towards the outermost layer (see Figure 2.5) (figure shown for explanation purposes only).

2.4.1.2) Second step: elution

Polymer fractions with different crystallinity are eluted during this step. This is done by increasing the temperature at a constant rate. The less crystalline fractions will elute first because they were the last fractions to crystallize during the cooling step of the Tref process and thus formed the outside layers in Figure 2.5. A Tref profile is obtained by plotting detector response against elution temperature. The elution step is illustrated in Scheme 2.12.

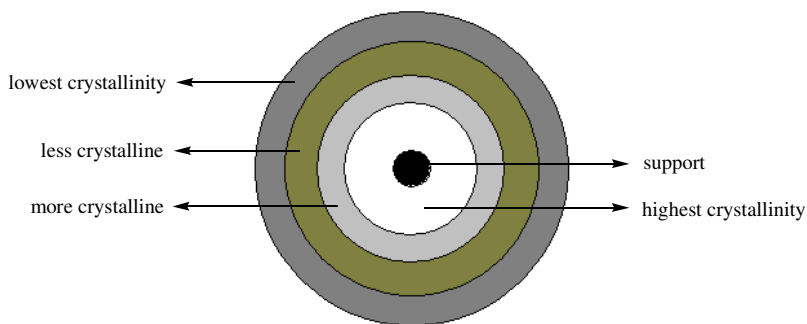
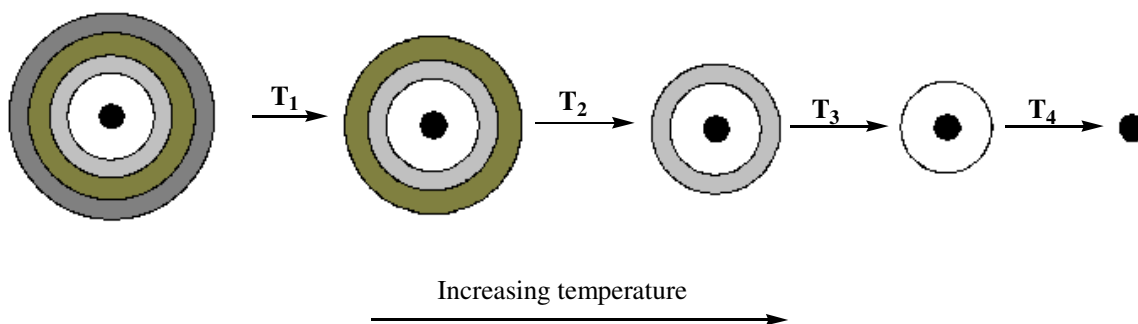


Figure 2.5: Illustration of different layers after Tref crystallization (first step).



Scheme 2.12: Illustration of Tref elution (second step).

In Figure 2.6 below the temperature profile of a typical Tref analysis is shown.

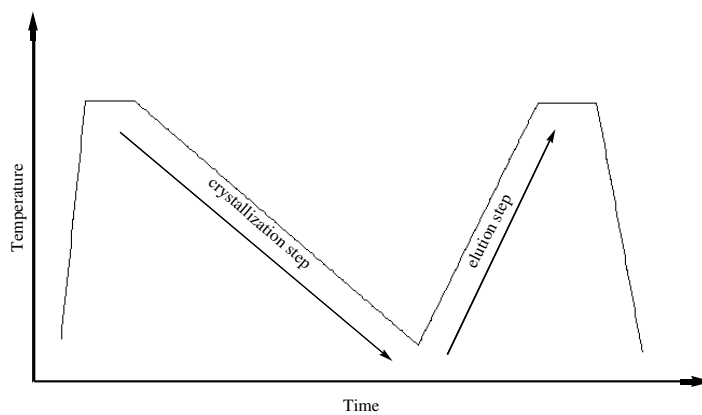


Figure 2.6: Temperature profile of crystallization and elution steps during Tref.

The Tref technique can either be run as an analytical Tref experiment or a preparative Tref experiment (p-Tref). Although the basic principles of these two experiments are very similar, the major differences are listed in Table 2.4.

Table 2.4: Comparison between preparative Tref and analytical Tref.

Analytical Tref	p-Tref
Fastest of the two experiments but not as much polymer information obtained.	Can obtained more information but also more time-consuming than analytical Tref
Smaller columns ; smaller sample size	Larger columns ; larger sample size
Continuous collection of fractions	Collection of fractions at fixed temperature intervals
Polymer information obtained on-line	Polymer information obtained off-line (additional techniques used for analysis)

It has been observed when analyzing polyethylene that the Tref curve is shifted about 10 °C to 20 °C over the newly developed Crystaf technique. This being due to the fact that operating conditions are far from thermodynamic equilibrium. The use of standards with known comonomer composition can be used to calibrate the system and solve the problem of peak shifting⁴².

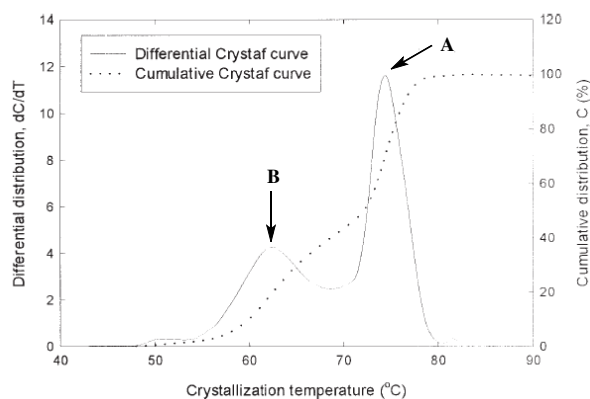
2.4.2) Crystallization analysis fractionation (Crystaf)

Due to the fact that Tref is a very tedious and slow technique, it recently encouraged the search for faster fractionation techniques. Crystallization analysis fraction (Crystaf) has become a common alternative technique to Tref for determining the distribution of chain crystallizabilities of semi-crystalline polymers^{43,44}. The technique has also become one of the most important techniques for polyolefin characterization⁴⁴. The reason for this is that Crystaf provides crucial information that is very helpful in understanding the structure-property relationship as well as the polymerization mechanism. The results obtained with Crystaf are comparable to that of Tref. The Crystaf instrumentation is easier to use, process has shorter analysis times, up to 5 polymer samples can be

analyzed concurrently and very little solvent is used during preparation and fractionation of samples. These are the main advantages over the Tref technique and it facilitates the collection of more data on the polymer structure⁴⁵. Crystaf is based on the analysis of the concentration of the polymer in solution during crystallization⁴⁶. The analysis consists of a single-step crystallization process as suppose to the two steps involved during a Tref analysis. Spectroscopic methods have often been used for determining and identifying blend components but it was found that these techniques struggle to differentiate between certain blend types (for example, homopolymer – copolymer blends or homopolymer – homopolymer blends)⁴⁷. Crystaf is currently being used to solve this problem.

2.4.2.1) Process

The polymer is dissolved in a suitable solvent and stirred in a vessel at high temperature. A high boiling point solvent is thus needed. After the polymer is completely dissolved, the temperature is decrease under controlled cooling. Polymer molecules will precipitate under the slow cooling rates according to their crystallizabilities⁴³. As more and more fractions precipitate, it lowers the concentration of the remaining polymer solution. The concentration of the solution is monitored as a function of crystallization temperature as the system is cooled down. During this process a concentration profile (cumulative curve) is generated. In order to observe the distribution of chain crystallizabilities, the first derivative of the cumulative curve is taken which represents the weight fraction of the precipitated polymer at each temperature⁴⁸. In most cases these curves are similar to those illustrated by a Tref profile. A typical Crystaf profile and is shown in Figure 2.7.



A - Higher crystalline fraction. Crystallize at higher temperatures.
B - Less crystalline fraction. Crystallize at lower temperatures.

Figure 2.7: Crystaf profile of a polyolefin blend.

The Crystaf separation process can be influenced by a number of molecular parameters⁴⁹. Some of the parameters are mentioned below:

- co-monomer type
- co-monomer content
- co-crystallization effects
- molecular weight

Another major effect that influences the analysis is the experimental conditions that are set by the operator. The paper published by Fischlschweiger et al.⁴⁹ showed that the experimental conditions, influencing the separation process, can be determined by mathematical modeling of the Crystaf technique. This is done by coupling of a mathematical model with an experimental analysis.

Due to the similar hardware shared by Tref and Crystaf, they are becoming complementary techniques in some applications. Efforts have been made to create one apparatus and combine the two techniques. The Crystaf instrument performs like an automated Tref with the addition of a pump, an injection valve and a Tref column⁴².

2.4.3) Turbidity Analysis

The usual methods used for studying kinetics of polymer crystallization do not differ a lot in their sensitivity towards growing spherulites. According to the article published by Heck et al.⁵⁰, reliable data are only obtained from crystallinity values close to the final values. They also mentioned that for growing spherulites with an end size of several micrometers, measurements will only start at a size of several hundred nanometers when using the usual techniques like differential calorimetry, dilatometry, X-ray scattering etc. This means that values obtained does not include the initial crystallization stages. An experimental method was needed with better sensitivity than conventional techniques. Heck et al.⁵⁰ found that measurements of the attenuation coefficient of light could be used. Other turbidity methods to study polymer crystallization have been applied rather long ago but only qualitative data could be obtained⁽⁵¹⁻⁵⁵⁾. Tref and Crystaf were traditionally used to study the short chain branching (SCB) of polyethylenes. Shan et. al³⁷ discovered that turbidity measurements are also capable of providing this information. They developed a turbidity fractionation analyzer (TFA) to study the crystallization and dissolution of a polymer in solution

and found that this technique had some advantages over the more usual methods. Some of the major advantages of the TFA are listed below:

- Short analysis times
- Crystallization of polymer from solution
- Dissolution of crystallized polymer into solution

Crystallization and dissolution is done in a single experiment³⁷. Following the article published by Shan et al, a similar instrument was built at the University of Stellenbosch⁵⁶.

2.4.3.1) Process

The polymer solution is placed in a quartz tube and positioned in an aluminium block. The polymer is dissolved as the temperature is increased. A diode laser beam is directed towards the tube and a photodiode detector at a 180° angle measures the intensity of this laser beam. Two more detectors are placed at 90° and 270° with respect to the tube and they detect scattered light during crystallization. As the temperature is decreased the polymer precipitates out of solution and thus lowers the intensity of the laser beam in the forward direction. Crystallization also increases the scattering detected by the two side detectors. These signals are sent to a computer system for analysis of the data. Similar to Crystaf, the first derivative of the raw data is needed for quantitative analysis. More recently three lasers are being used simultaneously to analyze crystallization and dissolution kinetics. An example of the raw data and first derivative curve from the crystallization analysis of a LDPE sample cooled at 0.5 °C/min is shown in Figure 2.8 and Figure 2.9 respectively. The solution was controlled cooled from 100 °C to 30 °C.

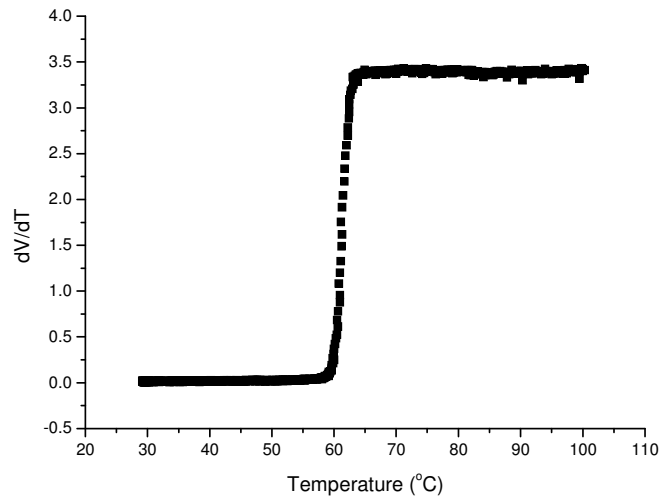


Figure 2.8: Raw data of a Scalls cooling scan.

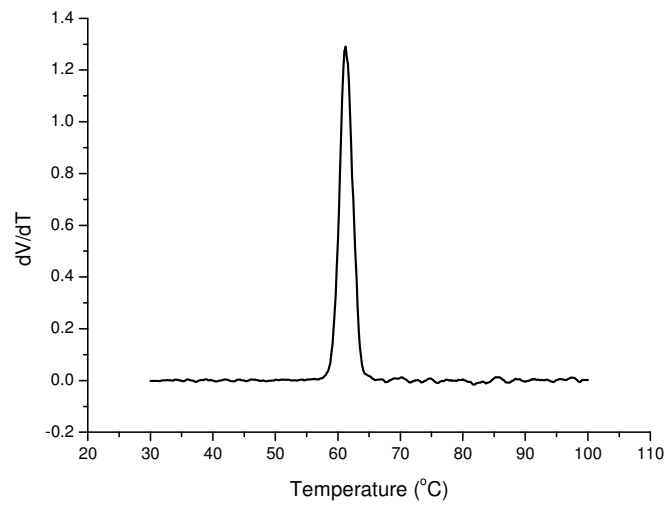


Figure 2.9: First derivative curve of raw data shown in Figure 2.8.

2.5) References

- 1) Raff, R., Lyle, E., *Historical Developments*, in *Crystalline Olefin Polymers, Part 1*, Raff, R.A.V. and Doak, K.W., Editors. 1965, John Wiley & Sons, Inc.: New York, p1-10.
- 2) Swallow, J.C., *The History of Polythene*, in *Polythene: The technology and uses of ethylene polymers*, Renfrew and Morgan, Editors. 1960, Ilffe & Sons Ltd.: London, p.1-10.
- 3) Dennis B. Malpass, *Introduction to Polymers of Ethylene*, in *Introduction to Industrial Polyethylene: Properties, Catalysts, Processes*, 2010, Scrivener Publishing LLC: United States, p.1-22.
- 4) Walter Kaminsky, *Polyolefins*, in *Handbook of Polymer Synthesis, Second Edition*, Kricheldorf, Nuyken, Swift, Editors, 2005, Marcel Dekker: New York, p.1-72.
- 5) Rossi, A., Zhang, J. & Odian, G., *Microstructure of ethylene - 1-butene copolymers produced by zirconocene/methylaluminumoxane catalysis*, *Macromolecules*, 1996, vol. 29, no. 7, pp. 2331-2338.
- 6) Czaja, K. & Bialek, M., *Microstructure of ethylene-1-hexene and ethylene-1-octene copolymers obtained over Ziegler - Natta catalysts supported on $MgCl_2(THF)_2$* , *Polymer*, 2001, vol. 42, no. 6, pp. 2289-2297.
- 7) Brydson, J.A., *Polyethylene* in *Plastics Materials, Seventh Edition*, 1999, Butterworth-Heinemann, Oxford, pp. 205-246.
- 8) MacDermott, *Chemical & Engineering News*, p.49, November 29, 1999.
- 9) Boor, Jr., J., *Ziegler-Natta Catalysts and Polymerizations*, 1979, Academic Press Inc., p.280.
- 10) Weckhuysen, B.M. & Schoonheydt, R.A., *Olefin polymerization over supported chromium oxide catalysts*, *Catalysis Today*, 1999, vol. 51, no. 2, pp. 215-221.
- 11) Weckhuysen, B.M., Wachs, I.E. & Schoonheydt, R.A., *Surface chemistry and spectroscopy of chromium in inorganic oxides*, *Chemical reviews*, 1996, vol. 96, no. 8, pp. 3327-3349.
- 12) Ruddick, V.J. & Badyal, J.P.S., *Early stages of ethylene polymerization using the Phillips $CrO_3/silica$ catalyst*, *Journal of Physical Chemistry B*, 1998, vol. 102, no. 16, pp. 2991-2994.

- 13) Groeneveld, C., Wittgen, P.P.M.M., Swinnen, H.P.M., Wernsen, A. & Schuit, G.C.A., *Hydrogenation of olefins and polymerization of ethene over chromium oxide/silica catalysts. V. In situ Infrared measurements and investigation of the polymer*, Journal of Catalysis, 1983, vol. 83, no. 2, pp. 346-361.
- 14) Jozwiak, W.K., Dalla Lana, I.G. & Fiedorow, R., *On the role of surface hydroxyls during the Cr/SiO₂-catalyzed polymerization of ethylene*, Journal of Catalysis, 1990, vol. 121, no. 1, pp. 183-195.
- 15) McGuinness, D.S., Davies, N.W., Horne, J. & Ivanov, I., *Unraveling the mechanism of polymerization with the phillips catalyst*, Organometallics, 2010, vol. 29, no. 22, pp. 6111-6116.
- 16) Cossee, P., *Ziegler-Natta catalysis I. Mechanism of polymerization of α -olefins with Ziegler-Natta catalysts*, Journal of Catalysis, 1964, vol. 3, no. 1, pp. 80-88.
- 17) Ivin, K.J., Rooney, J.J., Stewart, C.D., Green, M.L.H. & Mahtab, R., *Mechanism for the stereospecific polymerization of olefins by Ziegler-Natta catalysts*, Journal of the Chemical Society, Chemical Communications, 1978, no. 14, pp. 604-606.
- 18) Benedikt, G.M., Goodall, B.L., *Foreword*, in *Metallocene-Catalyzed Polymers: Materials, Properties, Processing & Markets*, 1998, Plastics Design Library: New York, p.v-viii.
- 19) Natta, G., Plno, P., Corradini, P., Danusso, F., Mantica, E., Mazzanti, G. & Moraglio, G., *Crystalline high polymers of α -olefins*, Journal of the American Chemical Society, 1955, vol. 77, no. 6, pp. 1708-1710.
- 20) Dennis B. Malpass, *Ziegler-Natta Catalysts*, in *Introduction to Industrial Polyethylene: Properties, Catalysts, Processes*, 2010, Scrivener Publishing LLC: United States, p.33-40.
- 21) Boor Jr., J., *Review of recent literature on Ziegler-type catalysts*, Industrial and Engineering Chemistry Product Research and Development, 1970, vol. 9, no. 4, pp. 437-456.
- 22) Petitjean, L., Pattou, D. & Ruiz-López, M.F., *Theoretical study of hydrogenolysis termination processes in ethylene polymerization*, Tetrahedron, 2001, vol. 57, no. 14, pp. 2769-2774.

- 23) Collman, J.P., *Principles and Applications of Organo transition metal Chemistry*, 1987, Mill Valley: California.
- 24) Breslow, D.S. & Newburg, N.R., *Bis-(cyclopentadienyl)-titanium dichloride alkylaluminum complexes as catalysts for the polymerization of ethylene*, *Journal of the American Chemical Society*, 1957, vol. 79, no. 18, pp. 5072-5073.
- 25) Ewen, J.A., *Mechanisms of stereochemical control in propylene polymerizations with soluble group 4B metallocene/methylalumoxane catalysts*, *Journal of the American Chemical Society*, 1984, vol. 106, no. 21, pp. 6355-6364.
- 26) Ewen, J.A., Jones, R.L., Razavi, A. & Ferrara, J.D., *Syndiospecific propylene polymerizations with group 4 metallocenes*, *Journal of the American Chemical Society*, 1988, vol. 110, no. 18, pp. 6255-6256.
- 27) Kaminsky, W., *New polymers by metallocene catalysis*, *Macromolecular Chemistry and Physics*, 1996, vol. 197, no. 12, pp. 3907-3945.
- 28) Tritto, I., Donetti, R., Sacchi, M.C., Locatelli, P. & Zannoni, G., *Dimethylzirconocene-methylaluminoxane catalyst for olefin polymerization: NMR study of reaction equilibria*, *Macromolecules*, 1997, vol. 30, no. 5, pp. 1247-1252.
- 29) Bouhadir, G., Amgoune, A. & Bourissou, D., *Phosphine-Boranes and Related Ambiphilic Compounds. Synthesis, Structure, and Coordination to Transition Metals*. *Advances in Organometallic Chemistry*, 2010, vol. 58, pp. 1-107.
- 30) Kaminsky, W., Piel, C. & Scharlach, K., *Polymerization of ethene and longer chained olefins by metallocene catalysis*, *Macromolecular Symposia*, 2005, vol. 226, pp. 25-34.
- 31) Dennis B. Malpass, *Single Site Catalysts*, in *Introduction to Industrial Polyethylene: Properties, Catalysts, Processes*, 2010, Scrivener Publishing LLC: United States, p.71-84.
- 32) Kaminsky, W., *Zirconocene catalysts for olefin polymerization*, *Catalysis Today*, 1994, vol. 20, no. 2, pp. 257-271.
- 33) Miller, R.L., *Crystalline and Spherulitic Properties*, in *Crystalline Olefin Polymers, Part 1*, Raff, R.A.V. and Doak, K.W., Editors. 1965, John Wiley & Sons, Inc.: New York, p.577-676.
- 34) Mandelkern, *Morphology*, in *Crystallization of Polymers*, 1964, McGraw-Hill: United States, p.291-337 (328).

- 35) Baer, E., *Engineering Design for Plastics; Polymer Science and Engineering Series*; ed. E. Baer; 1964, Van Nostrand Reinhold Company.
- 36) Bunn, C.W., *The Structure of Polythene*, in *Polythene: The technology and uses of ethylene polymers*, Renfrew and Morgan, Editors. 1960, Ilffe & Sons Ltd.: London, p.87-130.
- 37) Shan, C.L.P., Degroot, W.A., Hazlitt, L.G. & Gillespie, D., *A new turbidimetric approach to measuring polyethylene short chain branching distributions*, *Polymer*, 2005, vol. 46, no. 25, pp. 11755-11767.
- 38) Anantawaraskul, S., Soares, J.B.P. & Wood-Adams, P.M., *Fractionation of semi-crystalline polymers by crystallization analysis fractionation and temperature rising elution fractionation*, *Advanced Polymer Science*, 2005 vol 182, pp 1–54.
- 39) Wild, L. & Ryle, T. 1977, "Crystallizability distributions in polymers: A new analytical technique", American Chemical Society, *Polymer Preprints, Division of Polymer Chemistry*, vol. 18, no. 2, pp. 182-187.
- 40) Wild, L. *Advanced Polymer Science*, 1990, 98, 1-47.
- 41) Soares, J.B.P. & Hamielec, A.E., *Temperature rising elution fractionation of linear polyolefins*, *Polymer*, 1995, vol. 36, no. 8, pp. 1639-1654.
- 42) Monrabal, B., *Microstructure characterization of polyolefins. TREF and CRYSTAF*, in *Progress in Olefin Polymerization Catalysts and Polyolefin Materials*, Shiono, Nomura and Terano, Editors. 2006, pp. 35-42.
- 43) Anantawaraskul, S., Soares, J.B.P. & Wood-Adams, P.M., *An experimental and numerical study on crystallization analysis fractionation (Crystaf)*, *Macromolecular Symposia*, 2004, vol. 206, no. 1, pp. 57-68.
- 44) Soares, J.B.P. & Anantawaraskul, S., *Crystallization analysis fractionation*, *Journal of Polymer Science, Part B: Polymer Physics*, 2005, vol. 43, no. 13, pp. 1557-1570.
- 45) Britto, L.J.D., Soares, J.B.P., Penlidis, A. & Monrabal, B., *Polyolefin Analysis by Single-Step Crystallization Fractionation*, *Journal of Polymer Science, Part B: Polymer Physics*, 1999, vol. 37, no. 6, pp. 539-552.
- 46) Brüll, R., Pasch, H., Raubenheimer, H.G., Sanderson, R., Van Reenen, A.J. & Wahner, U.M., *Investigation of the melting and crystallization behavior of random propene/ α -olefin copolymers by DSC and CRYSTAF*, *Macromolecular Chemistry and Physics*, 2001, vol. 202, no. 8, pp. 1281-1288.

- 47) Pasch, H., Brüll, R., Wahner, U. & Monrabal, B., *Analysis of polyolefin blends by crystallization analysis fractionation*, Macromolecular Materials and Engineering, 2000, vol. 279, pp. 46-51.
- 48) Beigzadeh, D., Soares, J.B.P. & Duever, T.A., *Modeling of fractionation in CRYSTAF using Monte Carlo simulation of crystallizable sequence lengths: Ethylene/1-octene copolymers synthesized with single-site-type catalysts*, Journal of Applied Polymer Science, 2001, vol. 80, no. 12, pp. 2200-2206.
- 49) Fischlschweiger, M., Aust, N., Oberaigner, E.R. & Kock, C., *Mathematical modeling and optimization of run parameters of crystallization analysis fractionation (CRYSTAF)*, Macromolecular Chemistry and Physics, 2010, vol. 211, no. 4, pp. 383-392.
- 50) Heck, B., Kawai, T. & Strobl, G., *Time dependent light attenuation measurements used in studies of the kinetics of polymer crystallization*, Polymer, 2006, vol. 47, no. 15, pp. 5538-5543.
- 51) Hawkins, S.W. & Richards, R.B., *Light transmission and the formation and decay of spherulites in polythene*, Journal of Polymer Science, 1949, vol. 4, no. 4, pp. 515-522.
- 52) Keane, J.J. & Stein, R.S., *The scattering of light from thin polymer films. II. Scattering from polyethylene*, Journal of Polymer Science, 1956, vol. 20, no. 95, pp. 327-350.
- 53) Levy, B., *The development of crystallinity and transparency in irradiated polyethylene*, Journal of Applied Polymer Science, 1961, vol. 5, no. 16, pp. 408-423.
- 54) Mayhan, K.G., James, W.J. & Bosch, W., *Poly(ethylene terephthalate). I. Study of crystallization kinetics*, Journal of Applied Polymer Science, 1965 vol. 9, no. 11, pp. 3605-3616.
- 55) Stejskal, J., Horska, J. & Kratochvil, P., *Light scattering from polyethylene solutions*, Journal of Applied Polymer Science, 1982, vol. 27, no. 10, pp. 3929-3944.
- 56) Van Reenen, A.J., Rohwer, E.G., Walters, P., Lutz, M. & Brand, M., *Development and use of a turbidity analyzer for studying the solution crystallization of polyolefins*, Journal of Applied Polymer Science, 2008, vol. 109, no. 5, pp. 3238-3243.

Chapter 3

Experimental

This chapter focuses on the materials studied and experimental techniques used for analysis during this study.

3.1) Materials

3.1.1) Polymers

The types of polymers used in this study were linear low density polyethylene (LLDPE), low density polyethylene (LDPE), polypropylene (PP) and a polypropylene impact copolymer (PPIC).

Two different type of LLDPE were used. An ethylene-1-octene copolymer was obtained from Exxon Mobil (Exact 8201, MFI 1.1 g/min, density 0.882 g/cm³). Two ethylene-1-hexene copolymers made by different catalysts in specific trial was donated by Sasol Polymers (MFI = 2 g/10 min). Sasol Polymer also donated the LDPE used in the study. (see Table 3.1 for more details)

The PP was a Moplen[®] sample (98% isotactic, see also Table 3.1), while the PPIC (Sasol Polymers, Grade CMR 648) had an MFI of 8.5 g/10 min and a density of 0.904 g/cm³. The PPIC had an ethylene content of 12 wt%. Molecular weight data of the polymers used during this study are given in Table 3.1.

Table 3.1: Molecular weight data of polymers used during this study.

Polymer	M _n (g/mol)	M _w (g/mol)	PDI (M _w /M _n)
PE-1-octene	72 611	218 646	3.0
PE-1-hexene (sample 1)	28 645	208 924	7.3
PE-1-hexene (sample 2)	43 535	199 446	4.6
LDPE	20 411	141 410	6.9
PP	56 871	601 649	10.5
PPIC	45 011	266 098	5.9

3.1.2) Solvents

In the Tref experiments and preparation of polymer blends, xylene (Sigma-Aldrich, 99% purity) was used as solvent as received. During Scalls, Crystaf and HT-GPC experiments, TCB (1,2,4-trichlorobenzene) was used. The TCB was distilled and filtered twice (0.45 μm and 0.22 μm filters). Deuterated 1,1,2,2-Trichloroethane (TCE- d_2 , Sigma-Aldrich) was used as solvent for NMR analysis.

3.1.3) Stabilizers

During the blending of the polymers as well as in the Tref procedure, a mixture of Irgafos 168 [tris(2,4-di-tert-butylphenyl)phosphite] and Irganox 1010 was used to prevent degradation of the polymer during the heating process. The structures of these compounds are shown in Figure 3.1 and Figure 3.2.

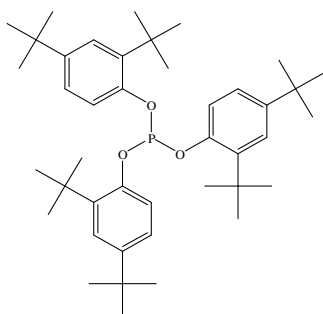


Figure 3.1: Structure of Irgafos 168

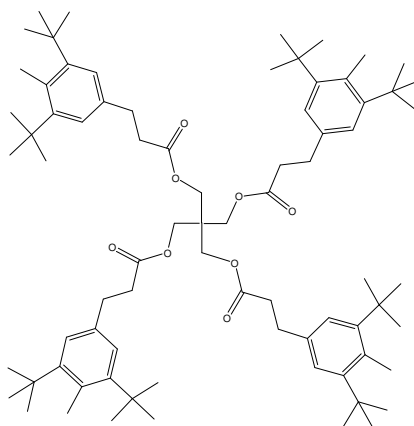


Figure 3.2: Structure of Irganox 1010

3.2) Preparation of polymer blends

Binary polymer blends were prepared. For Scalls analysis the sample weight was kept constant at 80 mg. The amount of each polymer component in the blend varied depending on the specific composition ratio to be analyzed. For example, an 80:20 LDPE:PP blend contained 80 wt% (64 mg) LDPE and 20 wt% (16 mg) PP. This method of blending was decided on, to be exactly sure of the composition ratio and the amount of each individual component in the analyzed sample.

3.3) Differential scanning calorimetry (DSC)

Crystallization and melting studies were done by differential scanning calorimetry (DSC). The instrument used was a TA Instruments Q100 calorimeter calibrated with an indium metal standard according to standard procedures. Cooling and heating rates were fixed at 10 °C/min. All samples were subjected to three cycles. The first comprised of heating the samples up to 190 °C for the LLDPE samples and 220 °C in the case of the PP homopolymers and ethylene-propylene rubber samples. This step was to remove all the thermal history. Samples were kept isothermally at these temperatures for 5 minutes and then cooled down to -40 °C to obtain the crystallization data. After cooling the second heating followed which was used for data analysis.

3.4) High temperature gel permeation chromatography (HT-GPC)

Molecular weight determination was done by high temperature gel permeation chromatography. A PL-GPC 220 high-temperature chromatogram system (Polymer Laboratories, Varian Inc., Amherst, MA) was used. The system was equipped with three PL gel columns and a differential refractive index detector. 1,2,4-Trichlorobenzene (TCB, distilled and filtered twice) was used as eluent at a flow rate of 1 ml/min with 0.0125% butylhydroxytoluene (BHT) as stabilizer. BHT was also used as a flow-rate marker. Samples were dissolved at 160 °C in TCB at concentration of 0.65 – 0.85 mg/ml and 200 µl of each sample were injected. Narrowly dispersed polystyrene standards (EasiCal, Polymer Laboratories) were used for calibration purposes.

3.5) Nuclear magnetic resonance spectroscopy (NMR)

Comonomer content of the LLDPE samples was determined by ¹³C-NMR spectroscopy. The analysis was done on a 600 Varian Unity Inova NMR spectrometer equipped with an Oxford

magnet operating at 600 MHz and also having a 5 mm inverse detection pulsed field gradient probe. Spectra were recorded at 120 °C. Samples were prepared by dissolving 60 mg of polymer with deuterated 1,1,2,2-tetrachloroethane (TCE-d₂) in a NMR tube. TCE-d₂ was used as internal reference at 74.5 ppm.

3.6) Temperature rising elution fractionation (Tref)

Polymer fractions were obtained through a preparative temperature rising elution fractionation (p-Tref) technique. The major differences between p-Tref and analytical Tref were pointed out in Chapter 2. Our instrumental system was built in-house. Polymers were dissolved in 3g quantities in xylene at 135 °C with addition of 2 wt% stabilizer (mixture of Irganox1010 and Irgafos168) to prevent degradation. After the polymer was fully dissolved, pre-heated silica sand (-50 to +70 mesh particle size, Sigma Aldrich) was added to the solution up to the point where the sand completely covered the solution.

3.6.1) Crystallization step

The reactor was placed into an oil-bath which was pre-heated at 130 °C and kept isothermally at this temperature for 2 hours. The crystallization process occurred on the silica sand support at a cooling rate of 1 °C/hour from 130 °C to 25 °C. Polymers formed several layers around the sand particles due to the difference in crystallizability of the polymer chains. Layers formed outwards in decreasing crystallizability.

3.6.2) Elution step

The crystallized polymer was transferred to a steel column and placed into a modified GC-oven¹. Fractions were collected through solvent elution by pumping heated xylene through the column while the temperature was increased to 120 °C in a controlled fashion. The solvent flow-rate was 40 ml/min and a FMI “Q” Model QG150 pump was used.

The eluted fractions were transferred to a round-bottom flask and the solvent was removed on a rotary evaporator. Samples were then placed in a vacuum oven to remove any residual solvent. An illustration of the Tref column is shown below in Figure 3.3.

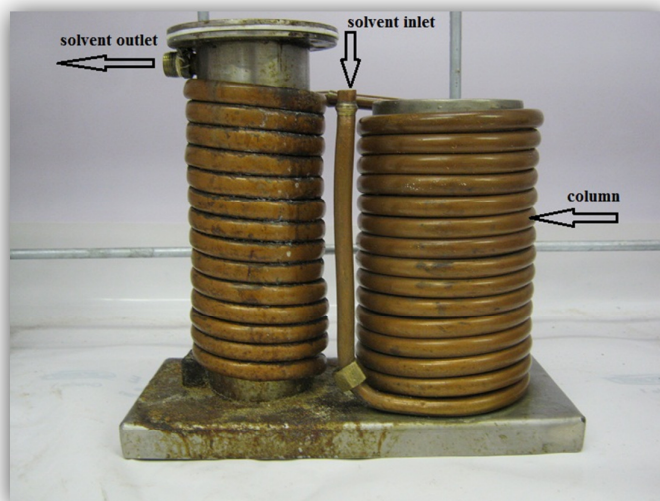


Figure 3.3: Tref column used in this study.

3.7) Crystallization analysis fractionation (Crystaf)

Solution crystallization studies were also performed by Crystaf for comparison with the Scalls results. The apparatus used was a model 200, manufactured by Polymer Char S.A. (Valencia, Spain). Samples of 20 mg were dissolved in 35 ml of 1,2,4-trichlorobenzene (TCB) in five vessels simultaneously (see Figure 3.4) at 160 °C and stabilized at this temperature for 1 hour. The solutions were cooled down to 30 °C at a rate of 0.1 °C/min to allow for sufficient crystallization to occur. During crystallization the polymer solution concentration was measured as a function of crystallization temperature.

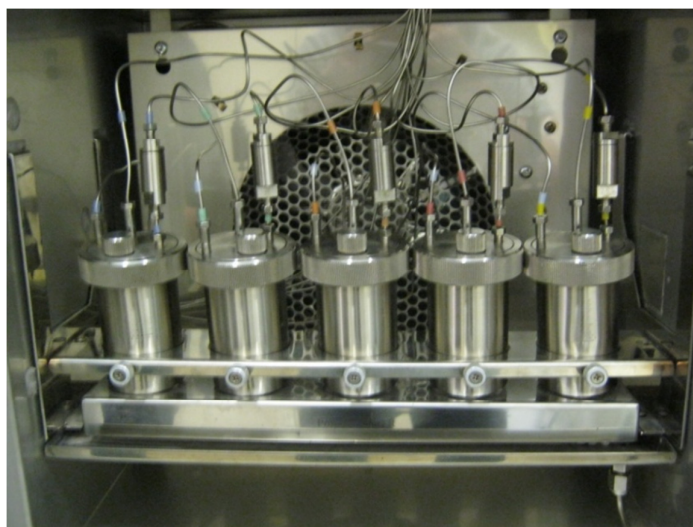


Figure 3.4: Reactor vessels inside Crystaf oven.

3.8) Solution crystallization analysis by laser light scattering (Scalls)

The instrumentation for this technique was built in-house and is based on the design of Shan et al². During Scalls analysis the polymer solution was placed in a quartz tube and positioned in an aluminium block mounted onto a magnetic heater stirrer. Three diode lasers; red, green and blue with wavelengths of 635 nm, 532 nm and 405 nm respectively were directed towards the polymer solution through an opening in the aluminium block. Photodiode detectors at an 180° angle measured the change in intensity of the laser beams during cooling and heating cycles. Filters were placed in front of the detectors to only allow light of certain wavelengths to the specific detector. Two detectors at 90° and 270° measure the scattered light during crystallization. Controlled cooling is obtained by the flow of water through channels in the aluminium block and a temperature controller is used to regulate temperature. Typical solutions for Scalls were prepared by dissolving 40 mg of polymer in 20 ml of 1,2,4-trichlorobezene (TCB). The solution was transferred to a quartz tube, placed into the aluminium block and heated up to 130 °C to allow for the entire polymer to dissolve. At controlled cooling rates the solutions were cooled down from 100 °C to room temperature. Cooling rates were varied between 0.2 °C/min and 1 °C/min. Heating rates for solution melting were varied between 1 °C/min and 1.5 °C/min. Figures 3.5 – 3.7 illustrate the Scalls setup.

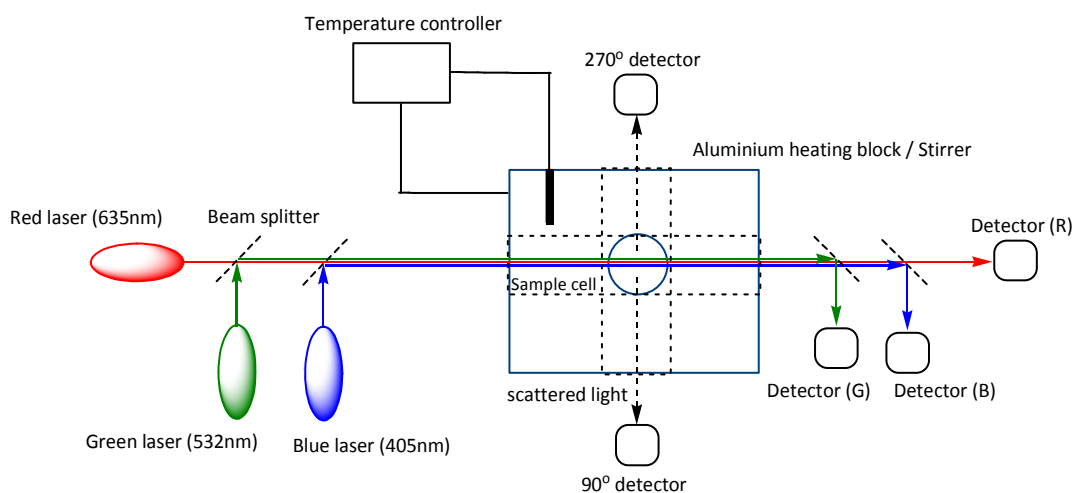


Figure 3.5: Schematic diagram of Scalls setup (viewed from the top).

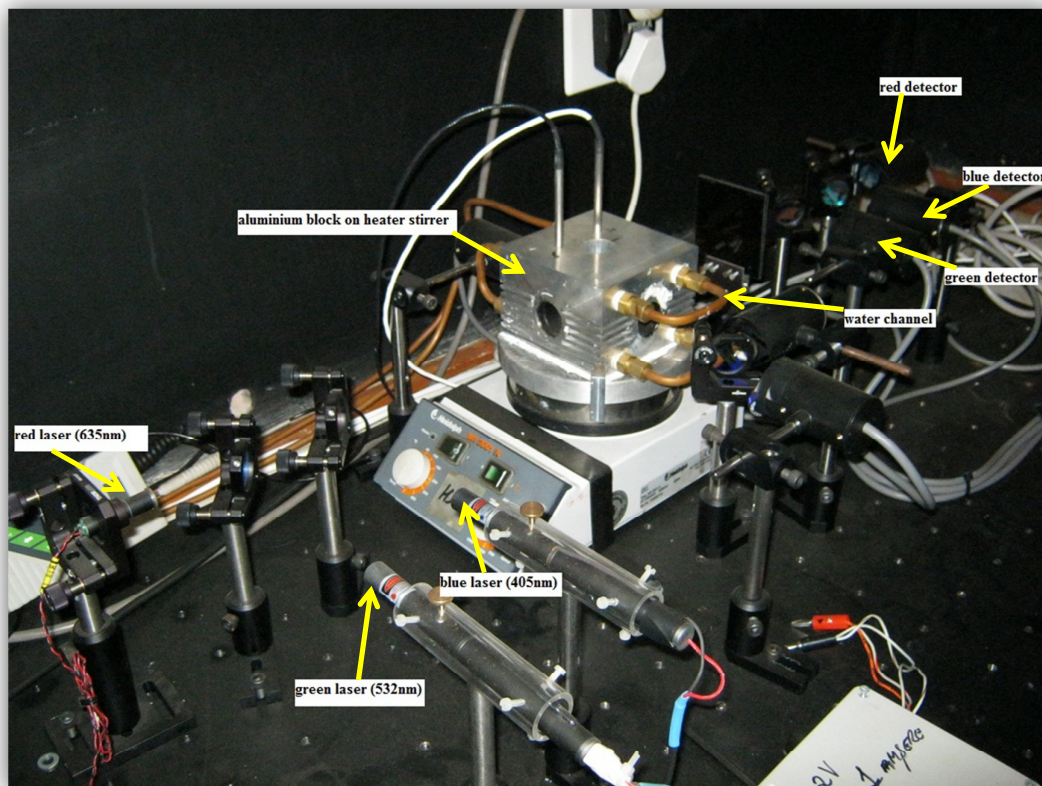


Figure 3.6: Experimental setup of Scalls instrumentation.

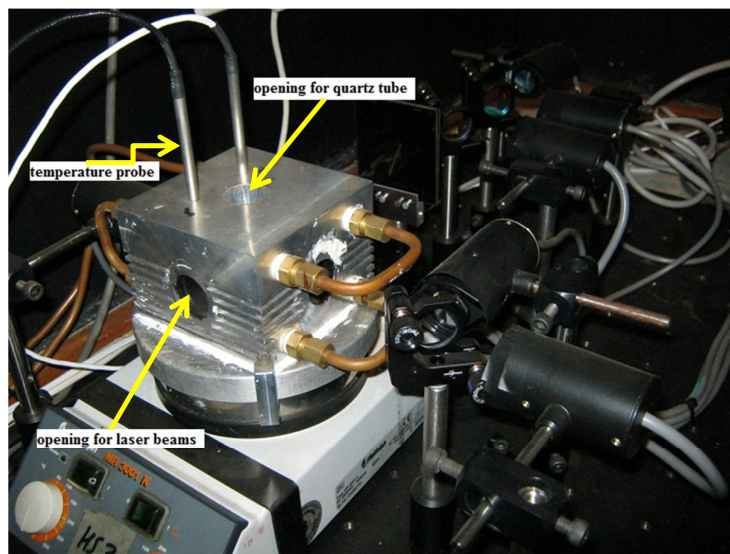


Figure 3.7: Aluminium block mounted on heater stirrer.

3.9) Particle size analysis

Particle size measurements were done using a Zetasizer Nano series particle analyzer. These measurements are performed through Dynamic light scattering (DLS) which measures Brownian motion and correlates the motions to the size of the polymer particles. Analyses were done straight after the cooling cycle from Scalls. The measurements were done at 30 °C. From one run, different distributions were obtained namely the intensity, volume and number distributions.

3.10) References

- 1) Rabie, A.J., *Blends with low-density polyethylene (LDPE) and plastomers*, MSc thesis, University of Stellenbosch, 2004.
- 2) Shan, C.L.P., Degroot, W.A., Hazlitt, L.G. & Gillespie, D., *A new turbidimetric approach to measuring polyethylene short chain branching distributions*, *Polymer*, 2005, vol. 46, no. 25, pp. 11755-11767.

Chapter 4

Results and Discussion

This chapter focuses on the results obtained from the solution crystallization of LLDPE homopolymers, polymer blends and fractionated polymers.

4.1) Introduction

As mentioned previously the technique used in this study is based on the design published by Shan et. al¹. The original design has been adapted and development of the instrumentation has been done².

4.2) Analysis of LLDPE samples

4.2.1) Crystallization analysis

The first part of the study comprised of the crystallization and solution melting analyses of different LLDPE copolymers. These LLDPE's differed in comonomer and catalysts used during preparation. The first aim was to see if we could differentiate between chemically similar but morphologically different polymers, in this case the LLDPE's. A second aim of this part of the study was to see responses of the different lasers (blue – 405 nm, green – 532 nm, red – 635 nm) and what information regarding the crystallization and melting events could be obtained from Scalls. The polymers used were two commercial LLDPE polymers; a heterogeneous Ziegler-catalyzed PE-1-hexene copolymer and a homogeneous metallocene-catalyzed PE-1-octene copolymer. (Data in Table 4.1). Figure 4.1 - 4.3 illustrate the crystallization data of these two polymers at different cooling rates. The three different colored peaks represent the signals of the corresponding three laser signals Peaks were normalized for ease of comparison of the different laser signals.

Table 4.1: Characterization data of LLDPE samples used

Polymer	Comonomer (mole%)	^a M _n (g/mol)	^b M _w (g/mol)	PDI (M _w / M _n)	^c T _m (°C)
PE-1-hexene	2	28 645	208 924	7.3	125.6
PE-1-octene	5	72 611	218 646	3.0	73.4

^aDetermined by ¹³C-NMR; ^anumber-average molecular weight; ^bweight-average molecular weight; ^cDSC melting temperature

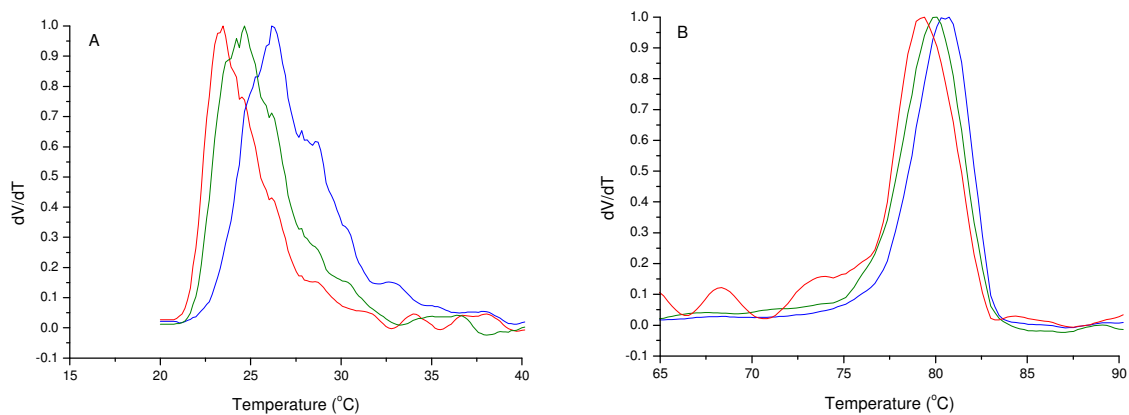


Figure 4.1: Comparison of crystallization data for (A) PE-1-octene and (B) PE-1-hexene at identical conditions (1 °C/min, 2 mg/ml). [Normalized curves]

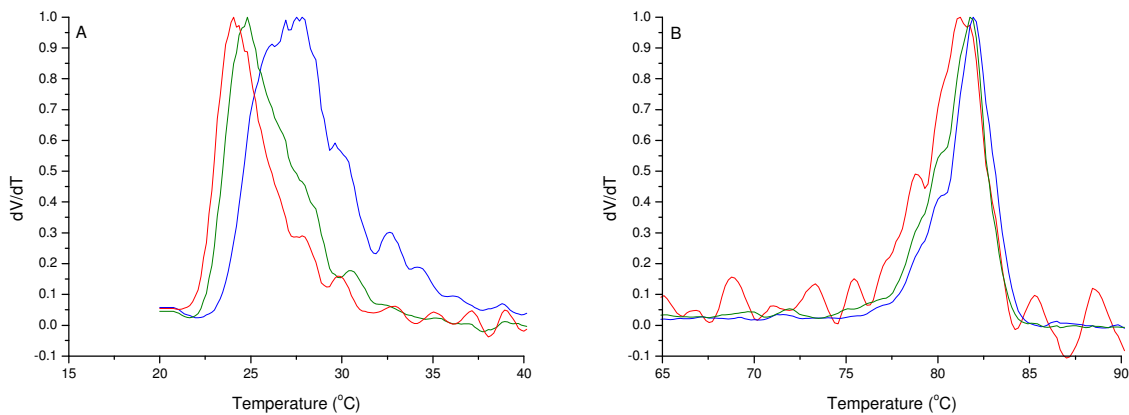


Figure 4.2: Comparison of crystallization data for (A) PE-1-octene and (B) PE-1-hexene at identical conditions (0.5 °C/min, 2 mg/ml). [Normalized curves]

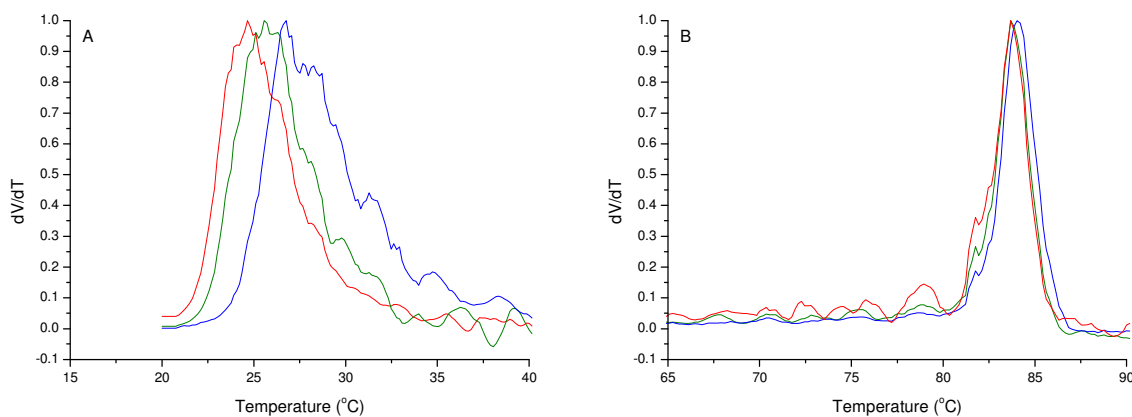


Figure 4.3: Comparison of crystallization data for (A) PE-1-octene and (B) PE-1-hexene at identical conditions (0.2 °C/min, 2 mg/ml). [Normalized curves]

A number of things are apparent from Figures 4.1 – 4.3. The range of crystallization of the 1-octene LLDPE and the 1-hexene LLDPE is significantly different (as would be expected) and the crystallization curves are different in shape and complexity as well. From the first derivative curves shown in Figure 4.1 – 4.3 it is difficult to see the broad temperature range needed for complete crystallization of the PE-1-hexene sample as the temperature scale shows no events below 65°C. This aspect will be explored in more detail later, when we looked at the crystallization kinetics using the raw data of the different laser responses. It is evident from all the crystallization results that the blue laser was the first to show a response, followed by the green and then the red laser. This is due to the differences in wavelengths of the three lasers. The blue laser picked up the occurrence of crystallization events earlier than the other two lasers. As the polymer crystals got larger in size, they started to scatter the higher wavelength laser beams. This implies that it is indeed possible to get information on the way the polymer crystals form from solution during cooling.

The cooling rate appears to have very little effect on the octene copolymer with a clear distinction remaining between the peaks associated with the different lasers. However when looked at the hexene copolymer, the signals of all the lasers clearly shifted towards higher temperatures as the cooling rate was decreased. Apart from the slight overall peak shifts towards higher temperatures when cooling down at a lower rate, another interesting result was observed when looking at the peak signals of the different lasers. A decrease in cooling rate caused the peaks of the three lasers to shift closer together. This effect was also detected when looked at the differences in peak temperatures of the blue laser which scattered first and the red laser which scattered last. Due to the broad temperature range over which the hexene copolymer crystallized, the peak temperature of the major peak was taken for comparison purposes. The difference in temperatures are shown in Table 4.2 and illustrated by ΔT_{BR} . Both polymers showed a shift of 0.3 °C as the cooling rate was changed from 0.5 °C/min to 0.2 °C/min. At a cooling rate of 1 °C/min, the octene copolymer showed a smaller ΔT_{BR} value than for the lower rates. This might have been due to some structural features in the polymer system. Overall the laser signal shifts provided important information on the crystallization kinetics and crystal growth of the polymers and indicated that at a lower cooling rate the crystal growth was more uniform. The octene copolymer crystallized over a smaller temperature range but the crystallization peaks were slightly less smooth at all cooling rates. These factors may directly be correlated to the difference in morphology of the two polymer structures.

Table 4.2: Data of crystallization peak temperatures

Laser signals	Cooling rate (°C/min)	Crystallization peak temperatures (°C)		ΔT_{BR}^a (°C)	
		PE-1-octene	PE-1-hexene	PE-1-octene	PE-1-hexene
Blue	0.2	27.7	84.0	3.1	0.3
Green		25.6	83.7		
red		24.6	83.7		
blue	0.5	27.5	81.9	3.5	0.6
green		24.8	81.7		
red		24.0	81.3		
blue	1	26.2	80.5	2.7	1.3
green		24.6	79.9		
red		23.5	79.2		

^aThe difference in peak temperature between blue and red laser signals.

The values of ΔT_{BR} , which basically gives a rough measurement of the rate at which crystallization occurs, appears to indicate that the 1-hexene copolymer crystallizes far more rapidly than the more homogeneous 1-octene LLDPE. This is at first glance rather puzzling, as one would expect the heterogeneous copolymer to crystallize over a broader temperature range. The duration of the crystallization event is somewhat difficult to calculate using the first derivative. See for example Figure 4.2b, where it is quite clear that smaller crystallization events occur at temperatures well below the major crystallization event.

The raw voltage data were used for these calculations as it gave a better indication of the onset and completion of crystallization. Figure 4.4 and Figure 4.5 presents the raw data of the two polymers at a cooling rate of 1 °C/min for the 405 nm signal. Anantawaraskul et. al³. mentioned that the onset of crystallization should be equal to the dissolution temperature at slow cooling rates. So, in order to establish a fixed point for the onset of crystallization, the dissolution peak temperature for the blue laser was taken as onset point. The completion of crystallization was taken at the end of the red laser signal as this laser was the last laser to scatter. If only one laser was to be used certain

crystallization events would not have been picked up and the duration of crystallization would appear less. This definitely points out an advantage of using lasers of different wavelengths over using only one laser. The calculations for the completion of crystallization were split into two sections namely stage 1 and stage 2. A clear illustration of the division of the two stages can be seen in Figure 4.6 and Figure 4.7. Stage 1 consisted of the crystallization times calculated from the crystallization onset until the peak maxima of the major crystallization peaks shown in Figure 4.1 – 4.3. The end of stage 1 thus corresponds to the laser signal at half height in the raw voltage curves. The onset of crystallization for the octene and hexene samples was at 43.3 °C and 92.5 °C respectively. Stage 2 had to do with the crystallization times from where stage 1 ended until the completion of crystallization. The crystallization process for the hexene sample was not completed within the temperature range used so the calculations were done until 30 °C. Equation 1 illustrates how the duration of crystallization was calculated and the subsequent values are given in Table 4.3 - 4.4.

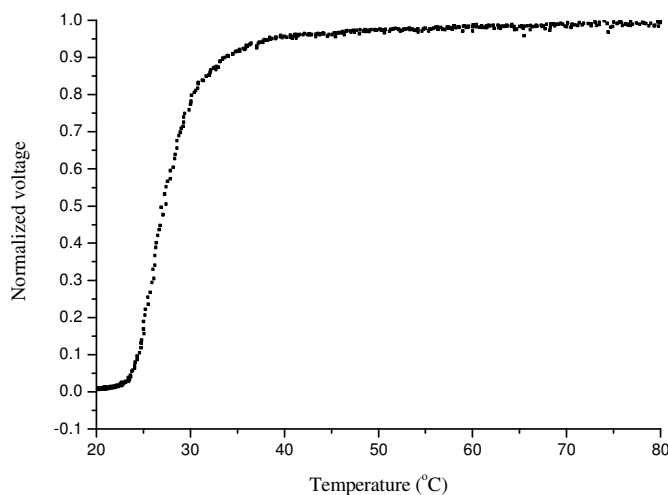


Figure 4.4: Normalized raw voltage curves for PE-1-octene cooled at 1 °C/min.

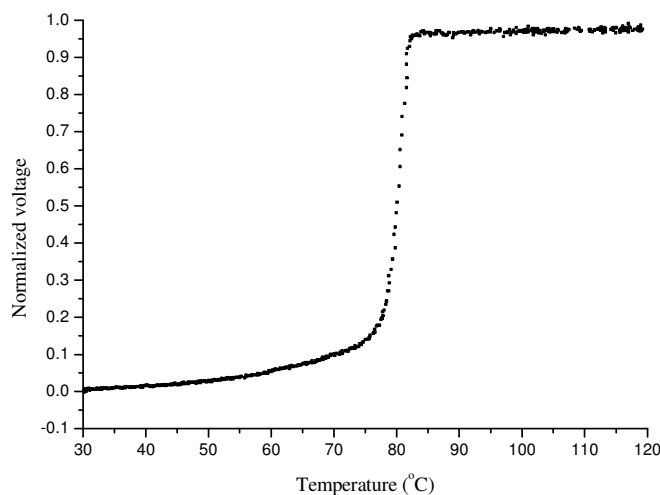


Figure 4.5: Normalized raw voltage curve for PE-1-hexene cooled at 1 °C/min.

$$\text{Duration of crystallization} = \frac{T_o - T_f}{\text{cooling rate}} \quad (1)$$

T_o = onset temperature at start of blue laser signal (°C)

T_f = final temperature at end of red laser signal (°C)

For the ease of comparing the crystallization times, a relative time for complete crystallization is also given. This was calculated by dividing all values by the highest value for the duration of crystallization (normalization of the duration of crystallization). The entry with the longest crystallization event at each cooling rate was taken as unity to get a better indication of the difference in duration of these events. These values are presented as the normalized crystallization times.

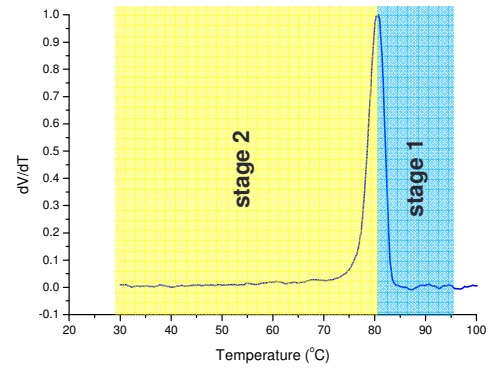
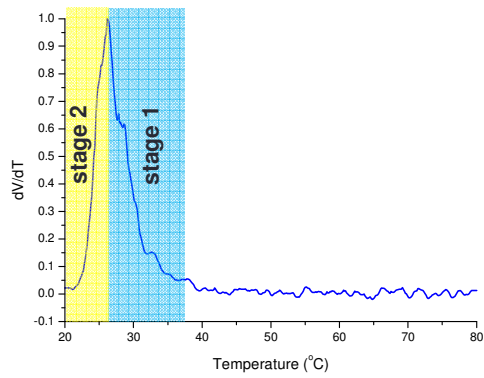
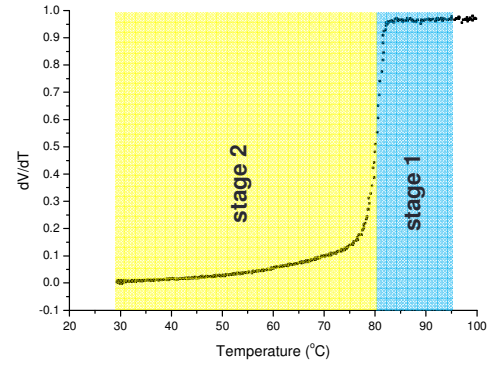
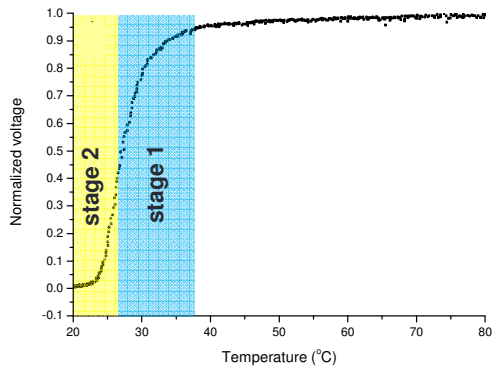


Figure 4.6: Crystallization stages for PE-1-octene.

Figure 4.7: Crystallization stages for PE-1-hexene.

Table 4.3: Duration of crystallization at different cooling rates for Stage 1

Polymer	T_{f1} (°C)	$T_o - T_{f1}$ (°C)	Duration of crystallization (min)	Relative duration of crystallization value
Cooling rate: 0.2 °C/min				
PE-1-octene	24.7	18.6	93	1
PE-1-hexene	83.6	8.9	44.5	0.48
Cooling rate: 0.5°C/min				
PE-1-octene	24.0	19.3	38.6	1
PE-1-hexene	81.2	22.6	22.6	0.56
Cooling rate: 1°C/min				
PE-1-octene	23.5	19.8	19.8	1
PE-1-hexene	79.4	13.1	13.1	0.66

T_o (octene) = 43.3 °C; T_o (hexene) = 92.5 °C; T_{f1} = temperature at end of stage 1

Table 4.4: Duration of crystallization at different cooling rates for Stage 2

Polymer	T_{f2} (°C)	$T_p - T_{f2}$ (°C)	Duration of crystallization (min)	Relative duration of crystallization value
Cooling rate: 0.2 °C/min				
PE-1-octene	22.5	2.2	11	0.04
PE-1-hexene	30	53.6	268	1
Cooling rate: 0.5°C/min				
PE-1-octene	22.8	1.2	2.4	0.02
PE-1-hexene	30	51.2	102.4	1
Cooling rate: 1°C/min				
PE-1-octene	22.1	1.4	1.4	0.03
PE-1-hexene	30	49.4	49.4	1

T_p = temperature at start of stage 2 = T_{f1} in stage 1

T_{f2} = temperature at end of stage 2

From the values given in Table 4.3 and Table 4.4 it can be seen that not only the peak temperatures are influenced by the change in cooling rate as shown in Table 4.2, but also the time needed for completion of crystallization are affected. It was found that crystallization occurs over a longer time period as the cooling rate was decreased. This data support the results from Figure 4.1 – 4.2 and Table 4.3 – 4.4. The increase in duration of crystallization correlates to the broadening of peaks as the cooling rates was decreased. During stage 1 the octene sample resulted in the highest crystallization time values. Figure 4.4 compliments these values where the octene copolymer resulted in a gradual decrease in laser intensity. A more rapid decrease in laser intensity was noticed during analysis of the hexene sample. Cooling down at 1 °C/min resulted in fairly similar crystallization times for the two polymers during stage 1. The higher values for the hexene sample during stage 2 are due to the higher heterogeneity of this sample as seen by the extensive tailing in the decrease of laser intensity shown in Figure 4.5. Solution crystallization analysis was also done by Crystaf to compare the results of the two techniques. No crystallization peaks could be seen in Crystaf for the PE-1-octene sample when cooled down to 30 °C at 0.1 °C/min. Figure 4.8 and Figure 4.9 compares the Crystaf and Scalls raw data as well as first derivative cooling profiles for the PE-1-hexene sample at cooling rates of 0.1 °C/min and 0.2 °C/min respectively. Due to the difference in cooling rates, the Crystaf peaks are slightly shifted to higher temperature. Overall the two techniques provide similar results and the heterogeneous nature of the polymer sample is clearly visible from both profiles.

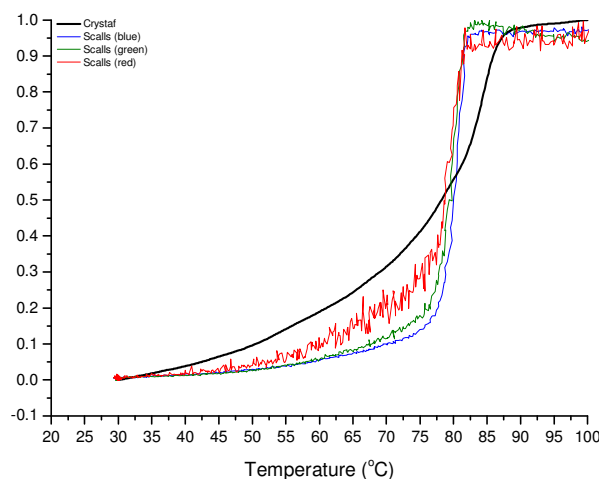


Figure 4.8: Raw voltage cooling profiles for Crystaf (0.1 °C/min) and Scalls (0.2 °C/min) for PE-1-hexene. [Normalized curves]

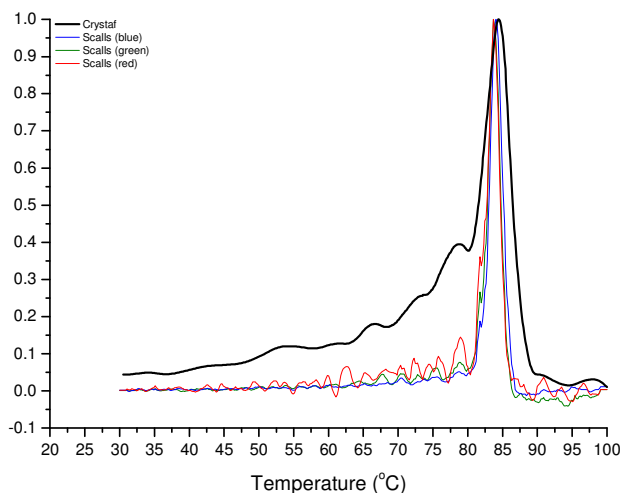


Figure 4.9: First derivative cooling profiles for Crystaf (0.1 °C/min) and Scalls (0.2 °C/min) for PE-1-hexene. [Normalized curves]

4.2.1.1) Particle size analysis

It was felt that particle size analyses of the formed crystallites could help understand the results obtained during a crystallization experiment. Particle size measurements were done using a Zetasizer instrument. Analyses were done straight after the cooling cycle from the Scalls analysis. The measurements were done at 30 °C. From one run, different distributions were obtained, namely the intensity, volume and number distribution of the particles. Both the intensity and volume distributions are based on the fact that larger particles scatter light more effectively. The volume distribution indicates the number of particles of specific sizes. The distribution curves for the two polymer samples are shown in Figure 4.10 – 4.12. A monomodal distribution was seen for the PE-1-octene copolymer. In the case of the PE-1-hexene sample, bimodal distributions were evident. These results indicated the difference in molecular heterogeneity between the two polymer samples. The octene copolymer was definitely a more homogeneous sample and hence the monomodal distribution. The bimodal distributions of the hexene copolymer compliment the Scalls crystallization data, from which it is apparent that this polymer crystallized over a much wider temperature range than the 1-octene copolymer.

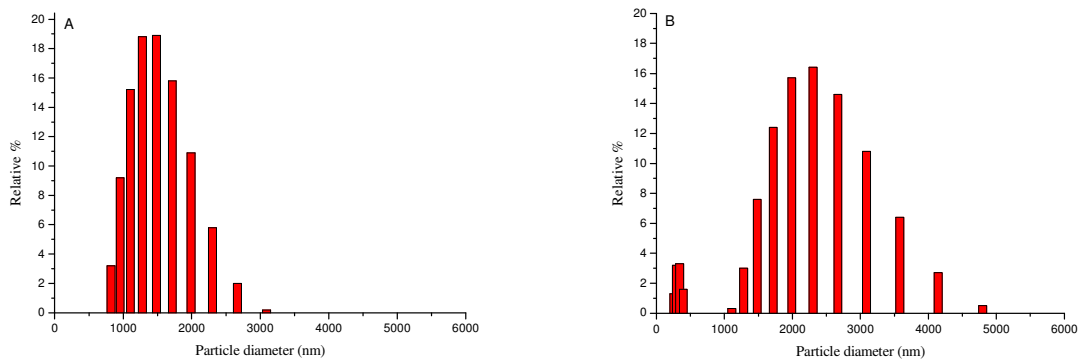


Figure 4.10: Intensity distributions of A) PE-1-octene and B) PE-1-hexene

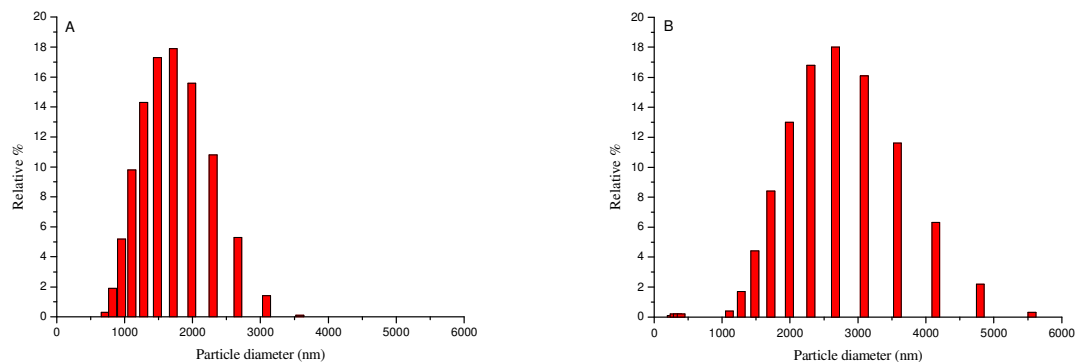


Figure 4.11: Volume distributions of A) PE-1-octene and B) PE-1-hexene

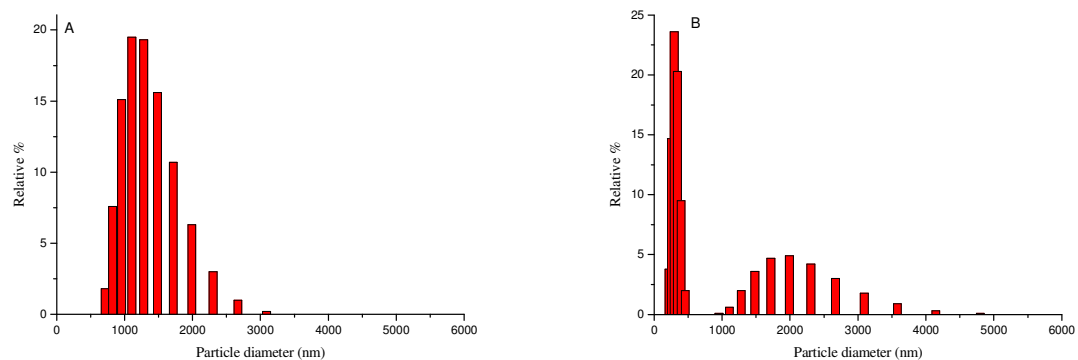


Figure 4.12: Number distributions of A) PE-1-octene and B) PE-1-hexene

4.2.2) Dissolution analysis

Upon completion of the cooling cycle, the process was reversed, and the turbid crystallized solution was heated up at a rate of 1 °C/min. The increase in laser beam intensities was measured as the polymer dissolved in solution. The heating profiles (Figure 4.13 – 4.14) also indicate that the crystallization processes were different for the two polymers. The heterogeneity of the hexene copolymer with regards to crystallizable sequences can be seen in the broad temperature range over which the polymer melted. A visible onset of melting could be seen at 40.2 °C. This polymer melted over a temperature range of almost 60 °C whereas the range for the octene copolymer was 30 °C. Melting of the crystallized hexene copolymer solution resulted in three laser signals at almost identical positions for the main melting peak, as can be seen in Figure 4.14. This implies that all the polymer crystals that formed during the cooling event melted at more or less the same time during the heating step. This was thus not the case for the higher α -olefin copolymer.

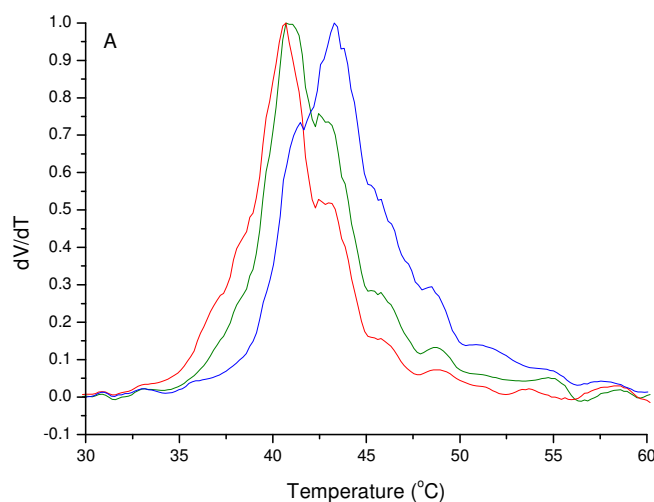


Figure 4.13: Heating profiles for PE-1-octene (1 °C/min; 2 mg/ml). [Normalized curves]

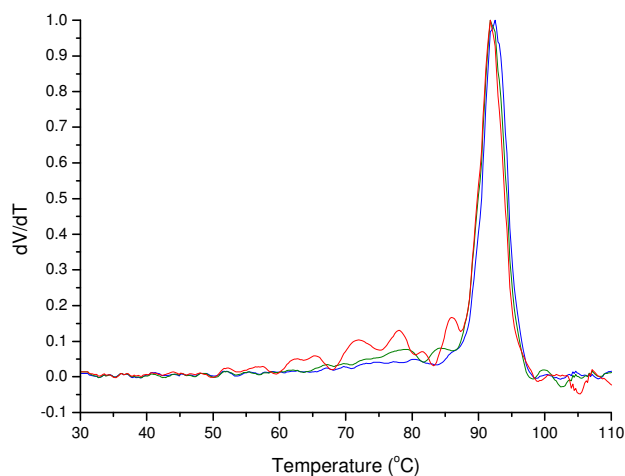


Figure 4.14: Heating profiles for PE-1-hexene (1 °C/min, 2 mg/ml). [Normalized curves]

As an additional study, the relative areas under the melting curves were calculated to get an idea of the different crystalline regions present in the two polymers. The total area was divided into 10 °C slices and the areas of the specific slices were indicated as a percentage relative to the total melting area. The results are illustrated in Table 4.5 and Figure 4.15 - 4.16 shows the relative areas as bar graphs.

Table 4.5: Relative areas under melting peaks

PE-1-octene									
Temperature range (°C)	Relative %			Relative area			Total area		
	blue	green	red	blue	green	red	blue	green	red
30.1 -40	8.5	20.0	34.3	0.583	1.197	1.859	6.871	5.972	5.418
40 - 50	81.3	74.5	63.0	5.589	4.447	3.413			
50 - 60.8	10.2	5.1	2.7	0.699	0.307	0.146			
PE-1-hexene									
Temperature range (°C)	Relative %			Relative area			Total area		
	blue	green	red	blue	green	red	blue	green	red
40.2 - 50	1.10	0.7	1.14	0.063	0.045	0.077	5.747	6.063	6.770
50 - 60	1.7	1.6	2.7	0.100	0.096	0.181			
60 - 70	3.2	4.0	6.4	0.182	0.241	0.435			
70 - 80	6.5	9.4	14.1	0.373	0.570	0.957			
80 - 90	15.5	19.5	20.4	0.890	1.181	1.382			
90 - 98.3	72.0	64.8	55.2	4.138	3.929	3.737			

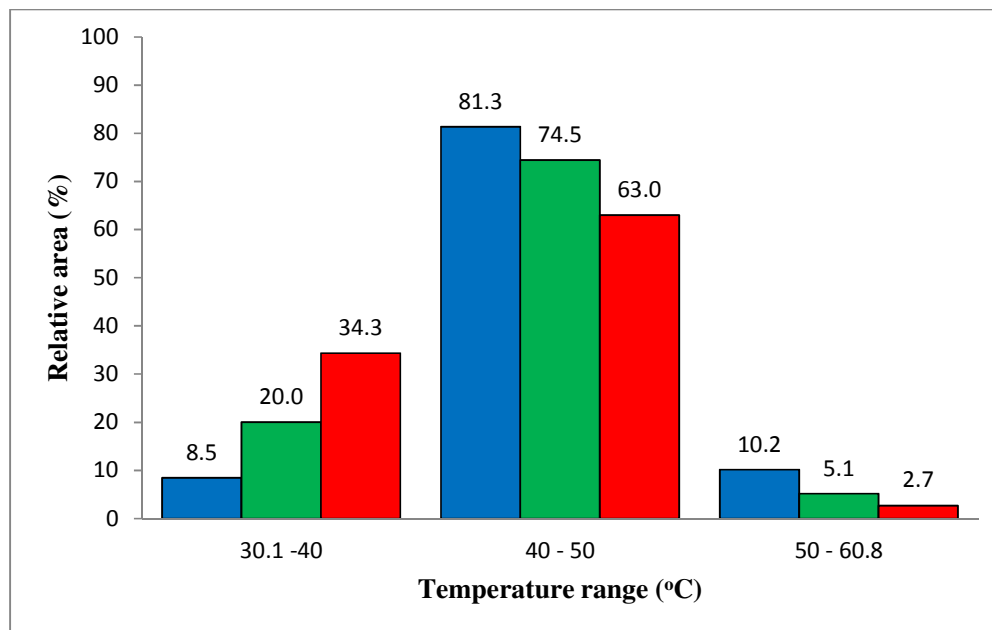


Figure 4.15: Relative area under melting peaks of different laser signals for PE-1-octene copolymer.

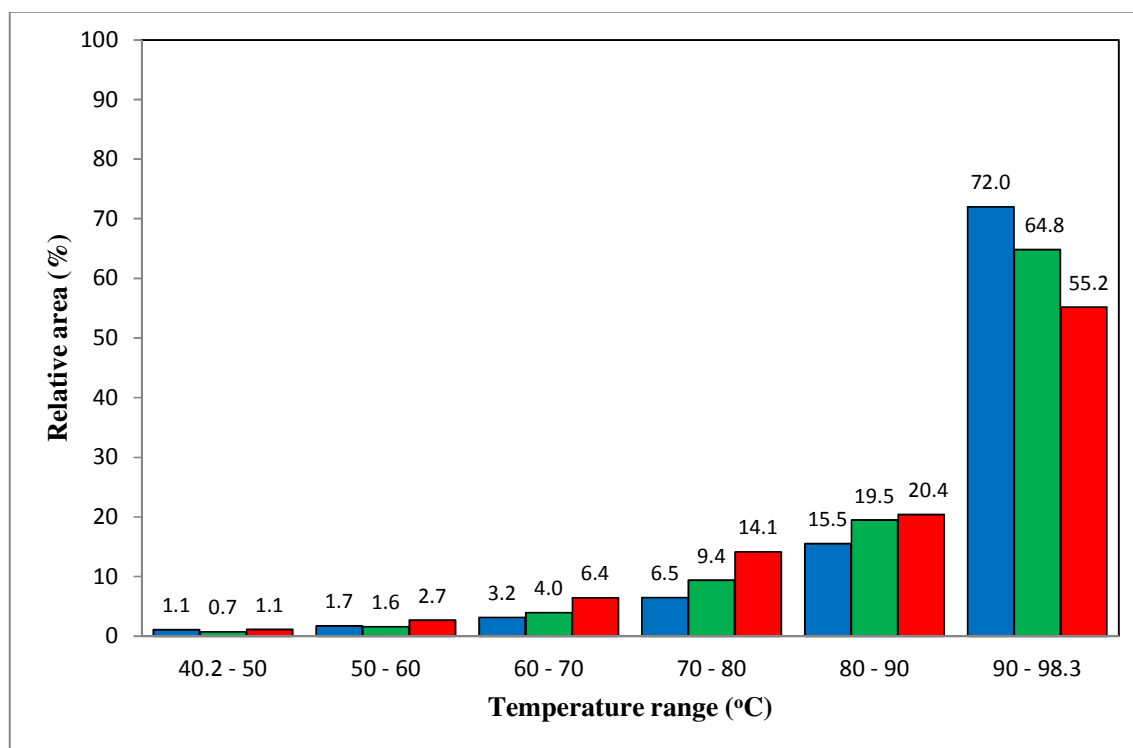


Figure 4.16: Relative area under melting peaks of different laser signals for PE-1-hexene copolymer.

A significant amount of information could therefore be obtained from the peak areas. First, it confirmed the molecular heterogeneity of the 1-hexene sample. Figure 4.15 illustrates the narrow temperature range over which the 1-octene sample melted. Second, information on the crystal sizes could be obtained by comparing the areas of the different laser signals. At higher temperatures the blue laser resulted in the largest area which corresponded to small changes during the melting event. When moving closer to the onset of melting, the red laser resulted in the largest area. The profile of the 1-hexene copolymer actually quite closely resembles that of a preparative Tref profile of a similar type of polymer (without the “soluble” fraction). To our mind, this clearly indicates that this method could be used to quantify molecular heterogeneity in a certain group of polyolefins.

4.3) Analysis of polymer fractions obtained by Tref

4.3.1) Introduction

The next part of the study comprised the fractionation of a polyolefin, and to analyze the fractions by Scalls and then compare the data with the Crystaf technique. The fractionation was done by Tref and the procedure can be found in the experimental part of this paper. A heterogeneous 1-hexene copolymer, prepared with a different catalyst to the previously analyzed hexene copolymer, was used for fractionation. The bulk polymer had a hexene content of 2 mol%. Fractions were obtained by solvent elution and collected at 60 °C, 70 °C, 80 °C and 90 °C. Table 4.6 shows the labeling of the Tref data and the molecular weight data can be found in Table 4.7.

Table 4.6: Tref fractions of PE-1-hexene copolymer collected for study

Elution temperature (°C)	Code
60	T60
70	T70
80	T80
90	T90

Table 4.7: Molecular weight data for fractions and bulk sample

Fraction	M _n (g/mol)	M _w (g/mol)	PDI
bulk	43 535	199 446	4.6
T60	31 582	103 846	3.3
T70	29 780	114 639	3.8
T80	43 756	136 748	3.1
T90	61 303	230 707	3.8

4.3.2) Crystallization analysis

Figure 4.17 – 4.19 display the Scalls crystallization profiles of the different laser signals for the Tref fractions analyzed at identical conditions. The different fractions could clearly be distinguished from both the cooling results due to the different temperature shifts. Crystallization temperatures obtained by Scalls are given in Table 4.8. Different crystalline regions and structures were present in the individual fractions leading to the peaks at different temperatures. Fractions T60, T80 and T90 gave rise to smooth curves of a unimodal nature during crystallization.

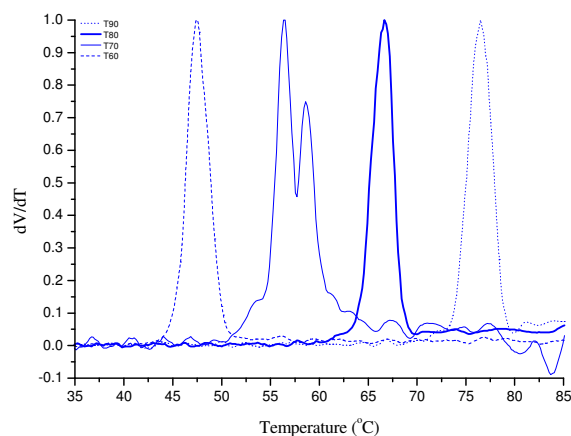


Figure 4.17: Normalized cooling profiles for Tref fractions of a PE-1-hexene copolymer analyzed by SCALLS. [blue laser ; 1 °C/min; 2 mg/ml]

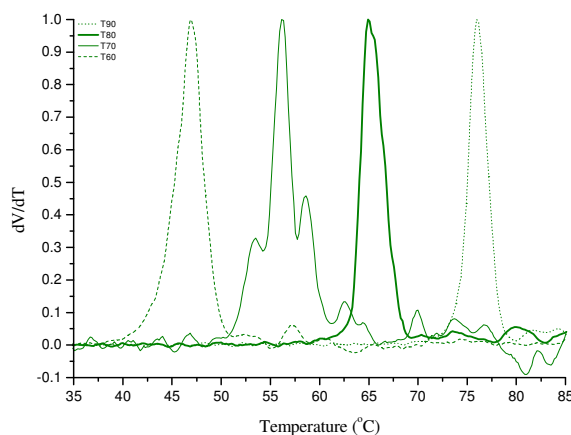


Figure 4.18: Normalized cooling profiles for Tref fractions of a PE-1-hexene copolymer analyzed by SCALLS. [green laser; 1 °C/min; 2 mg/ml]

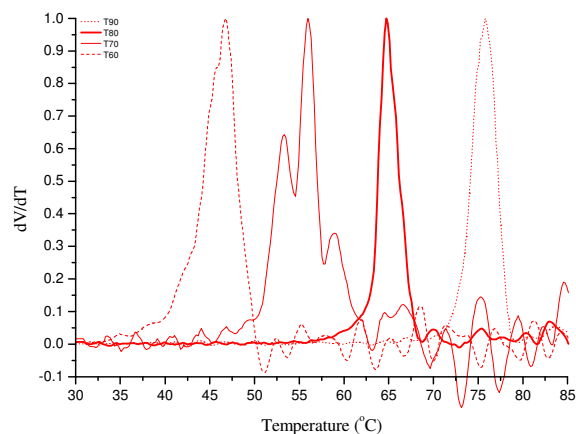


Figure 4.19: Normalized cooling profiles for Tref fractions of a PE-1-hexene copolymer analyzed by SCALLS: [red laser; 1 °C/min; 2 mg/ml]

Table 4.8: Crystallization peak temperatures for the different Tref fractions at cooling rate of 1 °C/min

Fraction	Scalls crystallization peak temperatures (°C)		
	blue laser	green laser	red laser
T60	47.5	46.8	46.7
T70	56.4	56.2	55.9
T80	66.6	64.8	64.7
T90	76.5	76.1	75.8

The values for the T70 fraction are that of the highest peaks in the cooling profiles. (Peak 2 in Table 4.)

In contrast, T70 showed an interesting crystallization profile. The peaks for this fraction showed definite bimodality for the blue laser and even trimodality for the green and red laser signals, indicating some structural heterogeneity. The peak temperatures for the peaks from the blue laser profile correlated well to the two peaks at higher temperatures in the green and red laser profiles. An overlay of these peaks is presented by Figure 4.20.

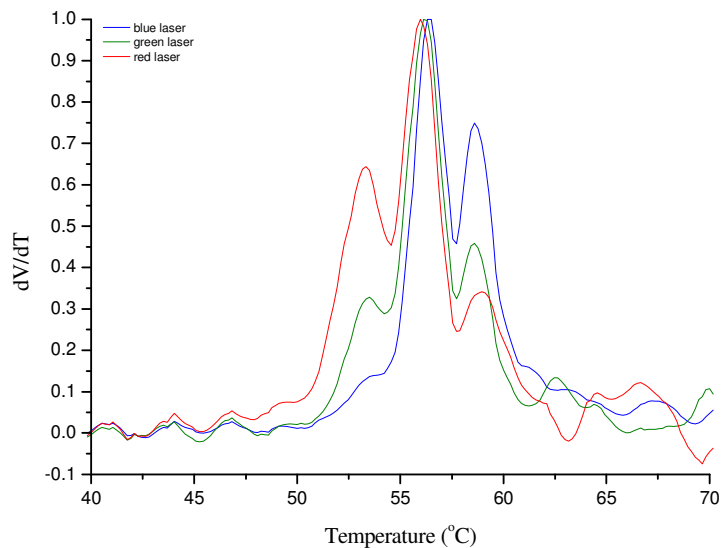


Figure 4.20: Different laser signals of T70 fraction cooling profile. [Normalized; 1 °C/min]

The first thing to note here is that the peak values for the three lasers are essentially identical, but the intensity of the peaks vary, with the 405 nm laser peak being more intense for peak 3, and the lowest intensity for peak 1. This seems to indicate that a fairly rapid increase in small crystallites are present at the temperature indicated by peak 3, and some of the crystals rapidly increase in size enough to cause scattering of the green and red lasers. This is followed by a secondary (or maybe different) crystallization event which is visible at peak 2, and another event evident at peak 3. The latter is most likely due to growth onto existing particles (green and red lasers) and some homogeneously nucleated new crystallization events (shoulder on blue laser peak).

Table 4.9: Peak temperatures for the T70 fraction cooled at 1 °C/min

Laser signal	Temperature (°C)		
	Peak 1	Peak 2	Peak 3
blue	*53.6	56.4	58.6
green	53.5	56.2	58.5
red	53.3	55.9	58.8

*Shoulder and not a fully resolved peak.

The Tref fractions were also analyzed by Crystaf and the data was compared to those obtained by the light scattering technique. The normalized Crystaf profiles for the fractions are shown in Figure 4.21. All fractions were subjected to identical experimental conditions. The T60 peak was very broad and made it difficult to select a peak maximum.

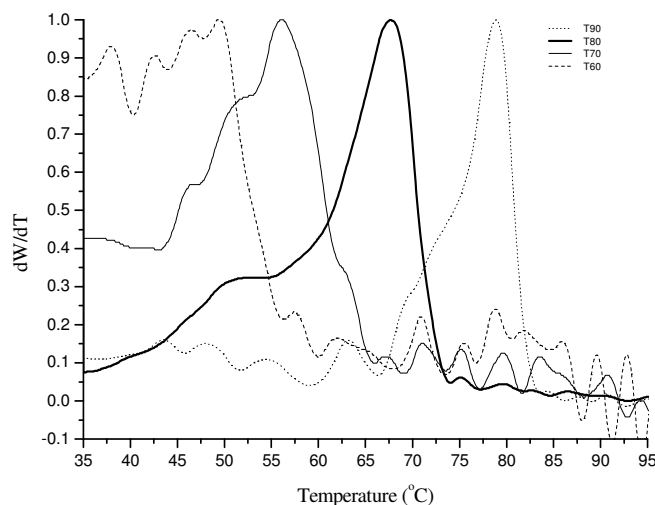


Figure 4.21: Normalized crystaf profiles of PE-1-hexene polymer fractions [0.1°C/min].

Similar to Scalls, the peaks of the different fraction are clearly shifted to different temperatures. According to the data from Figure 4.21, the fractions were more heterogeneous than the results initially obtained from light scattering. The reason for this was mainly the different cooling rate used in the two techniques. During the Crystaf analysis the cooling rate was 0.1 °C/min whereas the rate for the Scalls analysis was 1 °C/min. This large variation in cooling rates led to different crystallization behavior. Analysis by Scalls was a bit difficult at 0.1 °C/min and resulted in some complications with the controlled cooling of the instrument. However cooling down at a rate of 0.2 °C/min seemed to work fine and the fractions were again analyzed by Scalls and the results are illustrated in Figure 4.22 – 4.24.

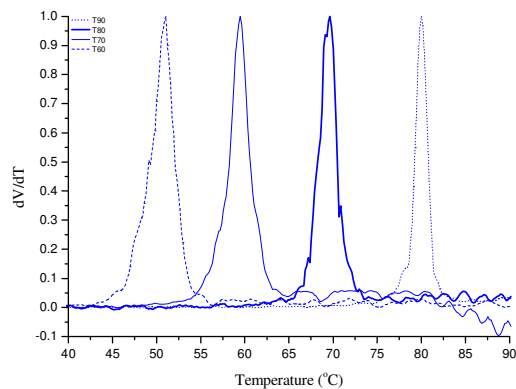


Figure 4.22: Normalized cooling profiles for the Tref fractions of a PE-1-hexene copolymer analyzed by Scalls. [blue laser; 0.2 °C/min; 2 mg/ml]

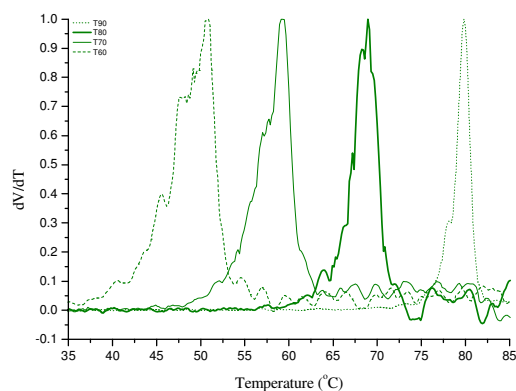


Figure 4.23: Normalized cooling profiles for the Tref fractions of a PE-1-hexene copolymer analyzed by Scalls. [green laser; 0.2 °C/min; 2 mg/ml]

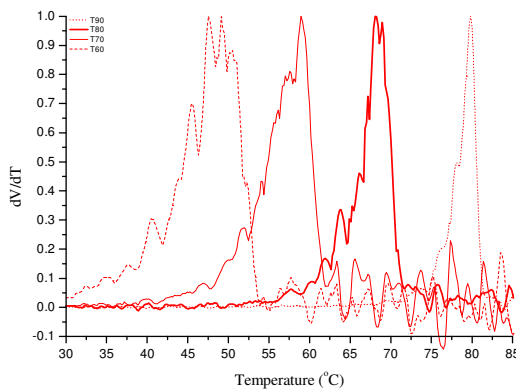


Figure 4.24: Normalized cooling profiles for the Tref fractions of a PE-1-hexene copolymer analyzed by Scalls. [red laser; 0.2 °C/min, 2mg/ml]

Similar to all the other operating cooling rates, the shifts of crystallization peaks were still clearly visible. After lowering the cooling rate from 1 °C/min to 0.2 °C/min, a notable shift in peak temperatures was observed. The peaks were broader and more comparable to the Crystaf data. Apart from the broadening of the profiles when moving from the blue laser through to the red laser, some shoulders became visible indicating the structural heterogeneity of the fractions. The data also showed that the T90 fraction was the most homogeneous fraction due to the narrowest crystallization signal. This was confirmed by the Crystaf profiles. Table 4.10 compares the temperatures of the peak maxima resulting from the two crystallization techniques used in the study. Looking at the values for the crystallization times at 0.2 °C/min information on the structural heterogeneity of the fractions could be obtained. The crystallization times were again calculated using equation 1 discussed in the previous section. The data is shown in Table 4.11 and it is clear that T90 was the most crystalline fraction as T90 crystallized over the shortest period of time. The peak widths of the cooling profiles compliment this results with T90 having the narrowest crystallization peaks. At both cooling rates the duration for complete crystallization follow the same trend when moving from T60 to T90. The T70 fraction appeared to deviate from this trend as it resulted in a higher value than T60. This might have been due to the heterogeneity of the T70 fraction as discussed earlier.

Table 4.10: Comparison of Crystaf and Scalls results done at similar conditions

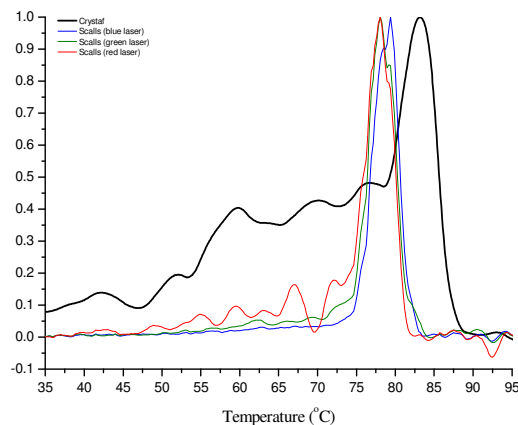
Fraction	Temperature of peak maxima (°C)			
	Crystaf [*]	blue laser	Scalls ⁺ green laser	red laser
^a T60	-	50.9	50.8	49.1
T70	56.1	59.5	59.2	58.9
T80	67.7	69.7	68.9	68.2
T90	78.9	80.1	79.9	79.8

^a The Crystaf peak for this fraction was very broad; difficult to get peak maximum
^{*} 0.1 °C/min; ⁺ 0.2 °C/min

Table 4.11: Duration of crystallization for Tref fractions analyzed by Scalls at different cooling rates

Polymer	T _o (°C)	T _f (°C)	T _o - T _f (°C)	Duration of crystallization (min)	Normalized crystallization time
Cooling rate: 0.2 °C/min					
T60	56.4	30	26.4	132	0.79
T70	64.7	31.4	33.3	166.5	1
T80	73.5	49.7	23.8	119	0.71
T90	84.2	74.5	9.7	48.5	0.29
Cooling rate: 1 °C/min					
T60	54.4	31.7	22.7	22.7	0.79
T70	68.6	39.9	28.7	28.7	1
T80	69.8	55.8	14	14	0.49
T90	79.9	68.8	11.1	11.1	0.39

The results listed in Table 4.10 indicate that the Scalls technique provides useful results similar to that of the traditionally used Crystaf setup. There were some minor dissimilarity in the data though, but largely the results obtained correlated reasonably well. Crystallization data for the unfractionated bulk polymer are illustrated in Figure 4.25. The main reason for the difference in peak temperatures was the cooling rates. The cooling rate for Crystaf analysis was 0.1°C/min and the crystallization step took over 11 hours to finish. During the Scalls run, the cooling rate was 1 °C/min and the crystallization step was done in 70 minutes with reasonably comparable results.

**Figure 4.25: Crystaf and Scalls crystallization profiles of unfractionated PE-1-hexene polymer.**

4.3.3) Dissolution analysis

Heating profiles of the polymer fractions can be found in Figure 4.26 - 4.28. From the profiles it can be seen that the T70 melting peak is slightly broader than that of the other three fractions and can be observed for the heating profiles of all three lasers and has an early onset of melting. This might have been due to the differences in solution crystallization events during the cooling step as well as the difference in crystalline regions of the fractions as previously shown by the multimodal nature of the T70 crystallization peaks. Another interesting observation was made when looked at the Tref elution temperatures in Table 4.6 and the peak temperatures of the fractions from the Scalls heating profiles. The experimental peak temperatures obtained by Scalls was in good correlation with the elution data. A comparison of the Tref and Scalls temperatures can be found in Table 4.12.

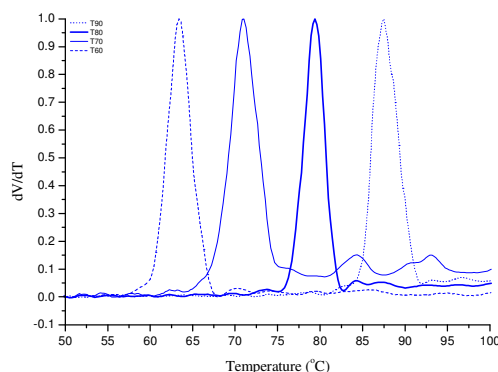


Figure 4.26: Normalized heating profiles for the Tref fractions of a PE-1-hexene copolymer analyzed by Scalls. [blue laser; 1.5 °C/min; 2 mg/ml]

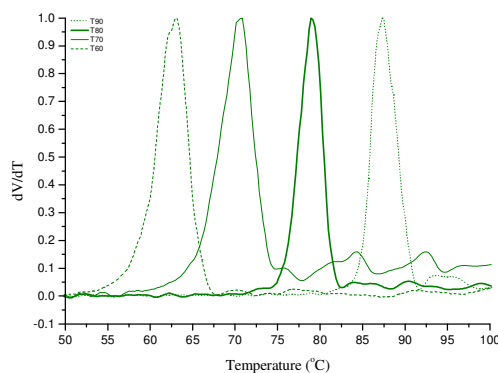


Figure 4.27: Normalized heating profiles for the Tref fractions of a PE-1-hexene copolymer analyzed by Scalls. [green laser; 1.5 °C/min; 2 mg/ml]

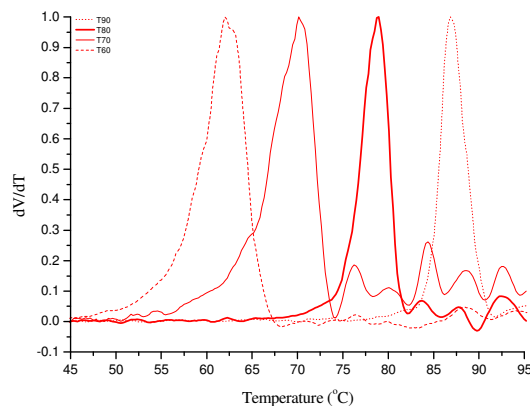


Figure 4.28: Normalized heating profiles for the Tref fractions of a PE-1-hexene copolymer analyzed by Scalls: [red laser; 1.5 °C/min; 2 mg/ml]

Table 4.12: Comparison of Tref elution temperatures and Scalls solution melting temperatures

Fraction	Tref elution temperature (°C)	Scalls melting peak temperatures (°C)		
		blue laser	green laser	red laser
T60	60	63.4	63.0	62.0
T70	70	70.9	70.6	70.2
T80	80	79.4	78.9	78.8
T90	90	87.5	87.4	86.9

Elution temperatures from Tref and solution melting temperatures from Scalls agreed very well. For the T60 and T70 fractions the Tref temperature was slightly lower than those obtained by Scalls and for the T80 and T90 fractions it was slightly higher than the Scalls temperatures. These differences are reasonable due to differences in factors like temperature-lag between the two techniques. Overall the results obtained were very similar.

4.4) Analysis of polymer blends

The part of the study comprised the analysis of polymer blends. Polymers were solution blended and the solution crystallization and melting was investigated by Scalls to see if this technique is able to detect the occurrence of phase separation during crystallization. Differential scanning calorimetry (DSC) was done first to see if there was any phase separation when samples were crystallized from the melt.

4.4.1) Isotactic polypropylene (iPP) – low density polyethylene (LDPE)

The incompatibility of LDPE/PP blends has been analyzed and explained in a number of studies and it has been shown that these two polymers are essentially immiscible in the melt and that two phases exist^{4,5}. In this study we use Scalls to study the compatibility of some LDPE/PP blends.

4.4.1.1) Crystallization analysis

The first blend to be studied was an isotactic polypropylene (iPP) and low density polyethylene (LDPE) polymer blend. The DSC endotherm and exotherm of a 50:50 wt% blend are given in Figure 4.29. The phase separation could clearly be seen by the presence of two distinct peaks for the crystallization and melting events. The peaks at higher temperatures were assigned to the PP and peaks at lower temperatures were due to the LDPE present in the blend.

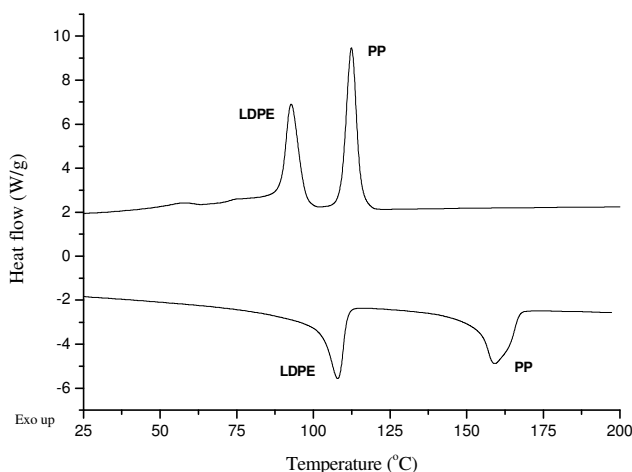


Figure 4.29: DSC profiles of 50:50 PP-LDPE blend.

Overlays of the Scalls cooling data for different blend compositions are given in Figure 4.30 – 4.32. Two main crystallization peaks were visible in all blends compositions similar to the DSC results, indicating the two separate phases. The crystallization peaks of the homopolymer LDPE and iPP, obtained from the blue laser, are given as references. The peak positions are different to the DSC results due to solvent effects during solution crystallization. The blends gave rise to peaks that were less smooth than those obtained for the homopolymers. This might have been due to some interaction between the two phases. As the composition ratio was varied, a clear shift in peak position was observed for the iPP phase. With less iPP present the polypropylene peak shifted to lower crystallization temperatures. There was no major shift in peak positions for LDPE although the peaks moved slightly closer to the homopolymer LDPE peak. From both calorimetry measurements and solution crystallization analysis, the phase separation could clearly be seen for this polymer blend.

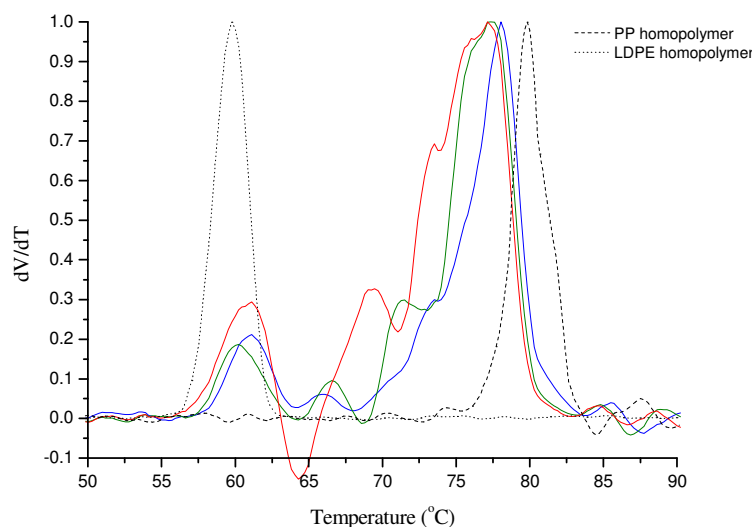


Figure 4.30: Overlay of Scalls cooling profiles for different lasers. [20:80 wt% PP-LDPE blend; 1 °C/min; 5 mg/ml; normalized peaks]

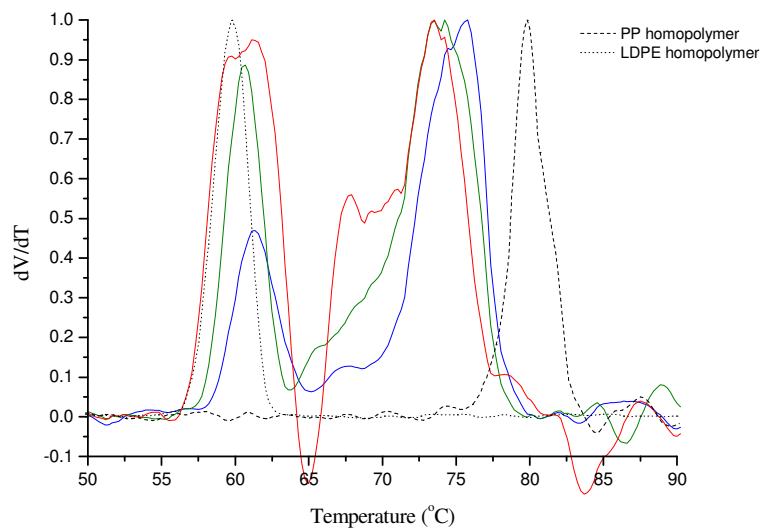


Figure 4.31: Overlay of Scalls cooling profiles for different lasers. [10:90 wt% PP-LDPE blend; 1 °C/min; 5 mg/ml; normalized peaks]

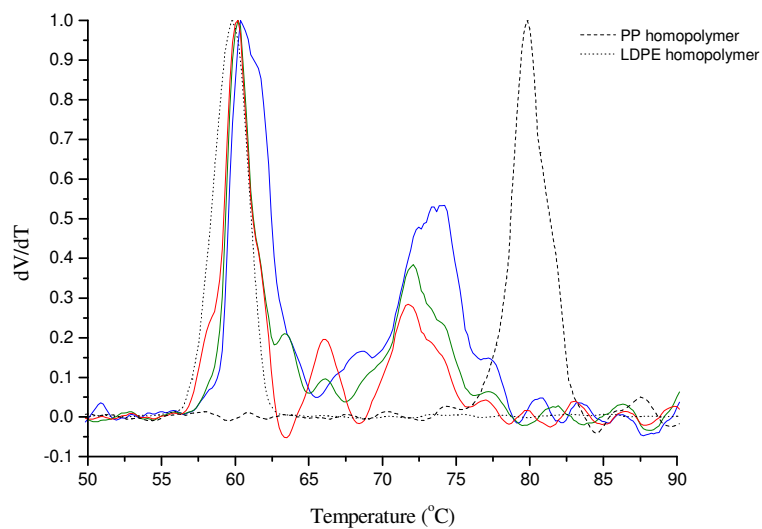


Figure 4.32: Overlay of Scalls cooling profiles for different lasers. [5:95 wt% PP-LDPE blend; 1 °C/min; 5 mg/ml; normalized peaks]

4.4.1.2) Dissolution analysis

After cooling the solutions to obtain the crystallization data, the temperature was increased to 120 °C at a rate 1 °C/min. The solution melting events were studied as the crystallized polymer solutions were heated up. Figures 4.33 – 4.35 show the heating profiles obtained by Scalls. A large number of scattering can be seen for all compositions between the peaks of the individual LDPE and PP components. It is unclear if this scattering was due to crystalline regions formed during the cooling stage because the crystallization profiles of PP was fairly broad and spanned over a wide temperature range as were illustrated in Figure 4.30 – 4.32. The LDPE and PP peaks were clearly separated from each other due to the phase separation during crystallization. From the Scalls solution melting analysis it is obvious that two different crystal regions were present namely a LDPE and PP region. When comparing the peaks of the blends with that of the homopolymers it was noticed that these peaks temperatures were very similar. Also the positions of the different laser signals were at similar temperatures. This indicates that although certain molecular regions crystallize before others (shift in laser signals), all crystal regions melted more or less at the same time and hence the overlapping melting peaks.

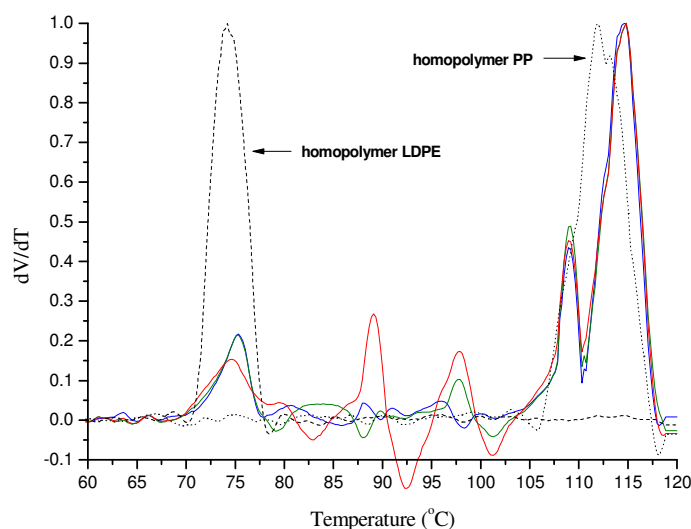


Figure 4.33: Overlay of Scalls heating profiles for different lasers. [20:80 wt% PP-LDPE blend, 1 °C/min; 5 mg/ml normalized peaks]

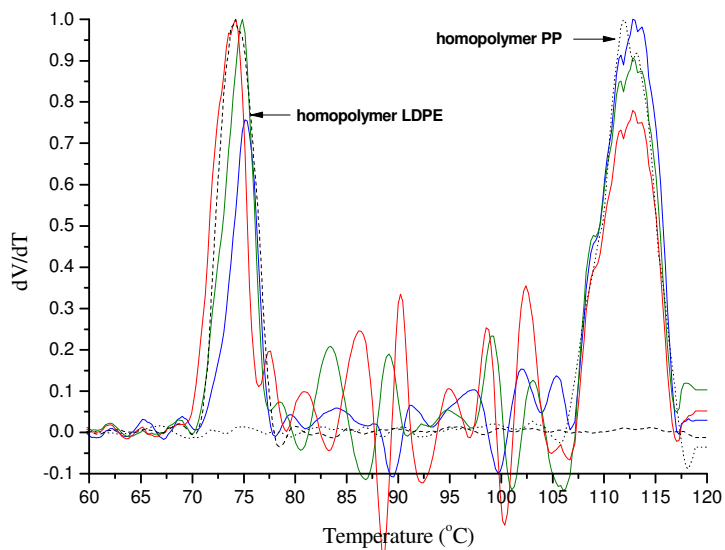


Figure 4.34: Overlay of Scalls heating profiles for different lasers. [10:90 wt% PP-LDPE blend, 1 °C/min; 5 mg/ml normalized peaks]

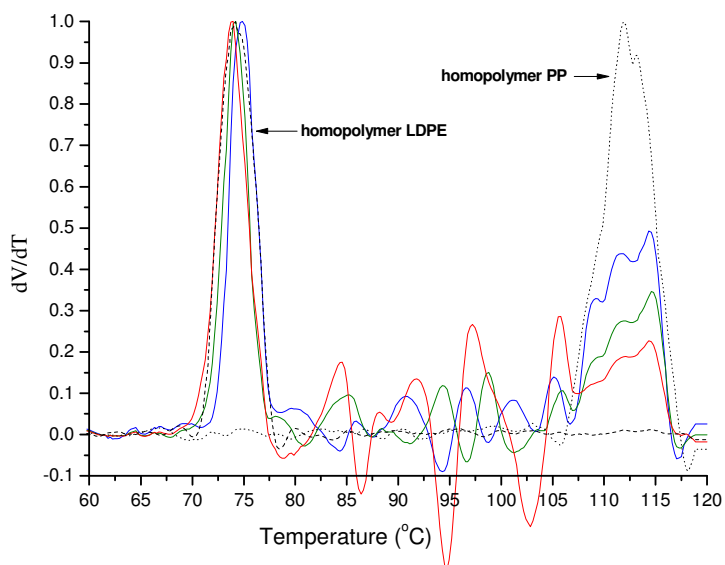


Figure 4.35: Overlay of Scalls heating profiles for different lasers. [5:95 wt% PP-LDPE blend, 1 °C/min; 5 mg/ml normalized peaks]

4.4.2) Isotactic polypropylene (iPP) – polypropylene impact copolymer (PPIC)

The second blend to be studied was a 50:50 wt% blend of an isotactic polypropylene homopolymer and polypropylene impact copolymer. Impact polypropylene is usually prepared through a cascade process where isotactic polypropylene is polymerized in the first reactor. After polymerizing the PP, it is sent to a second reactor where ethylene is added and resulting in the polymerization of polyethylene. It is clearly visible from the DSC exotherm and endotherm in Figure 4.36 that co-crystallization took place between the isotactic polypropylene part of PPIC and the homopolymer polypropylene due to the formation of only a single crystallization exotherm as well as only one melting endotherm. The amorphous rubber regions of the PPIC do not contribute to the crystallization events.

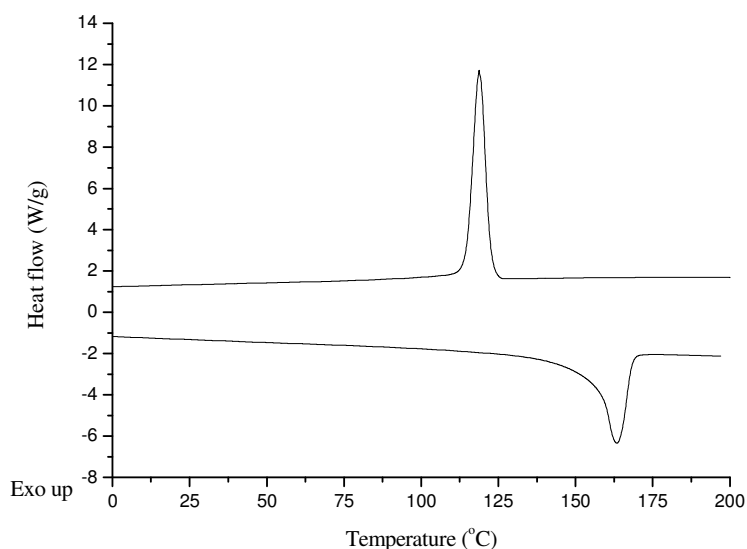


Figure 4.36: DSC profiles of 50:50 wt% PP-PPIC blend.

The solution crystallization and melting was done and the profiles are shown in Figure 4.37 and Figure 4.38 respectively. Similar to the DSC data only one crystallization peak was observed confirming the co-crystallization of the two phases in solution. The influence of the solvent during solution crystallization and solution melting can also be seen when looking at the variation of peak temperatures between the DSC and Scalls profiles. Both, crystallization and melting occurs at lower temperatures in solution.

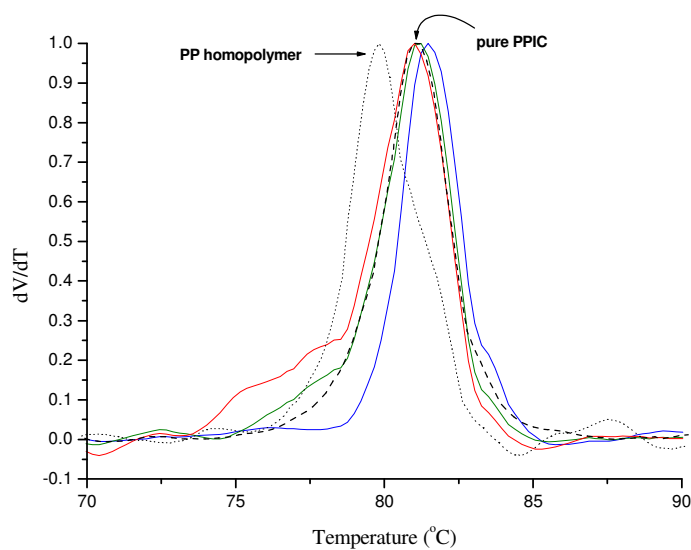


Figure 4.37: Overlay of Scalls cooling profiles for different lasers. [50:50 wt% PP-EPR blend; $1^{\circ}\text{C}/\text{min}$; 2 mg/ml; normalized peaks]

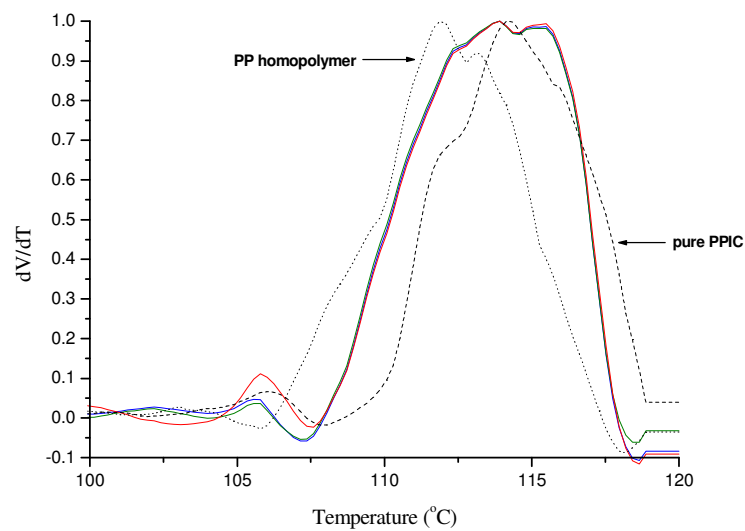


Figure 4.38: Overlay of Scalls heating profiles for different lasers. [50:50 PP-EPR blend; $1.5^{\circ}\text{C}/\text{min}$; 2mg/ml; normalized peaks]

4.5) References

- 1) Shan, C.L.P., Degroot, W.A., Hazlitt, L.G. & Gillespie, D. 2005, *A new turbidimetric approach to measuring polyethylene short chain branching distributions*, Polymer, vol. 46, no. 25, pp. 11755-11767.
- 2) Van Reenen, A.J., Rohwer, E.G., Walters, P., Lutz, M. & Brand, M. 2008, *Development and use of a turbidity analyzer for studying the solution crystallization of polyolefins*, Journal of Applied Polymer Science, vol. 109, no. 5, pp. 3238-3243.
- 3) Anantawaraskul, S., Soares, J.B.P. & Jirachathorn, P. 2007, *A mathematical model for the kinetics of crystallization in crystaf*, Macromolecular Symposia, vol. 257, pp. 94-102.
- 4) Bertin, S. & Robin, J.-. 2002, *Study and characterization of virgin and recycled LDPE/PP blends*, European Polymer Journal, vol. 38, no. 11, pp. 2255-2264.
- 5) Teh, J.W. 1983, *Structure and properties of polyethylene/polypropylene blend*, Journal of Applied Polymer Science, vol. 28, no. 2, pp. 605-618.

Chapter 5

Conclusions and Recommendations

This chapter concludes the results obtained and work done during this study. Some recommendations for future work are also given in this section.

5.1) Conclusions

5.1.1) Analysis of LLDPE samples

Two polymers, a 1-hexene and 1-octene LLDPE, with different comonomers and catalysts used during preparation were analyzed by Scalls. Solution crystallization and melting analyses revealed that we could differentiate between chemically similar but morphologically different LLDPE polymers with this unique light scattering technique. The use of different wavelength lasers (blue – 405 nm, green – 532 nm, red – 635 nm) clearly highlighted some major differences in crystallization and melting events of the two polymers. By looking at the peaks associated with the different lasers, important information on the crystallization kinetics and crystal growth could be obtained.

The range of crystallization for the 1-octene LLDPE was much narrower than that of the 1-hexene LLDPE and the crystallization curves were different in shape and complexity. Looking at the raw voltage data it was evident that the 1-hexene copolymer crystallized far more rapidly than the more homogeneous 1-octene sample. Crystallization data obtained from Scalls correlated well with Crystaf results but with much shorter analysis times. Slight peak shifts were visible between the results of the two different techniques but it was mainly due to the difference in cooling rates. Particle size analyses showed a bimodal particle size distribution for the 1-hexene copolymer which complimented the initial rapid crystallization followed by the extensive tailing resulting in a very broad range of crystallization.

Results obtained from the dissolution analyses showed that the crystallization processes were different for the two polymers. The difference in heterogeneity with regards to crystallizable sequences of the two LLDPE samples could be seen in the temperature range over which the polymers melted. Similar to the crystallization curves, the 1-octene sample melted over a narrower temperature range. The areas under the melting peaks confirmed the molecular heterogeneity of the 1-hexene sample. This study showed the potential of this unique light scattering technique for the analysis of solution crystallization and solution melting in polymers and both the crystallization and melting results indicated that this Scalls method could be used to quantify molecular heterogeneity in certain polyolefins.

5.1.2) Analysis of polymer fractions obtained by Tref

A 1-hexene LLDPE was fractionated by Tref and analyzed by Scalls. The different fractions could successfully be distinguished from both the cooling and heating profiles. The presence of multiple signals (bimodality and trimodality) for the T70 fraction indicated some structural heterogeneity for this fraction. Once again, in this case, the use of three different lasers gave an indication on the way the crystallites were formed during crystallization from solution. All results obtained from Scalls for the fractions as well as the unfractionated polymer were compared to Crystaf data and the results of the two techniques correlated well.

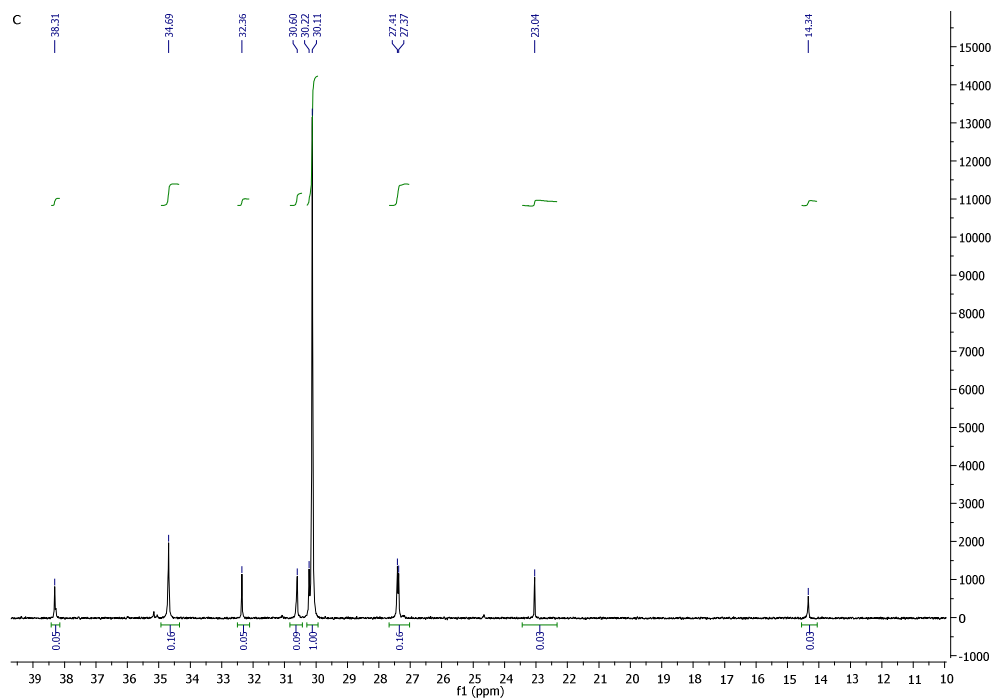
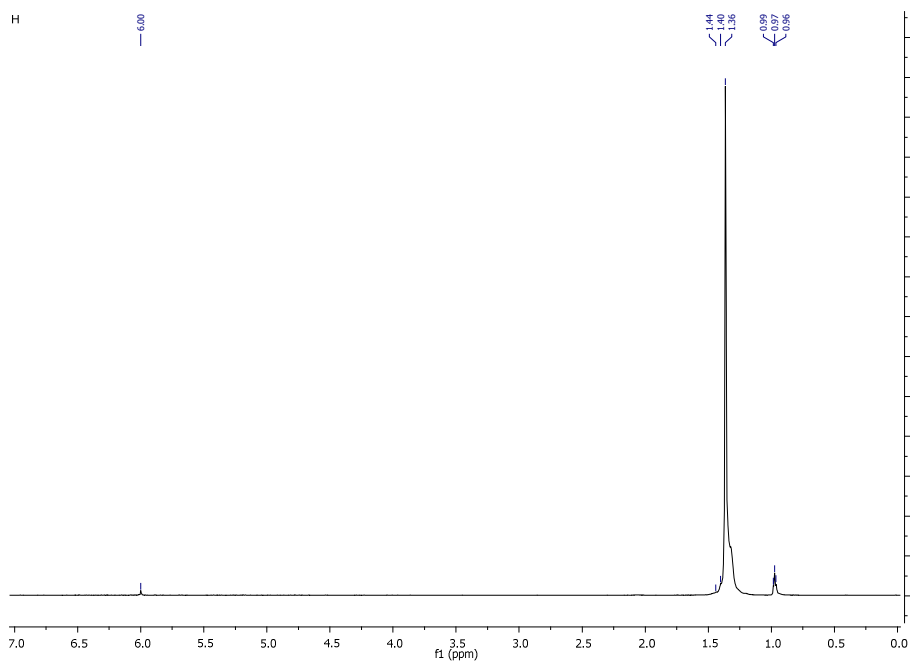
5.1.3) Analysis of polymer blends

For the immiscible blend (iPP – LDPE blend), the phase separation was clearly visible from both the crystallization and dissolution analyses with the presence of two distinct peaks, one peak corresponding to the isotactic polypropylene homopolymer and the second peak due to the polyethylene homopolymer. Peak shifts were visible as the blend compositions were varied. Analysis of the second blend (iPP – PPIC blend) resulted in a single crystallization and melting peak. This indicates that co-crystallization occurred between the polypropylene homopolymer and the isotactic polypropylene region in the PPIC. Differential scanning calorimetry showed similar results to those obtained by Scalls. It can be said that Scalls is an effective technique for examining the phase separation and co-crystallization events in certain polyolefin blends.

5.2) Recommendations

Due to the fact that water is being used to control cooling events during Scalls analyses, crystallization studies can only be controlled in a temperature range below 100 °C. In order to allow for the analysis of a wider range of polymers, improvement of the cooling system is important to achieve controlled cooling from above 100 °C. In addition, events that occur below the freezing temperature of TCB cannot be analyzed. Other solvents could be investigated.

Appendix A: NMR data

Figure A-1: ^{13}C NMR spectrum of PE-1-octene.Figure A-2: ^1H NMR spectrum of PE-1-octene.

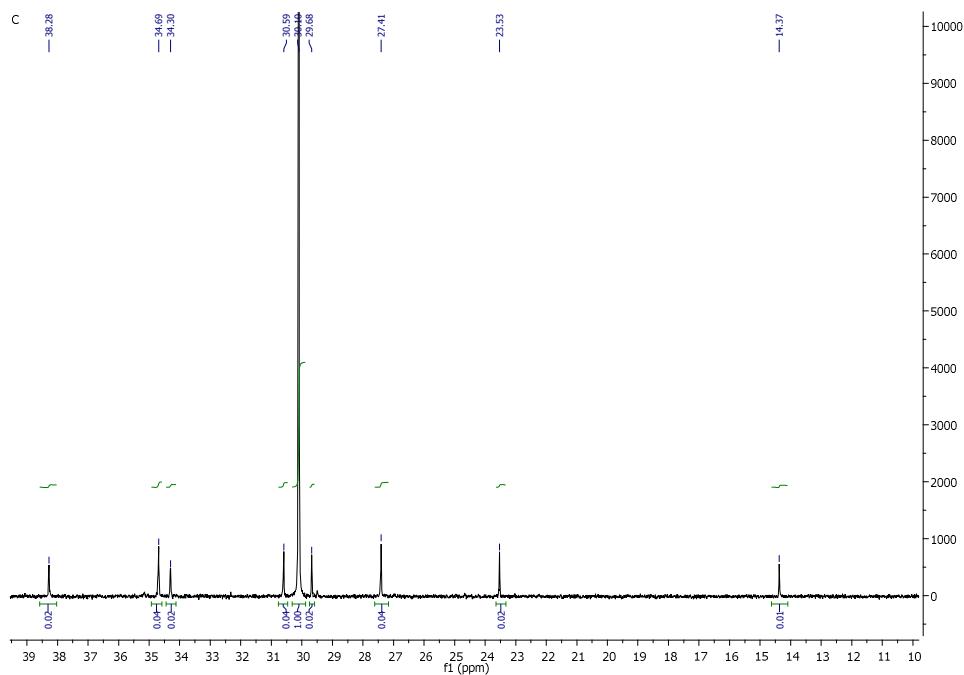


Figure A-3: ^{13}C NMR spectrum of PE-1-hexene used in first study.

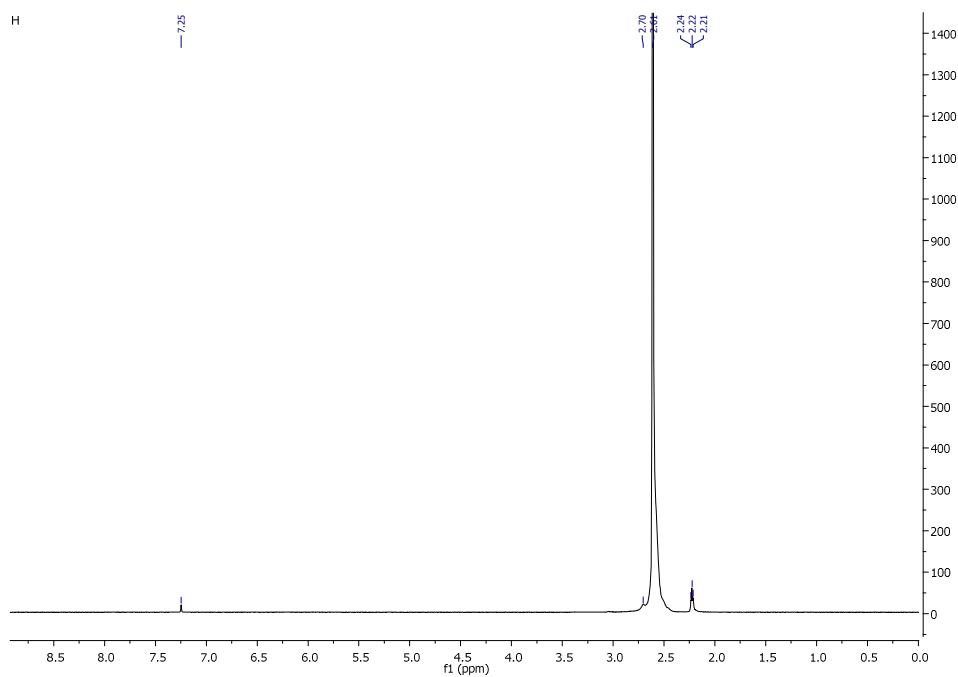


Figure A-4: ^1H NMR spectrum of PE-1-hexene used in first study.

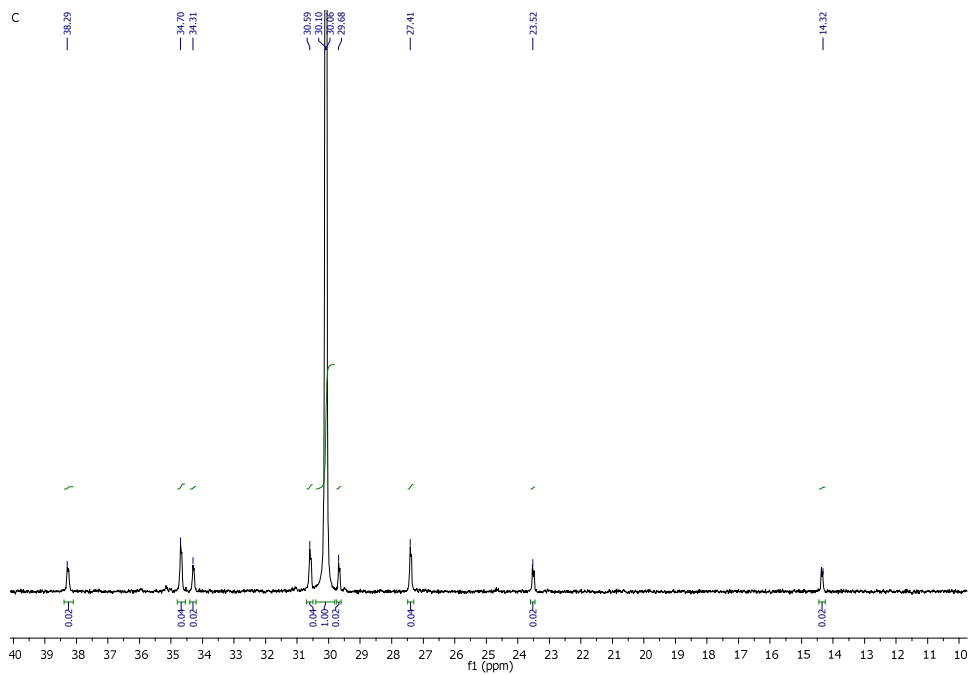


Figure A-5: ^{13}C NMR spectrum of PE-1-hexene used in fractionation study.

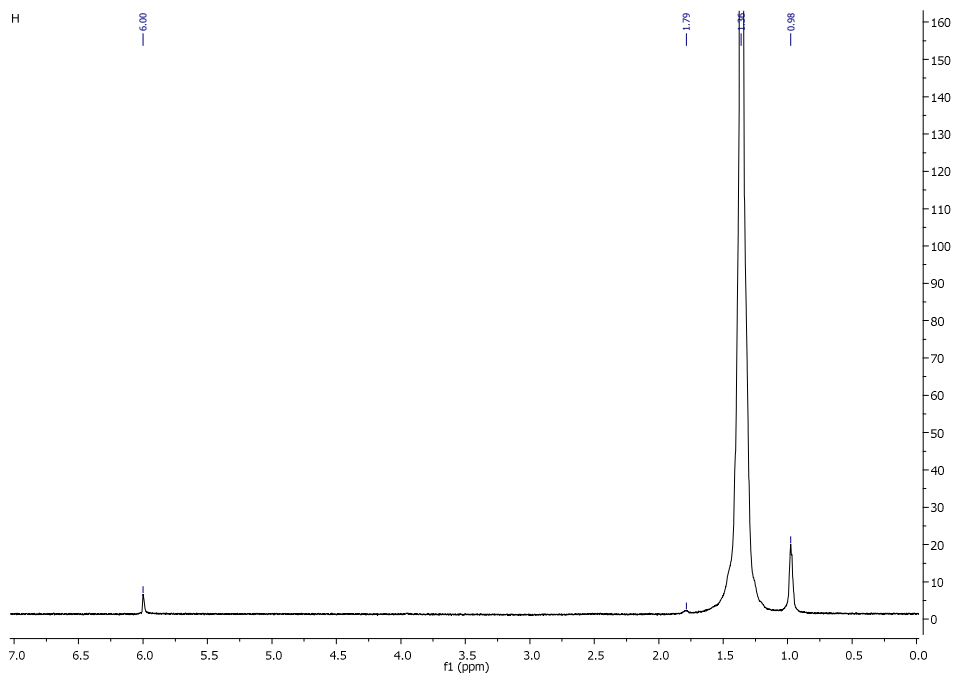
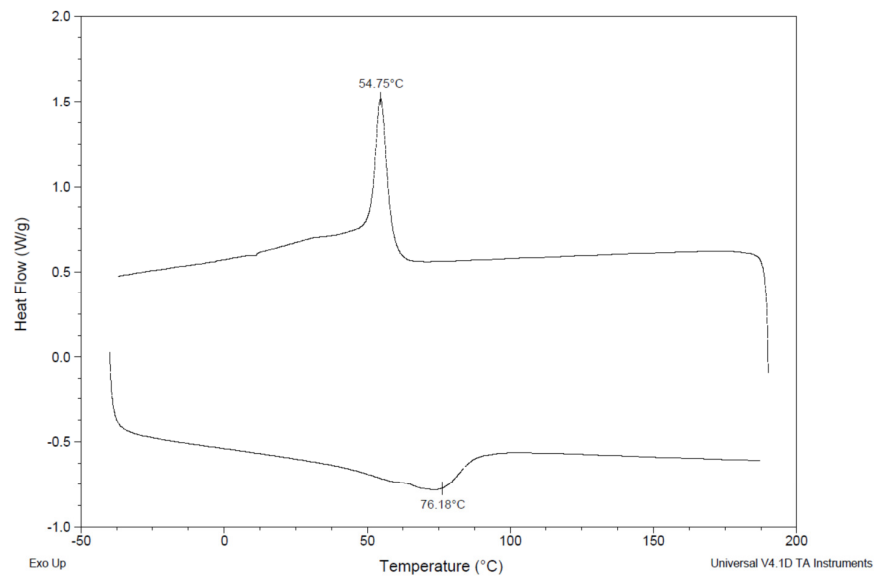
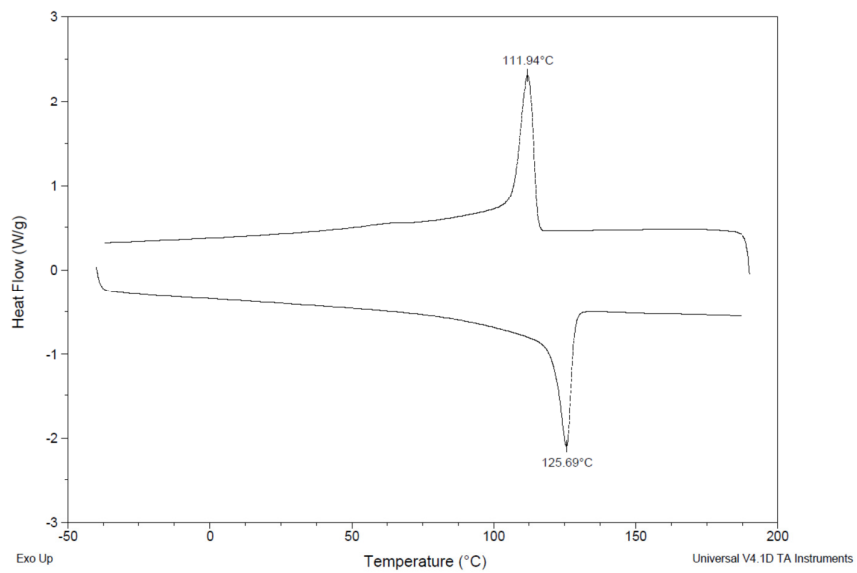


Figure A-6: ^1H NMR spectrum of PE-1-hexene used in fractionation study.

Appendix B: DSC data**Figure B-1: DSC results for PE-1-octene.****Figure B-2: DSC results for PEH1.**

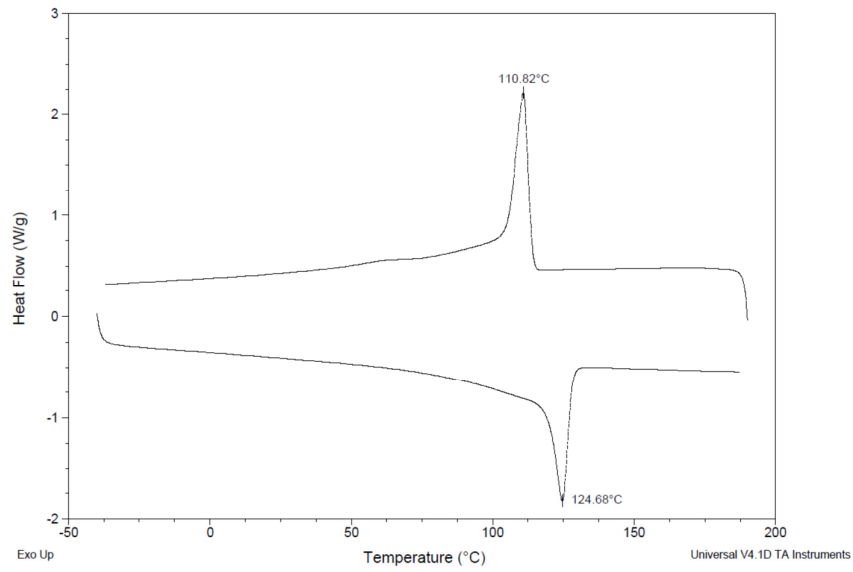


Figure B-3: DSC results for PEH2.

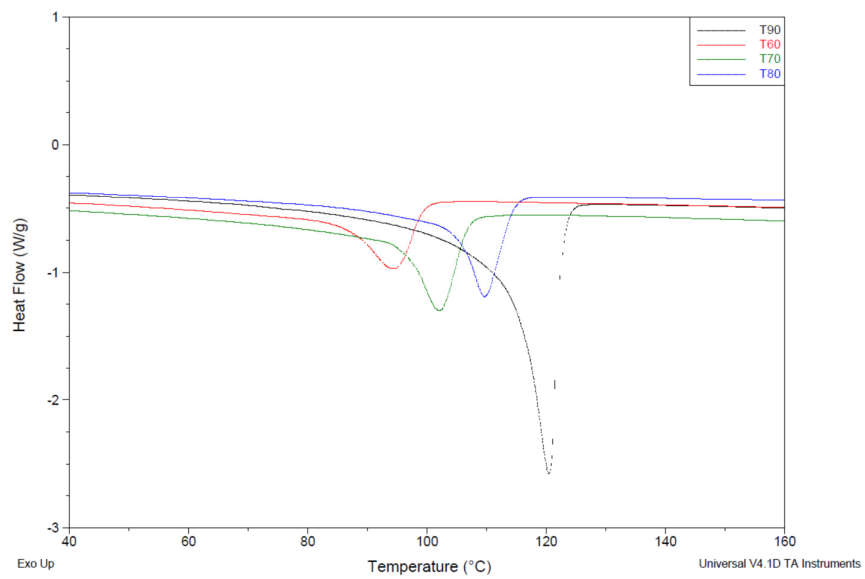


Figure B-4: DSC endotherms for Tref fractions of PEH2.

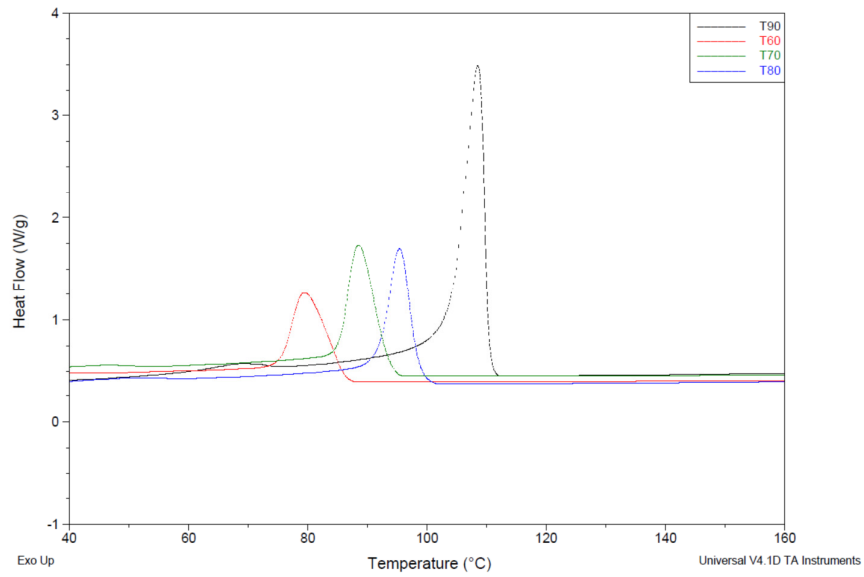


Figure B-5: DSC exotherms for Tref fractions of PEH2.

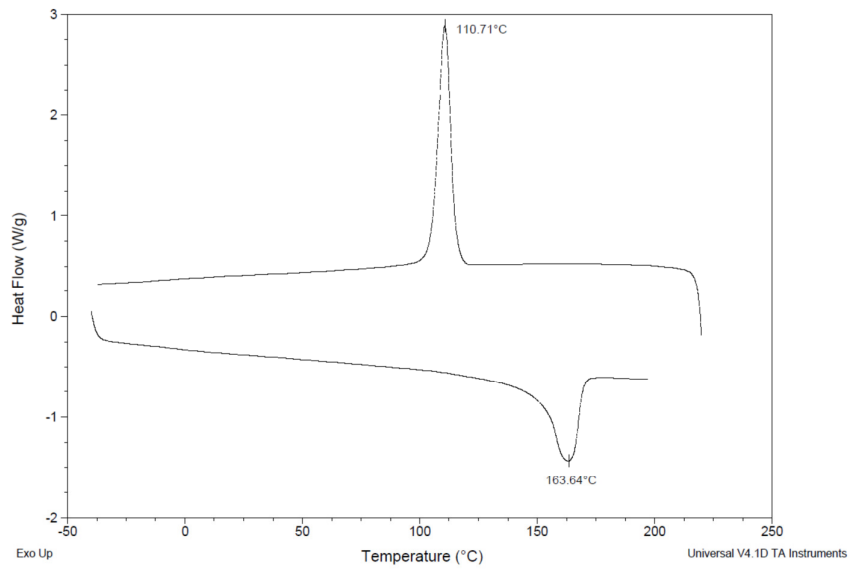


Figure B-6: DSC results for iPP.

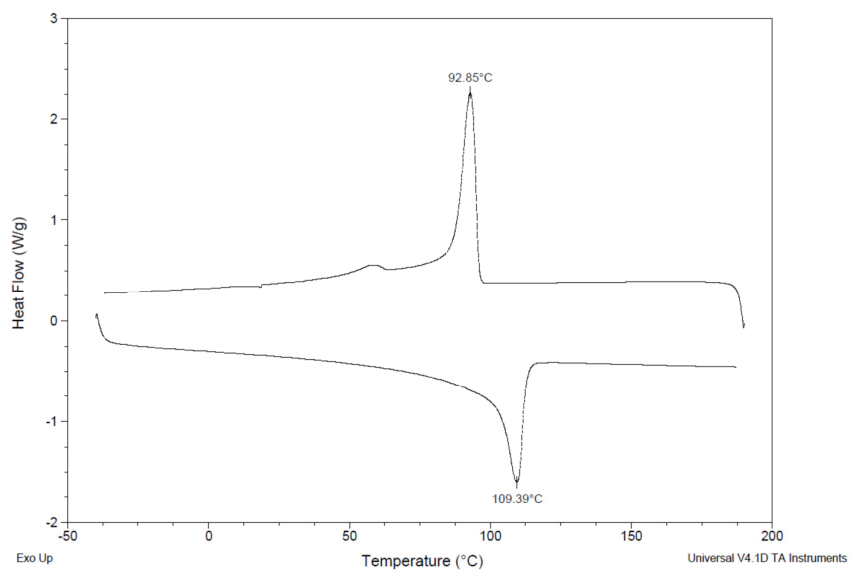


Figure B-7: DSC results for LDPE.

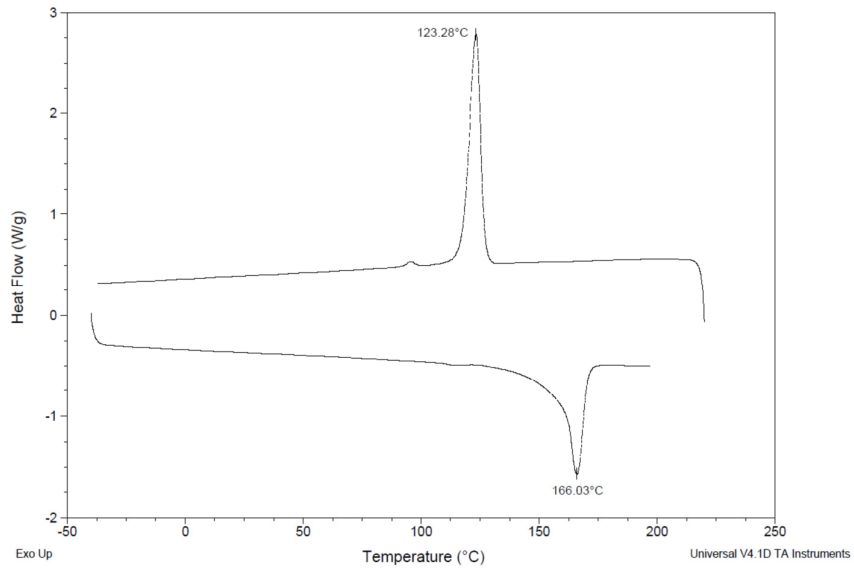
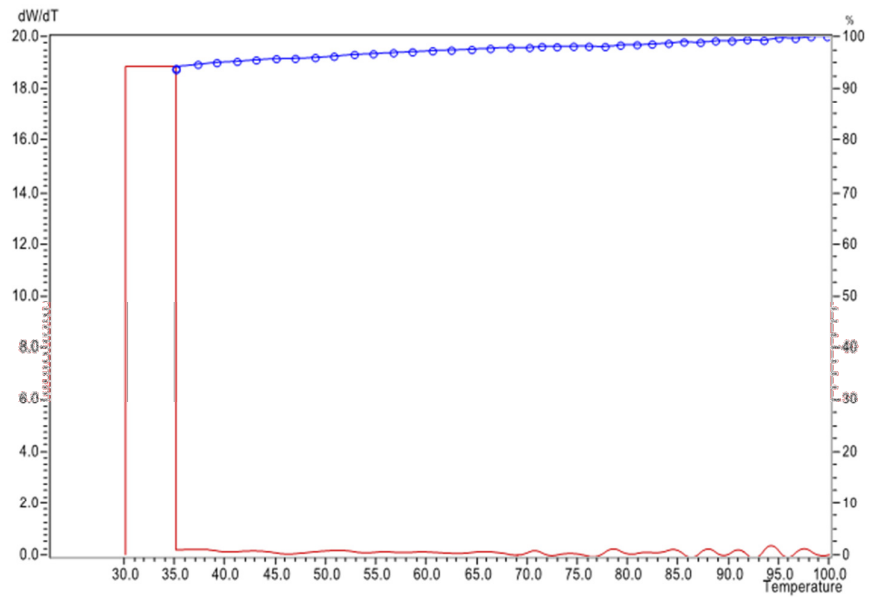
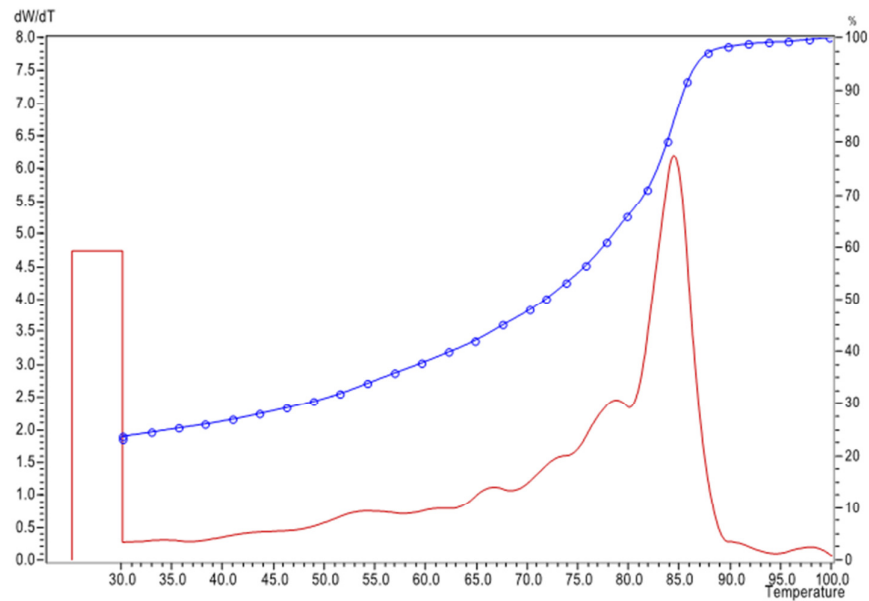


Figure B-8: DSC results for PPIC.

Appendix C: Crystaf data**Figure C-1: Crystaf profile of PE-1-octene.****Figure C-2: Crystaf profile of PEH1.**

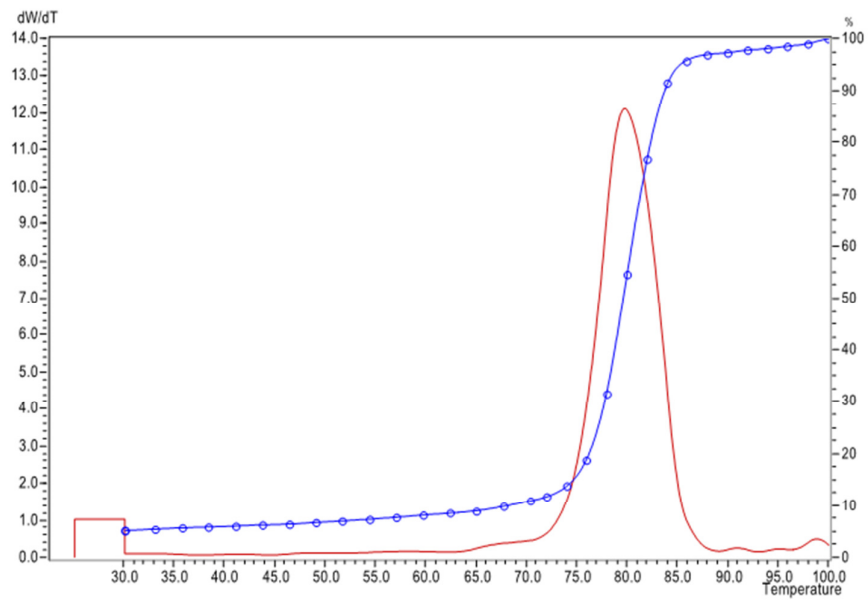


Figure C-3: Crystaf profile of iPP.

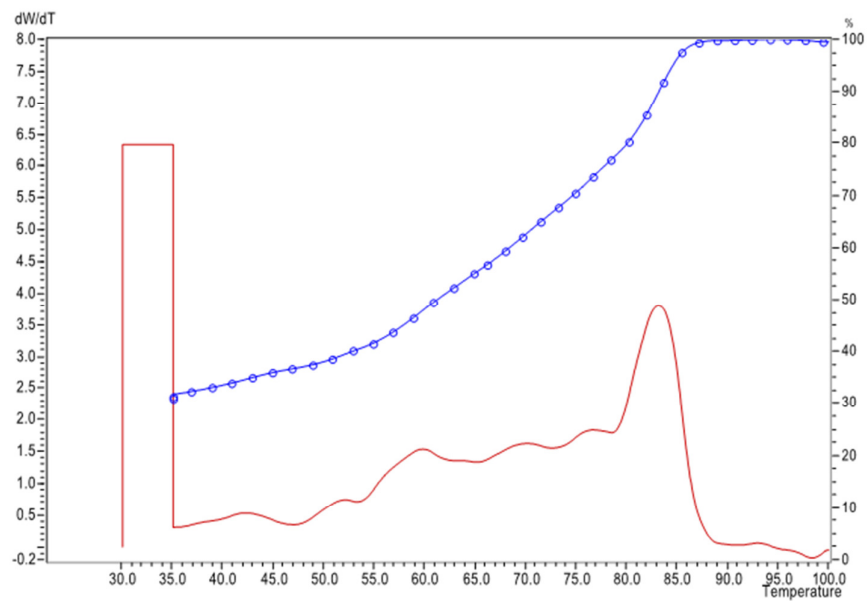


Figure C-4: Crystaf profile of PEH2.

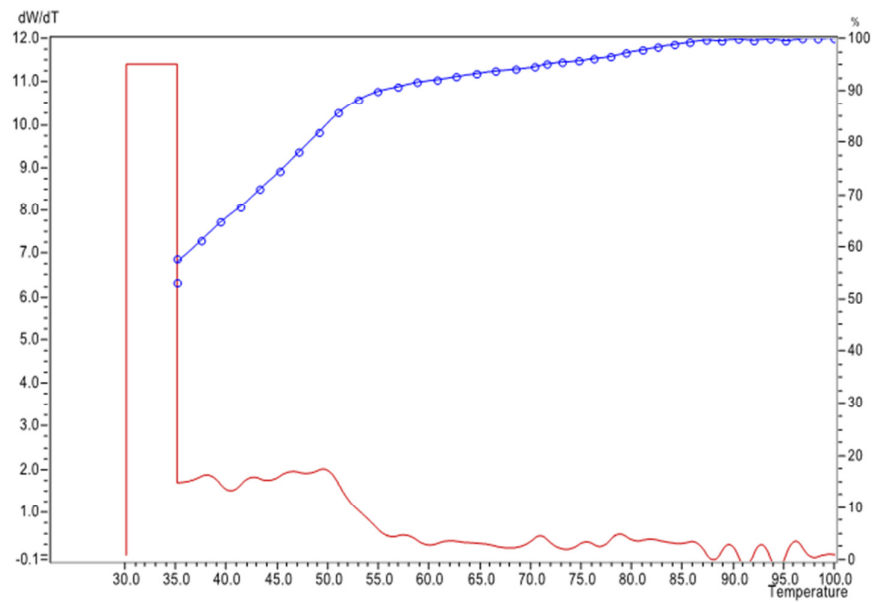


Figure C-5: Crystaf profile of PEH2 T60 fraction.

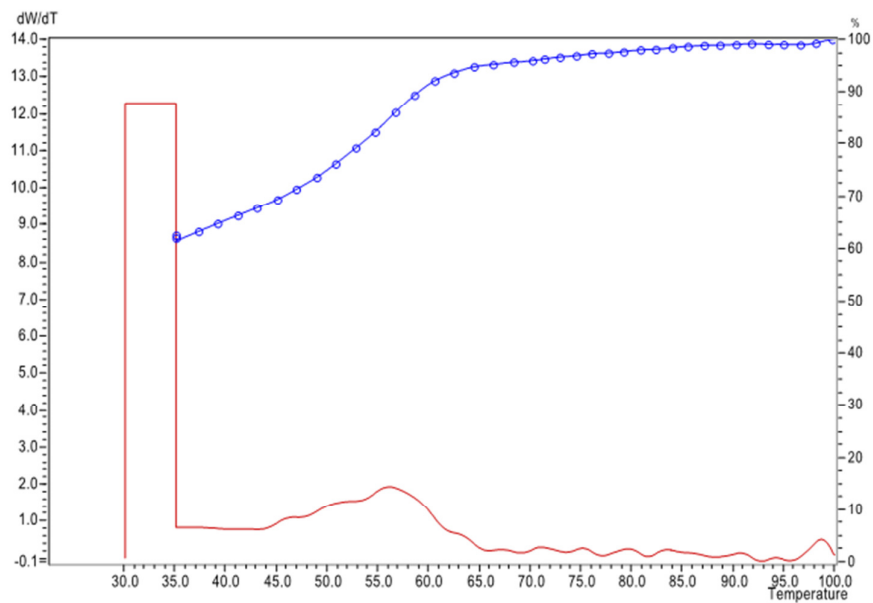


Figure C-6: Crystaf profile of PEH2 T70 fraction.

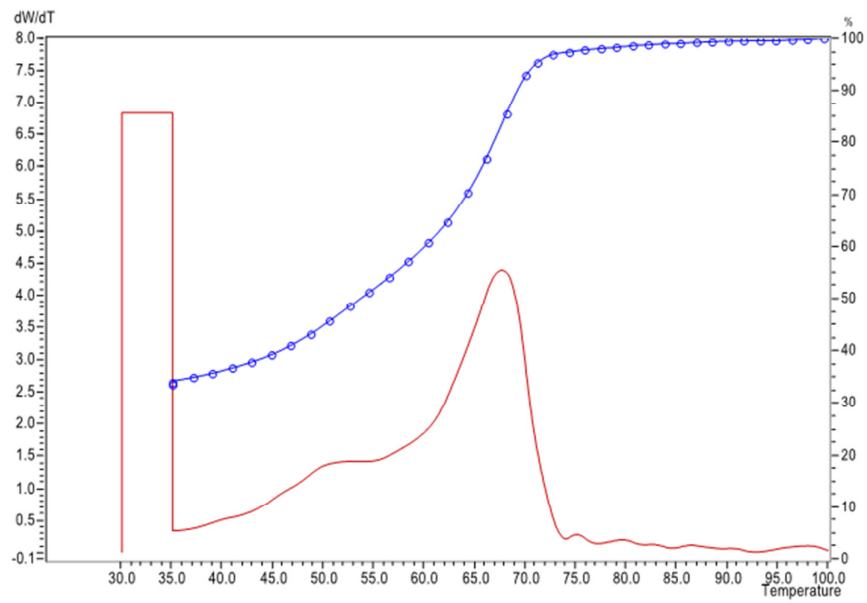


Figure C-7: Crystaf profile of PEH2 T80 fraction.

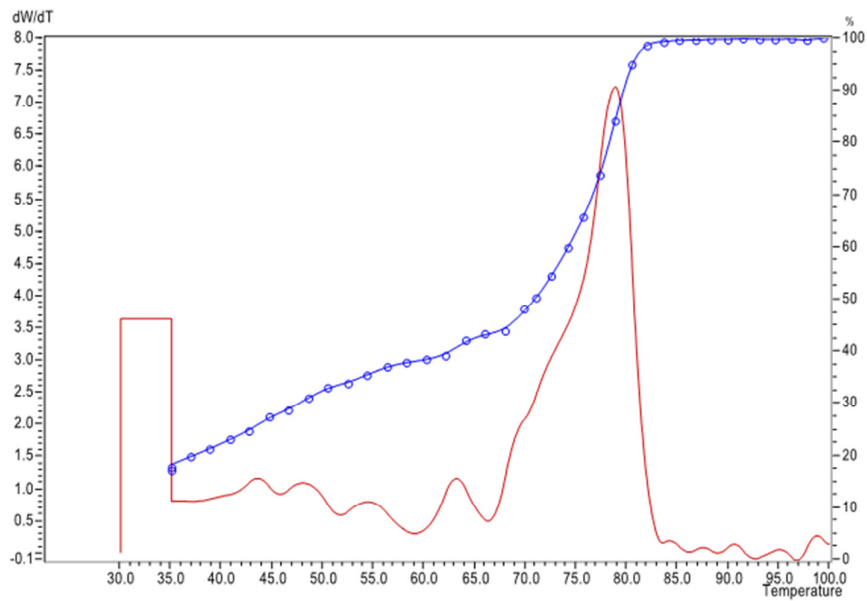


Figure C-8: Crystaf profile of PEH2 T90 fraction.